Radiology and Oncology

Publisher

Association of Radiology and Oncology

Affiliated with

Slovenian Medical Association – Slovenian Association of Radiology, Nuclear Medicine Society,
Slovenian Society for Radiotherapy and Oncology, and Slovenian Cancer Society
Croatian Medical Association – Croatian Society of Radiology
Societas Radiologorum Hungarorum
Friuli-Venezia Giulia regional groups of S.I.R.M.
Italian Society of Medical Radiology

Aims and scope

Radiology and Oncology is a journal devoted to publication of original contributions in diagnostic and interventional radiology, computerized tomography, ultrasound, magnetic resonance, nuclear medicine, radiotherapy, clinical and experimental oncology, radiobiology, radiophysics and radiation protection.

Editorial – progress of Radiology and Oncology

Dear authors, dear readers, dear reviewers of Radiology and Oncology. We would like to thank you for your contribution to the development and progress of the journal. Thanks to your effort the journal has grown through the last year, the number of manuscript submissions is gradually growing, providing the good platform for the quality of the accepted papers. The mainstream of Radiology and Oncology remains quality of the published articles; therefore, in 2011 we decide not to increase the number of published papers.

As you know, Thompson Reuters included us into the Journal Citation Reports/Science Edition database, starting in 2008. Therefore we expect this year to get the first Impact Factor (IF). According to the number of citations that are in the Web of Science database and are gradually growing, the IF should be decent. We believe that this will encourage all of us even more to strive for the quality of our journal.

The editorial policy of Radiology and Oncology is to publish in an open access. In order to follow this decision the journal is now available at www.vesitaopen.com as the open access journal. This will also enable us, hopefully this year, to enter Pub Med Central and PubMed database. In this way the journal will gain worldwide open access to all readers and writers in the field of radiology and oncology.

The open access policy has its advantages in broad accessibility of the papers, without any payment for the readers. However, it brings over the financial burden to the journal and also to the authors of the papers. Therefore, with time we will have to ask the authors to pay for the publication of the papers and their open access. In the transition phase we encourage the authors to pay the publication fee to the editorial office voluntarily. All authors are kindly encouraged to consider this option and help the journal to keep the open access policy.

We in the editorial office strive to be swift in processing the manuscripts. The time from the manuscript submission to acceptance of the paper for publication is in average 7 weeks. The accepted papers are then in approximately 3-4 weeks published E-ahead of print on the journal's web page.

At the end I would like to thank you again for your contribution to the journal and encourage you to submit high quality manuscripts to Radiology and Oncology and also encourage your colleagues and students to choose our journal for their publications.

Best regards,

Prof. Gregor Serša, Ph.D.
Editor in Chief

Viljem Kovač, M.D.
Executive Editor

contents

contents

radiophysics

slovenian abstracts

review

Magnetic nanoparticles as targeted delivery systems in oncology

Sara Prijic[1] and Gregor Sersa[2]

[1] Nanotesla Institute, Ljubljana, Slovenia

[2] Institute of Oncology Ljubljana, Department of Experimental Oncology, Ljubljana, Slovenia

Background. Many different types of nanoparticles, magnetic nanoparticles being just a category among them, offer exciting opportunities for technologies at the interfaces between chemistry, physics and biology. Some magnetic nanoparticles have already been utilized in clinical practice as contrast enhancing agents for magnetic resonance imaging (MRI). However, their physicochemical properties are constantly being improved upon also for other biological applications, such as magnetically-guided delivery systems for different therapeutics. By exposure of magnetic nanoparticles with attached therapeutics to an external magnetic field with appropriate characteristics, they are concentrated and retained at the preferred site which enables the targeted delivery of therapeutics to the desired spot.
Conclusions. The idea of binding chemotherapeutics to magnetic nanoparticles has been around for 30 years, however, no magnetic nanoparticles as delivery systems have yet been approved for clinical practice. Recently, binding of nucleic acids to magnetic nanoparticles has been demonstrated as a successful non-viral transfection method of different cell lines *in vitro*. With the optimization of this method called magnetofection, it will hopefully become another form of gene delivery for the treatment of cancer.

Key words: magnetic nanoparticles; nanotechnology; delivery systems; oncology; magnetofection; cancer therapy; magnetic targeting

Introduction

Nanotechnology is an interdisciplinary field of technological developments on the nanometer scale offering comprehensive applications also to biomedicine. Engineering particles a several tens of nanometers in diameter has opened new possibilities for targeting cells within an organism either for diagnostic or therapeutic purposes.

Magnetically-guided drug or gene targeting using magnetic nanoparticles is a promising approach for cancer chemotherapy and cancer gene therapy. The rationale behind these two treatment modalities is based on binding either chemotherapeutics or nucleic acids onto the surface of magnetic nanoparticles which are directed to and/ or retained at the tumor by means of an external magnetic field. Researchers have been studying magnetically-guided drug targeting since the late 1970's[1], however, magnetically-guided gene targeting has emerged as rapid and efficient approach in the beginning of the new millennium.[2] Magnetic nanoparticles have been explored predominantly in basic and translational research in the field of oncology although some of them have been already clinically approved as contrast enhancing agents for magnetic resonance imaging (MRI).[3]

Magnetic nanoparticles

What are nanoparticles?

To date, there is no uniform definition of a nanoparticle. According to Kreuter, a nanoparticle is a solid colloidal particle ranging in size from 1 to 1000 nm.[4] In nanomedicine, »nano« can be applied to materials or surfaces that are intentionally altered and manipulated at nanometer scale result-
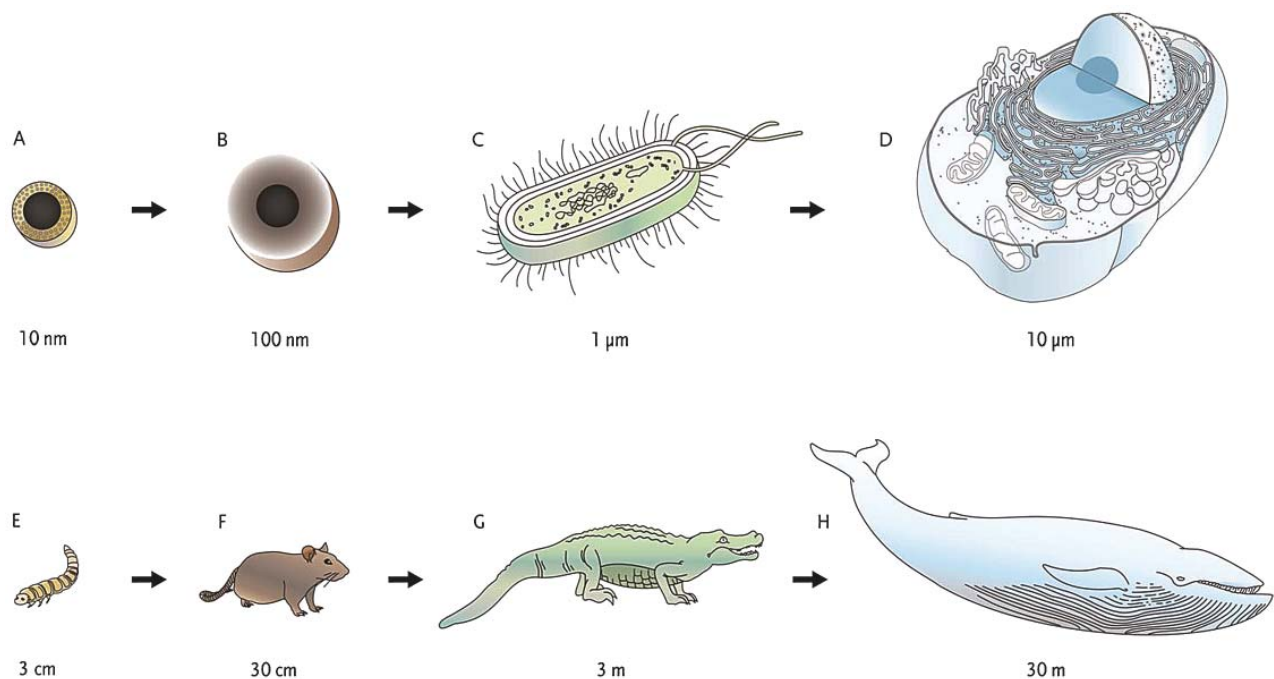
FIGURE 1. Illustrative demonstration of size comparison of a nanoparticle at the microscopic level with corresponding relations on the macroscopic level. Sizes at the microscopic level (A-D) are equivalent to the ones at the macroscopic level (E-H). Magnetic nanoparticle coated with a thin inorganic layer (A), magnetic nanoparticle coated with an organic polymer (B), prokaryotic cell (C) and eukaryotic cell (D) are in the same size relation as a mealworm (E), a rat (F), an alligator (G) and a blue whale (H), respectively.

ing in new properties.[5] Besides the differences in size, nanoparticles are also distinguished based on their shape and chemical composition (Table 1).

Despite the fact that many nanoparticles measure more than 100 nm in one dimension, a novel explanation of a nanoparticle based on the following foundations has emerged. First, the majority of nanoparticles for biomedical applications are prepared as colloidal dispersions, *i.e.* homogenous chemical mixtures of two separated phases. The homogeneity of dispersed-phase particles into a continuous-phase aqueous medium is only possible if dispersed-phase particles have a diameter between 5 and 200 nm.[6] Second, unique differences of physical properties that distinguish nanoparticles from atoms as well as from the bulk material are the most prominent below 100 nm. Hence, a nanoparticle is defined as a particle of any kind of material which has one or more dimensions equal to or smaller than 100 nm (Figure 1).[7]

What are magnetic nanoparticles?

Nanoparticles consisting of iron, nickel and/or cobalt which exhibit magnetic properties are called magnetic nanoparticles.[8] Elemental manganese which has a complex crystal structure and unusual magnetic properties can also display magnetic behavior after special physicochemical treatment.[9]

Briefly, the magnetic properties of a material are the reflection of magnetization which arises from magnetic moments of unpaired electrons due to their orbital motion around the nucleus of an atom and intrinsic spinning around their axes. Due to the thermal fluctuations of magnetic moments that reverse direction, some magnetic nanoparticles exhibit superparamagnetic properties which are defined as the nonappearance of magnetic behavior when the magnetic field is not present.[10] Superparamagnetic properties are observed at sizes smaller than 15 nm for iron oxide maghemite (γ-Fe_2O_3).[11] Hence, magnetic nanoparticles which are small enough, composed of iron oxide and display magnetic behavior only in the presence of a magnetic field are called superparamagnetic iron oxide nanoparticles (SPIONs). It is essential to use SPIONs in biomedical applications since the permanent magnetic behavior of magnetic particles within an organism would be redundant or even destructive when the magnetic field is removed. For example, magnetically induced deformation of endosomes containing paramagnetic nanoparticles

TABLE 1. Classification of nano-sized delivery systems by chemical compounds and shape. Magnetic nanoparticles which are most often used in biomedical applications are shadowed

CHEMICAL COMPOUNDS				SHAPE
ORGANIC	NATURAL	LIPIDS	Egg phosphatidylcholine (EPC), egg phosphatidyl glycerol (EPG)	Liposomes
		PROTEINS	Human serum albumin (HSA), gelatin	Nanoparticles*
		CARBON HYDRATES	Chitosan, alginate	Nanoparticles*
	SYNTHETIC	LIPIDS	Dipalmitoyl phosphatidylcholine (DPPC), dimyristoyl phosphatidylcholine (DMPC), dimyristoyl phosphatidylglycerol (DMPG), dipalmitoyl phosphatidic acid (DPPA), distearoyl phosphatidylcholine, cholesterol (Ch)	Liposomes
			Tricaprin, trilaurin, trimylistin, tripalmitin with gliceryl monostearate, cetyl palmitate, stearic acid	Solid lipid nanoparticles
		POLYMERS	**Homopolymers**: Poly(alkylcyanoacrylate) (PACA), poly(2-hydroxyethyl methacrylate) (pHEMA), poly(N-(2-hydroxypropyl)methacrylamide (pHPMA), polyvinylpyrrolidone (PVP), poly(methyl methacrylate) (PMMA), polyorthoesters, polycaprolactone (PCL), poly(vinyl alcohol) (PVA), poly(acrylic acid) (PAA), polylactides (PLA) **Copolymers**: Poly(alkylcyanoacrylate)-co-poly(ethylene glycol), poly(lactid acid)-co-poly(glycolic acid) (PLGA), poly(L,L-lactide-co-L-aspartic acid), poly(ethylene-co-vinyl acetate) (PEVA)	Dendrimers Nanoparicles* Nanocomposites Nanobrushes Nanotubes Micelles Nanogels
		SURFACTANTS	**Cationic**: Sodium dodecyl sulfate (SDS) **Anionic**: Cetyl trimethylammonium bromide (CTAB) **Non-ionic**: Copolymers of poly(ethylene oxide) and poly(propylene oxide)	Micelles
ORGANIC & INORGANIC		LIPIDS	DPPC/Ch/γ-Fe$_2$O$_3$, Fe$_3$O$_4$	Magnetic liposomes
INORGANIC	MAGNETIC	POLYMERS	Ni-Zn-ferrite/SiO$_2$, Fe-Ni/polymer, Co/polymer, PMMA/a-Fe$_2$O$_3$	Nanocomposites
		COMPOUNDS	Ni-Fe/SiO$_2$, Co/SiO$_2$, Fe-Co/SiO$_2$, Fe/Ni-ferrite, Ni-Zn-ferrite/SiO$_2$	Nanocomposites
		COMPOUNDS	**Iron**: γ-Fe$_2$O$_3$, Fe$_3$O$_4$	**Nanoparticles***
			MgFe$_2$O$_4$, MnFe$_2$O$_4$, FePt, NiFe$_2$O$_4$	Nanoparticles* Nanorods
			Nickel: NiO, NiFe$_2$O$_4$	
			Cobalt: Co$_3$O$_4$, CoFe$_2$O$_4$	
			Manganese: Mn$_3$O$_4$, MnO$_2$	
	NON-MAGNETIC	COMPOUNDS	CdSe/ZnS	Nanocrystals
			ZnO, Au, Ag, Cu, CdSe/ZnS, GaN, TiO$_2$, C, TiC, VO$_2$, V$_2$O$_5$, PbS, CdS, SiC, BiPO$_4$, AOB	Nanorods Nanoparticles*
			Calcium phosphate	Nanocomposites
		ELEMENTS	C	Fullerenes Nanotubes

* Nanoparticles include nanocapsules and/or nanospheres

was shown by the transmission electron microscope (TEM).[12]

Most studies discussed in this review refer to SPIONs, however not all of them. Hence, the superior term magnetic nanoparticles will be used also for SPIONs in order to make the manuscript more lucid and organized whereas the term SPIONs will be used only when emphasizing the importance of superparamagnetic behavior of the nanoparticles. The majority of magnetic nanoparticles as targeted delivery systems are chemically iron oxides (Table 1). Iron is essential to nearly all known organisms and even endogenic iron oxide nanoparticles were detected in the human hippocampus.[13,14] However, at the cellular basis, iron oxide causes direct cytotoxicity due to the generation of oxygen and nitrogen-based atoms with an unpaired electron, *i.e.* reactive oxygen and nitrogen species (ROS and RNS).[15] Therefore, magnetic nanoparticles are predominantly prepared through the use of core-shell methodology. As reviewed by Gupta and Gupta, the magnetic core of iron oxide nanoparticles is composed of magnetite (Fe_3O_4) and/or maghemite (γ-Fe_2O_3) whereas their shell surface coating can be of organic compounds, including surfactants and synthetic or natural polymers, or inorganic material, such as silica, carbon, precious metals or oxides.[16] Synthesis of core-shell type magnetic nanoparticles is important due to the several reasons: (i) protection of the magnetic core from oxidation, (ii) protection of the surface from chemical reactions, (iii) avoidance of aggregates and agglomerates formation due to Van der Waals forces, hydrophobic effects and magnetic attractions, (iv) facility of the various therapeutics attachment and (v) amplification of the cellular uptake rate.[17]

Biocompatibility of magnetic nanoparticles depends on the type of their surface coating which can be biodegradable (*e.g.* certain polymers) or non-biodegradable (*e.g.* silica) as well as on their size. The thickness of the coating determines the total size of magnetic nanoparticles, *i.e.* coating with an inorganic material in general results in smaller particles below 100 nm whereas a polymer coating is predominantly reflected in larger particles above 100 nm.[18,19] The type of the coating determines characteristics of the particle surface, such as hydrophilicity and surface charge.

For biomedical applications magnetic nanoparticles are predominantly prepared as ferrofluids, *i.e.* magnetic liquids, thus their surface charge is established by ionization of surface groups or by adsorption of charged species of a surrounding liquid medium onto the particle surface which re-

sults in a layer around the particle. The potential difference between the surrounding liquid medium and the layer around the particle is called the zeta potential. Particles with a zeta potential higher than 30 mV, either positive or negative, will repel each other, stay asunder and result in a stable ferrofluid.[6]

Why use magnetic nanoparticles?

The use of magnetic nanoparticles as drug or gene delivery systems can contribute to the effectiveness of cancer therapy in many ways. First, an advantage of using magnetic nanoparticles over non-magnetic ones is that magnetic behavior allows monitoring and quantitative determination of their biodistribution by MRI, which facilitates optimal dosing in cancer therapy. Second, targeting of tumors by magnetic nanoparticles can overcome some supplementary hindrances in more efficient treatment of cancer, such as insufficient penetration of certain therapeutics from the blood-stream into the tumor. Third, targeting of tumors with magnetically-guided nanoparticles provides site specificity and thus selectivity of the therapy, which results in reduced side effects and lower cost of the therapy. And last, exploiting the magnetic field as the driving force represents a non-invasive therapeutic approach.[10]

How to exploit magnetic nanoparticles?

The basic principle of using magnetic nanoparticles for targeting in oncology is to increase antitumor efficacy while at the same time reduce undesired systemic side effects towards normal tissues by (i) passive targeting, (ii) active targeting and/or (iii) targeting with an external magnetic field. Passive and active targeting can be achieved irrespective of nanoparticles possessing magnetic behavior. Passive targeting is referred to the extravasation of nanoparticles from the blood-stream into the tumor due to disorganized and leaky tumor vasculature.[20] Active targeting is related to appropriate ligands, predominantly monoclonal antibodies, their fragments, inhibitors of tyrosine kinase domains and most recently aptamers, which actively target tumor markers and are attached to nanoparticles.[21] Ligands can target extracellular matrix, surface receptors on endothelial cells of tumor vessels or pericytes and tumor cell surface receptors.[22] On the other hand, targeting by means of an external magnetic field can only be possible in the case of magnetic nanoparticles. Combining active target-

ing and targeting with a magnetic field provides double-targeting where the magnetic field represents an initial targeting vector that concentrates magnetic nanoparticles in the tumor followed by second level active targeting by means of ligands, bound onto the surface of magnetic nanoparticles that are specific for tumor cells.

Magnetic nanoparticles are in most cases manipulated by a magnetic field which is generated by high-field, high-gradient, rare earth magnets, such as neodymium iron boron (Nd-Fe-B) magnets. Nd-Fe-B magnets are the strongest type of permanent magnets which have been commercialized not earlier than 1986.[23] The basic principle of magnetically-guided targeting is to place a magnet over a targeted site, *i.e.* a tumor, in order to *in situ* concentrate and/or retain magnetic nanoparticles.

If targeting with an external magnetic field is in conjunction with bare magnetic nanoparticles with no attached therapeutics, such a kind of cancer therapy relies on intentional obstruction of tumor vessels. Cancer therapy aiming to obstruct tumor vessels with magnetically guided microparticles composed of carbonyl iron was performed in the early 1970s. Unfortunately, the material displayed low *in vivo* stability as well as a low ability to be guided by the magnetic field.[24] More than two decades later, magnetic nanoparticles were intravenously administered to mice prior to applying the magnetic field with a flux density of 200-500 mT for 20 min above the subcutaneously transplanted colon carcinomas or hypernephromas. This caused complete and permanent tumor remissions due to tumor blood vessels obstruction.[25] Compared to active targeting with antibody-bound magnetic nanoparticles, targeting with bare magnetic particles by sufficiently long exposure (6 h) to the magnetic field with a flux density of only 2.5 mT resulted in comparable retention at the targeted site, in this case lungs and heart.[26]

Pathways of magnetic nanoparticles within an organism

Efficient internalization of magnetic nanoparticles into targeted cells and subsequent therapy outcome are limited by several factors, such as (i) cytotoxicity, (ii) nanoparticle aggregation due to increased surface/volume ratio and (iii) short plasma half-life due to their elimination from the bloodstream by phagocytic cells. In general, biocompatibility of magnetic nanoparticles mainly depends on their

physicochemical properties whereas the route of administration and characteristics of an applied magnetic field also affect cellular uptake and biodistribution.[27,28]

Cellular pathways

It is known that different therapeutics get in contact with cells mainly by Brownian motion during a given incubation time. Hence, the crucial limitation in achieving more efficient delivery of therapeutics to the cells is the lack of contact between the delivery system and cellular surface. The contact between the therapeutics and cellular surface can be increased by exploiting the gravitational force[29] as well as magnetic force.

Sedimentation

Manipulating the magnetic force *in vitro* leads to accelerated sedimentation of magnetic nanoparticles onto the cellular surface and does not directly affect their internalization.[30,31] Magnetic nanoparticles exposed to Nd-Fe-B magnets with the remanence of approximately 1 T, *i.e.* the strength of the magnetic field at the core of the magnet, were detected *in vitro* onto the cellular surface within a few minutes.[32]

Internalization

Once the magnetic nanoparticles are located onto the cellular surface, fast internalization begins. Results obtained by mechanics modeling demonstrate that particles in the size range of tens to hundreds of nanometers can enter cells even in the absence of clathrin or caveolin-mediated endocytosis.[33] However, the majority of experimental studies concluded that internalization of magnetic nanoparticles was mediated through endocytosis, beginning with the invagination of the plasma membrane at either clathrin-coated pits or caveolaes.[18,31,34-36] The extent of involvement of clathrin-dependent and caveolae-mediated endocytosis seems to be cell dependent.[31]

Irrespective of nanoparticles possessing magnetic behavior, authors of studies have reported about more efficient membrane crossing and cellular uptake of smaller particles in comparison to larger ones, *e.g.* 10-20 nm *vs.* 1000 nm and 70 nm *vs.* 200 nm.[37,38]

Malignant cells are more prone to internalization of magnetic nanoparticles than normal cells (Figure 2).[18,35,39,40] The reason is that malignant cells
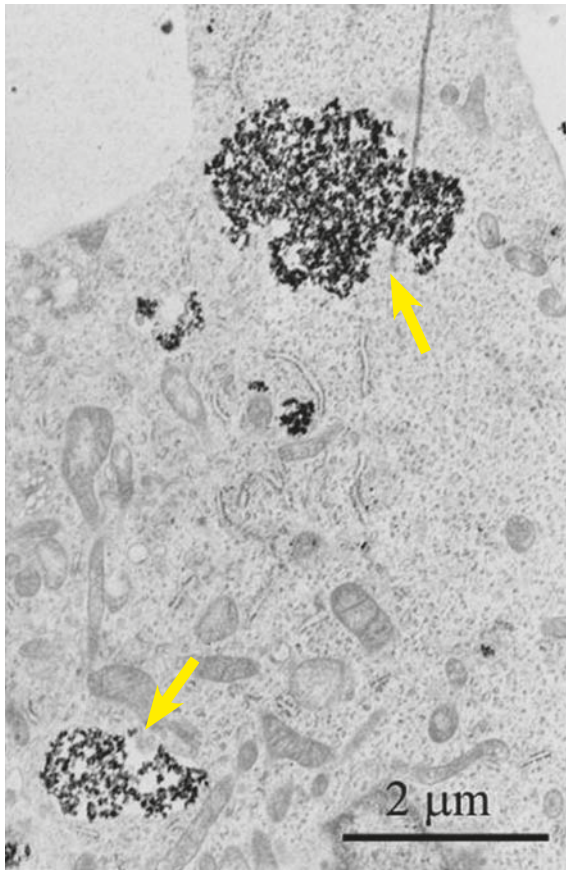
FIGURE 2. Transmission electron micrograph of human melanoma SK-MEL-28 cell, taken 4 h after the cell has been exposed to 100 μg SPIONs/ml. Arrows indicate enlarged endosomes with high accumulation of SPIONs.

possess a higher endocytotic potential than normal cells due to their enhanced requirement for nutrients in virtue of their high metabolic activity and proliferation rate.[41] This makes magnetic nanoparticles especially suitable for delivery of anticancer therapeutics into tumor cells.

Cellular trafficking

Once internalized, magnetic nanoparticles with attached therapeutics remain within the maturing endosomes until they fuse with lysosomes where they are exposed to digestive enzymes. Linkage between a magnetic nanoparticle and a therapeutic has to overcome degradation within body fluids but has to achieve fast and simple cleavage once magnetic nanoparticles are internalized into cells. Various molecules can be linked to magnetic nanoparticles in order to release their cargo from the endocytotic-degradative pathway.

In the case of gene delivery, endosomal escape of nucleic acids is in most cases achieved by the proton sponge effect of endosomolytic polymers, such as polyethylenimine (PEI).[31,42-44] Due to the large number of amino groups PEI possesses a high buffering capacity which in the acidic environment of the endolysosomes induces proton entry and accumulation, followed by passive chloride influx leading to osmotic swelling of the endolysosomes. Endolysosomes burst releasing their content into the cytoplasm.[45] Irrespective of the applied magnetic field, binding of PEI to the surface of magnetic nanoparticles increased transfection efficiency of anti-GFP siRNA in stably transduced cervical cancer HeLa cells with GFP for 20% at siRNA concentrations as low as 8 nM.[42] Moreover, under magnetic field guidance, addition of free PEI to already PEI-modified magnetic nanoparticles resulted in an approximately 8-fold increase in transfection efficiency of the *luciferase* reporter gene to Swiss albino mouse fibroblasts (NIH 3T3) in comparison to transfection using just PEI-modified magnetic nanoparticles.[42]

However, as PEI is vastly cytotoxic[44,46], also other molecules are attached to magnetic nanoparticles, such as fusogenic peptides and cell-penetrating peptides (CPPs).[28,47,48] Fusogenic peptides, *e.g.* INF-7, are able to form membrane channels in response to low pH which leads to the disruption of an endosome.[49,50] CPPs, *e.g.* Tat peptides, are a family of proteins containing short cationic or amphiphatic polypeptide sequences, termed the protein transduction domain that have the ability to cross cellular membranes while carrying macromolecules.[51,52]

Penetration into the nucleus

The nuclear membrane allows passive transport of substances below 50 kDa whereas other substances can only enter the nucleus by active transport through nuclear pore complex (NPC). NPC consists of importins, heterodimeric proteins of α and β subunits, which bind to a specific recognition sequence called the nuclear localization signals (NLSs) of the importing substance. NLSs consist of arginine and lysine sequences which help in the transportation of the substance from the cytoplasm to the nucleus.[53] In order to avoid the use of the intrinsic machinery of the viruses to enter the nucleus and to enhance transfection efficacy, synthetic NLSs have been produced and bound to magnetic nanoparticles. For example, magnetic nanoparticles successfully entered the nucleus of HeLa cells only when modified with NLSs peptide.[54]

Biodistribution within an organism

As reviewed by Soenen and Cuyper, biodistribution of magnetic nanoparticles depends on their physicochemical properties, such as size, hydrophilicity and surface charge.[15] Irrespective of nanoparticles possessing magnetic behavior, with increasing their surface charge and decreasing hydrophilicity, the capacity of plasma protein absorption increases which leads to their recognition by phagocytic cells.[55] By increasing the size, renal clearance is omitted, however, nanoparticle recognition by phagocytic cells increases which results in their accumulation in the liver, spleen and lymph nodes.[56]

Different *in vivo* studies in mice and rats showed that magnetic nanoparticles after intravenous administration predominantly accumulated in the liver and spleen: 55% of the injected iron composing 190 nm magnetic nanoparticles localized in the liver after 6 h, but was reduced to 20% after 24 h.[57] The level of iron in the spleen after 3 weeks corresponded to 25% of the injected dose.[58] Significantly increased iron levels were also detected in the heart and brain, however these were notably lower than these in the liver and spleen.[57] Biodistribution of magnetic nanoparticles in the mice after intra-peritoneal route was similar to that of intravenous administration: the highest concentrations of magnetic nanoparticles were observed in liver and spleen.[59] If magnetic nanoparticles are guided by means of a magnetic field, they concentrate in the area of interest (Figure 3). For example, when 70 nm magnetic nanoparticles were injected into mice through the tail vein and directed to the heart and kidneys by means of magnetic field with flux density of only 2.5 mT for 6 h, they concentrated in the heart and kidneys as well as in the lungs.[26] Biodistribution of magnetic nanoparticles after different administration routes is schematically presented in the Figure 3.

Toxicity studies

Toxicity of magnetic nanoparticles

Toxicity studies of magnetic nanoparticles are scarce. The first tolerance study with carbohydrate-coated magnetic nanoparticles as potential delivery systems was performed in nude mice and showed no median lethal dose (LD$_{50}$), no alterations in the blood haematological and biochemical profiles as well as no organomegalies were observed after injection of magnetic nanoparticles. However, when
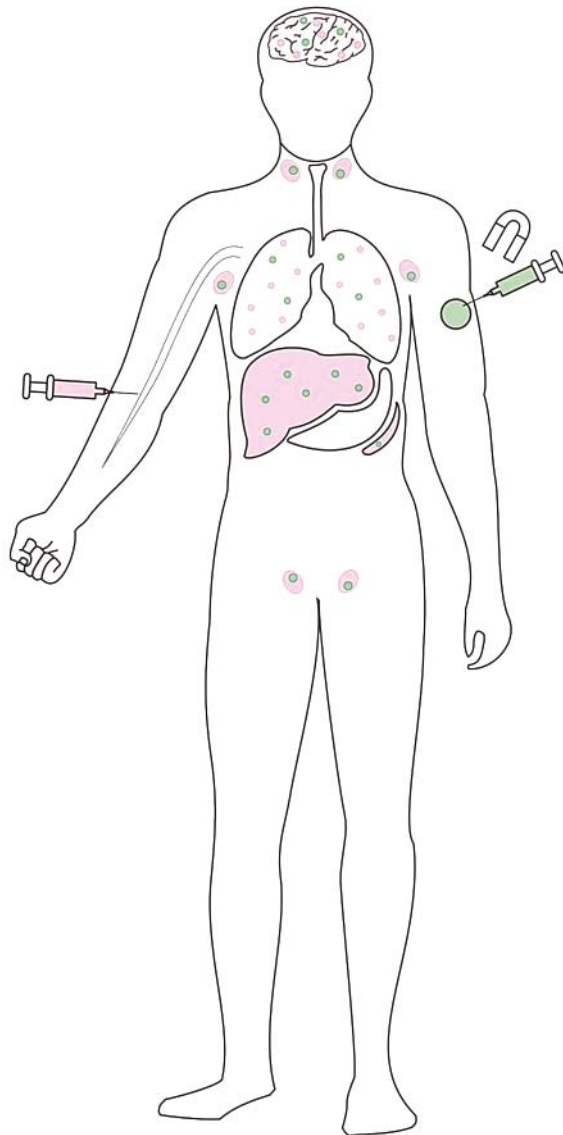
FIGURE 3. Biodistribution of magnetic nanoparticles within the body after different administration routes. After intravenous administration (pink syringe) magnetic nanoparticles predominantly accumulate in the liver, spleen and lymph nodes (pink areas). However, the blood flow also takes them to other organs, *e.g.* lungs, brain (pink dots). After intra-tumoral administration and exposure to the magnet (green syringe), magnetic nanoparticles concentrate in the tumor (green area). However, a small quantity can also be also found in the organs throughout the body, *e.g.* liver, lungs, lymph nodes, brain, spleen (green dots), which depends on leakage of the tumoral vasculature.

10-20% of the blood volume was infused with the ferrofluid, short episodes of lethargy and resistance of food uptake were detected.[25] On the other hand tartrate and citrate-coated magnetic nanoparticles, administrated intra-peritoneally in mice, caused severe inflammatory reactions in the peritoneal

cavity and around the hilum of spleen and kidneys, indicating that adsorption of carboxylic acids at physiological pH and isotonic conditions did not inevitably result in a biocompatible ferrofluid.[60] Coating of magnetic nanoparticles with dextran despite of more than 6 months retention in the liver and spleen of mice caused no alterations observable in histology specimens of these organs.[61] Similarly, histological analysis of liver, spleen and kidney after intravenous administration of oleic acid-coated magnetic nanoparticles did not show any alterations in these organs. However, lipid peroxidation indicating oxidative stress was elevated and returned to a normal value within 3 weeks.[57]

Toxicity of an external magnetic field

Questions remain about the possibility of adverse side effects related to electromagnetic fields. According to the U.S. National Institute of Environmental Health Sciences (NIEHS), there is a weak association between magnetic field exposure of flux density as small as 0.0003 mT and an increased risk of childhood leukemia.[62] According to numerous MRI examinations, a static magnetic field of flux densities from 0.5 to 2 T does not cause any known side effects and therefore the patient compliance is high.[63] On the other hand, rats developed aversive and avoidance behavior when the field was increased up to ultra-high fields of flux densities of 4 T and 7 T, respectively.[64]

There are some inconsistent reports about cellular toxicity or adverse side effects caused by magnetic field exposure which might be due to the cell type dependent mechanisms. It seems that cells deriving from mesenchymal descent are more prone to the magnetic field exposure than other normal and malignant cells.[47,65-68] Evidently, in order to provide assurance that the magnetic field accurately does not cause any side effects there is a vital need to perform additional *in vitro* as well as *in vivo* studies.

Applications of magnetic nanoparticles in oncology

Diagnostic purposes

For diagnostic purposes magnetic nanoparticles are utilized as contrast enhancing agents for MRI in order to improve spatial resolution and provide earlier lesion detection.[69] SPIONs are replacing paramagnetic gadolinium-based MRI contrast agents due to their superior *in vivo* behavior and biocom-

patibility with some of them already being FDA-approved. Earliest magnetic nanoparticles for MRI were administered into the bloodstream and within minutes cleared by mononuclear phagocytic cells of the reticuloendothelial system. Their subsequent accumulation into the liver and spleen improved visualization of focal lesions with a few millimeters diameter.[70-72] In 1996, the first liver-specific MRI contrast agent, Feridex I.V.®, came to the market which was soon followed by GastroMARK®, a contrast agent for MRI of the gastrointestinal tract. Modification of physicochemical properties of magnetic nanoparticles resulted in their prolonged blood half-life and vascular penetration which enabled visualization of other tissues and organs within the rats.[73,74] For example, Chertok *et al.* visualized accumulation of magnetically-guided nanoparticles in experimentally-induced rat gliosarcomas after intravenous administration by MRI.[75] Currently, magnetic nanoparticles are being investigated for visualization of lymph node metastases which are otherwise undetectable by existent technology equipment.[76] Moreover, as reviewed by Jain *et al.*, SPIONs with minor macrophage uptake and prolonged blood half-life have found preferential application in sentinel lymph node imaging as contrast enhancing agents for MRI.[77]

Concerning diagnostic, prognostic and even therapeutic implications, magnetic nanoparticles are also used in magnetic-activated cell sorting (MACS®) for magnetic separation of different tumor cells and cancer stem cells out of the bloodstream or tissue by the recognition of CD surface antigens.[78-81] Briefly, magnetic nanoparticles coated with immunospecific agents tag target cells which are then separated from other biological entities by passing through an external magnetic field.

Therapeutic purposes

For therapeutic purposes no magnetic nanoparticles have yet been approved for clinical use. However, the majority are being investigated as drug or gene delivery systems whereas to a considerably smaller extent they are being explored for the treatment of cancer by magnetic hyperthermia.

Magnetic hyperthermia

Magnetic hyperthermia is local therapeutic modality for the treatment of cancer which is founded on the fact that magnetic nanoparticles produce heat when exposed to an alternating current (AC) magnetic field. The therapy comprehends administra-

tion of magnetic nanoparticles into the tumor followed by an AC magnetic field exposure. Cancer cells loaded with magnetic nanoparticles are subjected to irreversible damage of temperatures above 42-43°C whereas normal cells withstand temperatures up to 46°C.[39] Moreover, heat alters some receptor molecules on the surface of cancer cells which enhances their recognition by natural killer cells.[82] In 2005, the first phase I clinical trial was carried out in a patient with a recurrent prostatic tumor concluding that magnetic hyperthermia is a feasible and well tolerated treatment modality.[83] Two years later in combination with radiotherapy, magnetic hyperthermia was performed in 14 brain-cancer patients demonstrating that the therapy was well tolerated by all the patients with minimal or no clinical effect.[84]

Drug carriers

Magnetically-guided drug carriers in the treatment of cancer date back to the late 1970s, however, no such magnetic nanoparticles have yet been clinically approved. Only nanoparticles without magnetic properties, *i.e.* liposomes encapsulating anthracyclines (daunorubicin and doxorubicin), and nanoparticulate albumin-bound paclitaxel are used for the treatment of different types of solid tumors and metastatic breast cancer, respectively.[85]

The idea of using magnetic microspheres as vehicles for drug delivery in cancer therapy was first introduced by Widder *et al*.[1] In 1983 they performed the first preclinical study in rats. Selective targeting with intravenously administrated magnetic albumin microspheres containing low doses of doxorubicin resulted in total remission of 77% (17/22) of tumors after only one regimen of drug therapy.[86]

As late as 1996, the very first preclinical and clinical studies on magnetic nanoparticles for cancer therapy were done. It is essential to mention that the following magnetically-guided drug carriers were barely classified among nanoparticles since they measured 0.5 - 5.0 μm. A preclinical study of magnetically-guided nanoparticles as delivery systems in cancer therapy was performed in a xenotransplanted human colon as well as renal cancer tumor-bearing mice. After intravenous injection and magnetic guidance of epidoxorubicin attached to magnetic nanoparticles, complete remissions of tumors were observed.[25] The first clinical phase-I magnetically-guided drug-targeted study was carried out in 14 patients with advanced unsuccessfully pretreated solid tumors.

Intravenous administration of epidoxorubicin attached to magnetic nanoparticles resulted in transient serum iron elevations in almost all patients after the therapy, which did not cause any clinical symptoms, and in some patients increased ferritin levels in the blood were observed. In 50% (7/14) of the patients, magnetic nanoparticles were detected within the tumors. However, only a slight reduction of tumor size occurred in merely 14% (2/14) of the patients.[87]

Later, the same research group utilized mitoxantrone attached to magnetic nanoparticles of the ferrofluid (magnetic liquid) (FF-MTX) aiming to compare the antitumor efficacy of FF-MTX given by different administration routes. The treatment was performed in rabbits bearing squamous cell carcinomas (VX-2) which showed complete and permanent remission after intra-arterial administration of FF-MTX. However, intravenous application of FF-MTX did not result in statistically significant tumor remission in comparison to the control group.[88]

The following preclinical and clinical trials of two research groups focused on the delivery of doxorubicin hydrochloride adsorbed to magnetic targeted carriers (MTC-DOX) by selective arterial catheterization of the hepatic artery.[89-91] A preclinical trial was performed in a swine model. By magnetic targeting, extravasation of MTC-DOX through the vascular wall was obtained, leading to their localization and retention in the tissue at the targeted site. The severity of liver necrosis correlated to the severity of embolization following treatment and was observed only in the animals which received the highest dose of MTC-DOX whereas no adverse effects were determined at the MTC-DOX low-dose group.[89] Clinical trials with MTC-DOX were carried out in patients with inoperable hepatocellular carcinomas. No clinically significant toxicity was observed. However, all patients experienced abdominal pain during MTC-DOX administration which was intravenously controlled with analgesics.[90,91] In the first phase I/II study, localization of MTC-DOX in the tumors was achieved in 94% (30/32) of all the patients with one complete and two partial responses.[90] In the second study MTC-DOX was observed in 100% (4/4) of the tumors with 64-91% of the tumor volume loaded with magnetic nanoparticles. However, this resulted in only one partial response.[91] A subsequent phase II/III multinational clinical study with MTC-DOX enrolling 240 patients with hepatocellular carcinoma was prematurely stopped as there was no increase in median survival time for MTC-DOX
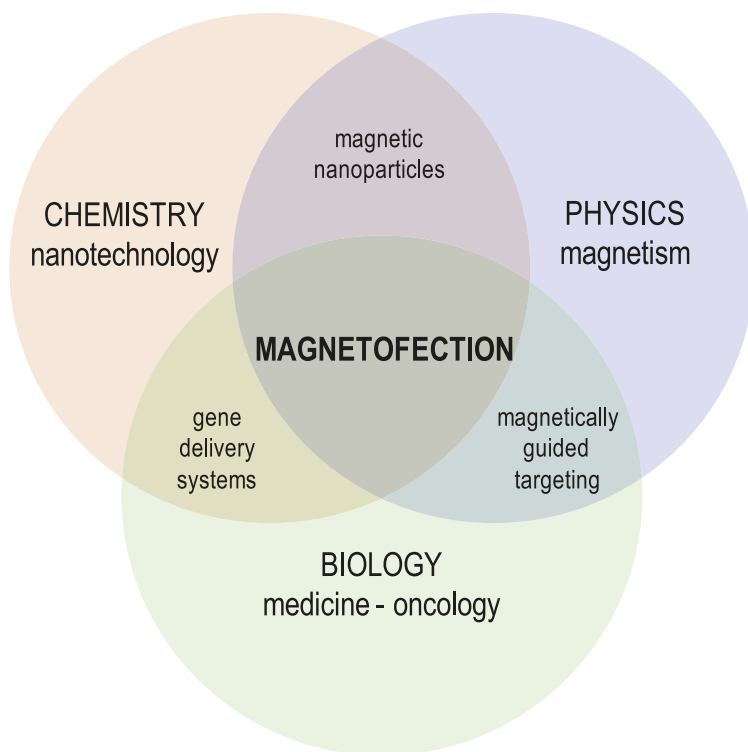
FIGURE 4. Schematic presentation of interdisciplinary approach resulting in magnetofection at the cross-section.

treated patients relative to patients treated with IV doxorubicin.[92]

To sum up, preclinical studies turned out in complete and permanent tumor remission; however, dose escalation clinical trials resulted in no clinically significant toxicities but had a relatively poor tumor response.

Nucleic acid carriers

In addition to chemotherapy, recent progress in gene therapy has made it a realistic option for the treatment of cancer.[93,94] The idea of using magnetic nanoparticles as gene delivery systems emerged in the year 2000, combining expertise of chemistry, biology, medicine and physics. This new interdisciplinary approach has already shown some promising results in preclinical studies.[95-98]

Until the new millennium, the majority of studies focusing on gene delivery for therapeutic approaches used viruses as transport vehicles for nucleic acids. In order to avoid the disadvantages of viral based gene delivery, such as receptor dependent host tropism, pre-existing immunity of the host, induced immune response by the virus, potential recombination of viral and host cell ge-

netic material and large-scale infrastructure for virion production, new methods have begun developing.[99]

Non-viral methods of gene transfer can be divided into three major groups: injection of naked plasmid DNA (pDNA), chemical and physical approaches.[100] In 1990, first *in vivo* study injecting naked pDNA into mouse muscle was performed. In the injected tissue significant elevations of all three reporter genes encoding chloramphenicol acetyltransferase, luciferase and beta-galactosidase were observed.[101] Later, injection of naked pDNA was repeated by others, as well as in other organs.[102,103] In an effort to increase transfection efficiency, development of various physical approaches has begun. The general principle of nucleic acid internalization by physical approaches, which include microinjection, hydrodynamic delivery, biolistics, electroporation, sonoporation and impalefection, is based on disruption of the cell membrane to facilitate nucleic acid uptake.[104-109] However, nucleic acids still remain exposed to biochemical degradation which reduces transfection efficacy; thus attaching or encapsulating nucleic acids within nanoparticles, which mediate their internalization by membrane fusion and/or endocytosis, results in increased transfection efficiency *in vitro* in comparison to some physical approaches.[110]

Progress in the field of nanotechnology and new trends in gene biology contributed to the development of a novel method called magnetofection, which unites the advantages of physical and chemical approaches in one system (Figure 4). The method is based on binding the nucleic acids to magnetic nanoparticles that concentrate and transfect cells in the area of interest by means of a magnetic field.[2] For cancer therapy, a high-field, high-gradient, rare earth permanent magnet, such as Nd-Fe-B magnet, is placed above the solid tumor in order to retain administrated magnetic nanoparticles with bound nucleic acids *in situ* until they internalize and transfect malignant cells.[97,98] Although magnetofection is considered a nonviral method of gene transfer, viral vectors can be supplementary attached to magnetic nanoparticles in order to additionally increase transfection efficiency.[111] In 2000, the use of magnetic microparticles for transfection *in vitro* was first demonstrated in carcinoma C12S cells and *in vivo* in mice using an adeno-associated virus linked to magnetic microspheres *via* heparin. The study resulted in enhanced green fluorescent protein (GFP) expression due to the increase in contact between the delivery system and the cell.[112] In these terms,

the immunity-based problems arising from the use of viral vectors for gene transfer remain; therefore, studies of virus-associated magnetic nanoparticles will not be discussed in this review.

Magnetofection in vitro and ex vivo

Currently there are several commercially available magnetic nanoparticles measuring 50 to 200 nm in diameter, *e.g.* CombiMAG, PolyMAG and TransMAG[PEI], which have been used in many *in vitro* and some *in vivo* studies of magnetofection.[2,28,31,42,95-98,113] It is noteworthy that these vectors represent a hybrid system characterized by the iron oxide inner core and a coat consisting of PEI, which is a well known transfection agent.[114]

All *in vitro* studies confirmed efficient magnetofection of a variety of cell lines with various nucleic acids, in most cases pDNA followed by small interfering RNA (siRNA), short hairpin RNA (shRNA) and antisense oligonucleotides, associated to magnetic nanoparticles and guided by a magnetic field generated by Nd-Fe-B magnets.[2,28,31,42,95,96] Magnetofection of pDNA encoding GFP on mouse melanoma B16F1 cells is presented in Figure 4. The studies also demonstrated that magnetofection is superior to other standard transfection protocols, mostly lipofection.[95,115]

The first *in vitro* study demonstrated enhancement in *LacZ* reporter gene transfection of mouse embryonic fibroblasts NIH3T3 and Chinese hamster ovary (CHO) cells up to several 100-fold compared to transfection in the absence of magnetic field. In addition, a minimal dose of pDNA (0.1 μg) was sufficient to achieve high transfection levels.[2] The highest increase in transfection efficiency of human umbilical vein endothelial cells (HUVEC) with the *luciferase* reporter gene by magnetofection was about 360-fold compared to various conventional transfection methods.[95] However, it is worth to note that magnetic nanoparticles in the latter study were additionally coupled to lipid-based transfection reagents, Effectene® and FuGENE®, as well as to a combination of the polymer-lipid transfection enhancer PEI/DOTAP-cholesterol, which greatly contributed to the increase in transfection efficiency. Other *in vitro* and *ex vivo* magnetofection-based studies also showed enhanced transfection efficacy of *luciferase*, *enhanced GFP (EGFP)* and *Discosoma sp. red fluorescent protein (DsRed)* reporter genes to various cell lines, however, to a lesser extent, *i.e.* from 3-fold to 36-fold.[116-119]

Refinements of the technique resulted in significantly reduced time needed for the transfec-
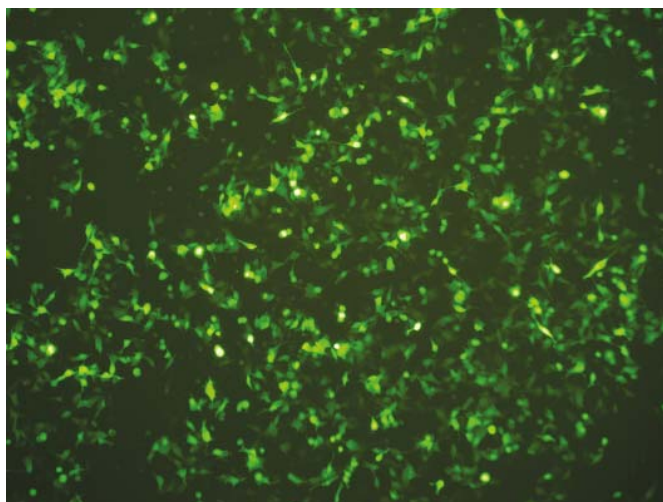
FIGURE 5. Photomicrograph of mouse melanoma B16F1 cells, taken 24 h after magnetofection of pDNA encoding GFP was performed, demonstrating high transfection efficiency. Image taken under visible light condition (A) and image taken under fluorescence epi-illumination (B) (x 60 magnification).

tion process to be completed (transfection time) in comparison to other non-viral gene delivery approaches. Under magnetic field guidance, the transfection time of HUVEC with oligodesoxynucleotides (ODN) against the p22[phox] subunit of endothelial NAD(P)H-oxidase bound to magnetic nanoparticles was decreased to a few minutes whereas it required 24 h when ODN were coupled only to Effectene®.[96] Cationic lipid-coated magnetic nanoparticles associated with transferrin demonstrated a 300-fold increase in transfection efficiency of the *luciferase* reporter gene in comparison to well established and efficient PEI polyplexes and Lipofectin™ after 15 min incubation.[115] Similarly, Chorny *et al.* managed to efficiently transfect aortic smooth muscle cells A10 and bovine aortic

endothelial cells (BAEC) with the use of polymer-coated magnetic nanoparticles attached to pDNA encoding EGFP just after 15 min of exposure to the magnetic field. The negligible transfection was observed in the absence of the magnetic field.[120]

Therefore, magnetofection is defined as enhanced delivery of nucleic acids associated with magnetic nanoparticles to the cells under the influence of a magnetic field.[2]

The majority of magnetofection studies utilized a static magnetic field, however, two research groups have also focused on the application of a pulsed magnetic field. The Swiss group utilized electromagnets and reported that transfection efficiency of reporter genes was the highest when magnetic nanoparticles were first sedimented by exposure to the permanent magnet before application of the pulsating magnetic field.[121] The mechanism behind this observation could be an alteration in the permeability of cell membranes by pulsed magnetic field after the increased sedimentation by a static magnetic field enhanced the contact between the cells and magnetic nanoparticles. In another study of the same group, at least a 6-fold increase in transfection efficiency of the *EGFP* reporter gene to various primary cell lines was shown when a combination of static and pulsating magnetic field was used compared to the presence of static magnetic field alone. The transfection was the lowest when the cells were exposed only to the pulsed magnetic field.[119] On the other hand, the American group utilized a computer-controlled stepper motor-driven horizontally oscillating magnet array system which produced increased magnetic field strength and a gradient with no heating in comparison to electromagnets used by the Swiss group. The lateral motion of the horizontally oscillating magnet array system at an amplitude 200 μm and frequency 2 Hz promoted extra energy and mechanical stimulation which increased particles sedimentation onto the cellular surface. The result was a 4-fold greater transfection of the *luciferase* reporter gene to human lung epithelial NCI-H292 cells than that of Lipofectamine™ 2000 and more than a 2-fold greater than transfection performed under a static magnetic field. The oscillating array system also had little or no effect on cell viability.[122]

Magnetofection in vivo

Although authors of several studies have reported about the suitability of magnetofection of reporter genes *in vitro*, some improvements are still required to make the method efficient enough to be widely used for *in vivo* applications.

To demonstrate that magnetofection of reporter genes *in vivo* is feasible, two studies using pDNA encoding beta-galactosidase and luciferase were performed in rats, mice and pigs.[2,113] In addition, a magnetofection study using Cy3-fluorescence-labeled antisense ODN was carried out in mice by the same extended research group.[96] Initial preclinical *in vivo* trial of *LacZ* reporter gene delivery was performed in ilea lumens of rats using viral vector-free magnetic nanoparticles and in stomach lumens of mice using adenovirus-associated magnetic nanoparticles. Efficient transfection was observed in lamina propria of ileum as well as in crypts of fundic glands after 20 min of exposure to the magnetic field. For additional proof-of-principle, magnetofection of the *luciferase* reporter gene was done in the ear veins of pigs. Luciferase expression was observed in all vein samples under the influence of magnetic field whereas no transfection was found distally from the magnet position and in other organs.[2] In another study, the same magnetic nanoparticles were coupled to lipid 67 (GL67) and pDNA encoding luciferase, thus forming ternary complexes. GL67 is a cationic lipid considered as the gold standard for *in vivo* airway gene transfer. The authors aimed to compare magnetofection efficacy of ternary complexes to transfection efficacy of plane GL67/pDNA. Surprisingly, *in vivo* transfection of the murine nasal epithelium with plane GL67/pDNA resulted in an approximately 90-fold higher luciferase expression than that observed by magnetofection. The authors referred the poor outcome of magnetofection to the size of magnetic nanoparticles (200 nm), their coating and characteristics of the magnetic field applied, suggesting that smaller particles with a modified surface coating could have been more efficient in crossing extracellular barriers as well as intracellular membranes in the airway epithelium.[113] The third *in vivo* study was performed in mice in order to investigate whether magnetofection is feasible strategy for directing antisense ODN, complexed to magnetic nanoparticles, to a targeted site *via* arterial catheterization. Nd-Fe-B magnet was held above the right testis throughout the infusion of Cy3-labeled antisense ODN, coupled to magnetic nanoparticles, *via* femoral catheter and for another additional 4 min. The study demonstrated site-specific magnetofection of the ipsilateral arterioles of the cremaster muscle whereas contralateral vessels of the same muscle, which were not exposed to an external magnetic field, were not transfected.[96]

Magnetofection of therapeutic genes *in vivo* was published in two papers, both dealing with veterinary clinical trial consisting of dose-escalation neoadjuvant gene therapy to surgery.[97,98] The aim of neoadjuvant immunostimulatory gene therapy in the treatment of cancer is to induce local production of cytokines which triggers systemic antitumor immunity.[123] Both studies were carried out in feline fibrosarcomas by the same research group in which immunostimulatory therapeutic genes were applied by magnetofection. In the study of Jahnke *et al.*, dose-escalation study was performed with a combination of pDNA encoding three different cytokines: feline interleukin-2 (feIL-2), feline interferon-gamma (feIFN-γ) and feline granulocyte-macrophage colony-stimulating factor (feGM-CSF). Altogether six cats developed local recurrences during 1-year observation period, four of them received the highest dose of the total amount of pDNA (1350 μg pDNA; 450 μg per plasmid).[97] That was clarified by bell-shaped dose dependence of IL-2.[124,125] Moreover, one cat in this group (12.5%) showed adverse events. However, the study concluded that the highest dose was well tolerated as the only adverse events occurred once and were self-limiting. Due to the early recurrences the authors suggested to include in a subsequent phase-II study also the second highest dose of pDNA (450 μg pDNA; 150 μg per plasmid).[97] In the study of Hüttinger *et al.*, magnetofection of pDNA encoding feGM-CSF was performed 14 days prior to surgery. Results of the study demonstrated that ten of the treated animals (50%) were recurrence-free after 360 days of observation. Moreover, the highest dose (1250 μg) of pDNA applied was shown to be safe for phase-II testing.[98]

Future directions

New technologies have enabled synthesis of biocompatible magnetic nanoparticles that can be functionalized with therapeutic molecules. The transfection method using magnetic nanoparticles, which are manipulated by an external magnetic field, is called magnetofection. It is a promising strategy that can lead to targeted delivery of pDNA carrying therapeutic genes, siRNA or other gene therapy approaches. Due to its physical properties of delivery, the approach is feasible on different tissues; foreseen can be tumors, muscle, skin and others. In this field of research very little was done. When the protocols for synthesis of magnetic nanoparticles and their functionalization with nucleic acids are standardized along with contemporary optimization of magnetic field parameters, the field will open for broader and in depth investigations, that may in near future also bring magnetofection into the clinical trials.

Acknowledgement

References

1. Widder KJ, Senyei AE, Ranney DF. Magnetically responsive microspheres and other carriers for the biophysical targeting of antitumor agents. *Adv Pharmacol Chemother* 1979; **16:** 213-71.

2. Scherer F, Anton M, Schillinger U, Henke J, Bergemann C, Krüger A, et al. Magnetofection: enhancing and targeting gene delivery by magnetic force in vitro and in vivo. *Gene Ther* 2002; **9:** 102-9.

3. Morana G, Salviato E, Guarise A. Contrast agents for hepatic MRI. *Cancer Imaging* 2007; **7 Spec No A:** S24-7.

4. Kreuter J. Drug targeting with nanoparticles. *Eur J Drug Metab Pharmacokinet* 1994; **19:** 253-6.

5. Filipponi L, Sutherland D, editors. Nanotechnology: a brief introduction [Internet]. Aarhus: University of Aarhus; 2007 [cited 2010 March 11]. Available from: http://www.nanocap.eu.

6. Hunter R. Electrokinetics and the zeta potential. In: Hunter R, editor. *Foundations of colloid science*. New York: Oxford University Press; 2001. p. 373-434.

7. Auffan M, Rose J, Bottero JY, Lowry GV, Jolivet JP, Wiesner MR. Towards a definition of inorganic nanoparticles from an environmental, health and safety perspective. *Nat Nanotechnol* 2009; **4:** 634-41.

8. Gubin S. Introduction. In: Gubin S, editor. *Magnetic nanoparticles*. Weinheim: Wiley-VCH; 2009. p. 1-24.

9. Bondi JF, Oyler KD, Ke X, Schiffer P, Schaak RE. Chemical synthesis of air-stable manganese nanoparticles. *J Am Chem Soc* 2009; **131:** 9144-5.

10. Alexiou C, Jurgons R. Magnetic drug targeting. In: Andrä W, Nowak H, editors. *Magnetism in medicine: a handbook*. Berlin: Wiley-VCH; 2007. p. 596-605.

11. Lowery T. Nanomaterials-based magnetic sensors switch biosensors. In: Kumar C, editor. *Nanomaterials for the life sciences*. Weinheim: Wiley-VCH; 2009. p. 3-54.

12. Wilhelm C, Cebers A, Bacri JC, Gazeau F. Deformation of intracellular endosomes under a magnetic field. *Eur Biophys J* 2003; **32:** 655-60.

13. Kirschvink JL, Kobayashi-Kirschvink A, Woodford BJ. Magnetite biomineralization in the human brain. *Proc Natl Acad Sci U S A* 1992; **89:** 7683-7.

14. Schultheiss-Grassi PP, Wessiken R, Dobson J. TEM investigations of biogenic magnetite extracted from the human hippocampus. *Biochim Biophys Acta* 1999; **1426:** 212-6.

15. Soenen SJ, De Cuyper M. Assessing cytotoxicity of (iron oxide-based) nanoparticles: an overview of different methods exemplified with cationic magnetoliposomes. *Contrast Media Mol Imaging* 2009; **4:** 207-19.

16. Gupta AK, Gupta M. Synthesis and surface engineering of iron oxide nanoparticles for biomedical applications. *Biomaterials* 2005; **26:** 3995-4021.

17. Phenrat T, Saleh N, Sirk K, Tilton RD, Lowry GV. Aggregation and sedimentation of aqueous nanoscale zerovalent iron dispersions. *Environ Sci Technol* 2007; **41:** 284-90.

18. Prijic S, Scancar J, Romih R, Cemazar M, Bregar VB, Znidarsic A, et al. Increased cellular uptake of biocompatible superparamagnetic iron oxide nanoparticles into malignant cells by an external magnetic field. *J Membr Biol* 2010; **236:** 167-79.

19. Chertok B, David AE, Yang VC. Polyethyleneimine-modified iron oxide nanoparticles for brain tumor drug delivery using magnetic targeting and intra-carotid administration. *Biomaterials* 2010; **31:** 6317-24.

20. Matsumura Y, Maeda H. A new concept for macromolecular therapeutics in cancer chemotherapy: mechanism of tumoritropic accumulation of proteins and the antitumor agent smancs. *Cancer Res* 1986; **46:** 6387-92.

21. Byrne JD, Betancourt T, Brannon-Peppas L. Active targeting schemes for nanoparticle systems in cancer therapeutics. *Adv Drug Deliv Rev* 2008; **60:** 1615-26.

22. Leuschner C, Kumar CS, Hansel W, Soboyejo W, Zhou J, Hormes J. LHRH-conjugated magnetic iron oxide nanoparticles for detection of breast cancer metastases. *Breast Cancer Res Treat* 2006; **99:** 163-76.

23. Babincova M, Babinec P. Magnetic drug delivery and targeting: principles and applications. *Biomed Pap Med Fac Univ Palacky Olomouc Czech Repub* 2009; **153:** 243-50.

24. Mosso JA, Rand RW. Ferromagnetic silicone vascular occlusion: a technic for selective infarction of tumors and organs. *Ann Surg* 1973; **178:** 663-8.

25. Lübbe AS, Bergemann C, Huhnt W, Fricke T, Riess H, Brock JW, et al. Preclinical experiences with magnetic drug targeting: tolerance and efficacy. *Cancer Res* 1996; **56:** 4694-701.

26. Kumar A, Jena PK, Behera S, Lockey RF, Mohapatra S. Multifunctional magnetic nanoparticles for targeted delivery. *Nanomedicine* 2010; **6:** 64-9.

27. Chouly C, Pouliquen D, Lucet I, Jeune JJ, Jallet P. Development of superparamagnetic nanoparticles for MRI: effect of particle size, charge and surface nature on biodistribution. *J Microencapsul* 1996; **13:** 245-55.

28. Mykhaylyk O, Zelphati O, Hammerschmid E, Anton M, Rosenecker J, Plank C. Recent advances in magnetofection and its potential to deliver siRNAs in vitro. *Methods Mol Biol* 2009; **487:** 111-46.

29. Luo D, Saltzman WM. Enhancement of transfection by physical concentration of DNA at the cell surface. *Nat Biotechnol* 2000; **18:** 893-5.

30. Plank C, Schillinger U, Scherer F, Bergemann C, Rémy JS, Krötz F, et al. The magnetofection method: using magnetic force to enhance gene delivery. *Biol Chem* 2003; **384:** 737-47.

31. Huth S, Lausier J, Gersting SW, Rudolph C, Plank C, Welsch U, et al. Insights into the mechanism of magnetofection using PEI-based magnetofectins for gene transfer. *J Gene Med* 2004; **6:** 923-36.

32. Plank C, Scherer F, Schillinger U, Bergemann C, Anton M. Magnetofection: enhancing and targeting gene delivery with superparamagnetic nanoparticles and magnetic fields. *J Liposome Res* 2003; **13:** 29-32.

33. Gao H, Shi W, Freund LB. Mechanics of receptor-mediated endocytosis. *Proc Natl Acad Sci U S A* 2005; **102:** 9469-74.

34. Kim JS, Yoon TJ, Yu KN, Noh MS, Woo M, Kim BG, et al. Cellular uptake of magnetic nanoparticle is mediated through energy-dependent endocytosis in A549 cells. *J Vet Sci* 2006; **7:** 321-6.

35. Ma YJ, Gu HC. Study on the endocytosis and the internalization mechanism of aminosilane-coated Fe3O4 nanoparticles in vitro. *J Mater Sci Mater Med* 2007; **18:** 2145-9.

36. Petri-Fink A, Chastellain M, Juillerat-Jeanneret L, Ferrari A, Hofmann H. Development of functionalized superparamagnetic iron oxide nanoparticles for interaction with human cancer cells. *Biomaterials* 2005; **26:** 2685-94.

37. Prabha S, Zhou WZ, Panyam J, Labhasetwar V. Size-dependency of nanoparticle-mediated gene transfection: studies with fractionated nanoparticles. *Int J Pharm* 2002; **244:** 105-15.

38. Zauner W, Farrow NA, Haines AM. In vitro uptake of polystyrene microspheres: effect of particle size, cell line and cell density. *J Control Release* 2001; **71:** 39-51.

39. Jordan A, Scholz R, Wust P, Schirra K, Schiestel T, Schmidt H, et al. Endocytosis of dextran and silan-coated magnetite nanoparticles and the effect of intracellular hyperthermia on human mammary carcinoma cells in vitro. *J Magn Magn Mater* 1999; **194:** 185-96.

40. Wilhelm C, Billotey C, Roger J, Pons JN, Bacri JC, Gazeau F. Intracellular uptake of anionic superparamagnetic nanoparticles as a function of their surface coating. *Biomaterials* 2003; **24:** 1001-11.

41. Sincai M, Ganga D, Ganga M, Argherie D, Bica D. Antitumor effect of magnetite nanoparticles in cat mammary adenocarcinoma. *J Magn Magn Mater* 2005; **293:** 438-41.

42. Mykhaylyk O, Antequera YS, Vlaskou D, Plank C. Generation of magnetic nonviral gene transfer agents and magnetofection in vitro. *Nat Protoc* 2007; **2:** 2391-411.

43. Wei W, Xu C, Wu H. Use of PEI-coated magnetic iron oxide nanoparticles as gene vectors. *J Huazhong Univ Sci Technolog Med Sci* 2004; **24:** 618-20.

44. Chen CB, Chen JY, Lee WC. Fast transfection of mammalian cells using superparamagnetic nanoparticles under strong magnetic field. *J Nanosci Nanotechnol* 2009; **9:** 2651-9.

45. Godbey WT, Wu KK, Mikos AG. Tracking the intracellular path of poly(ethylenimine)/DNA complexes for gene delivery. *Proc Natl Acad Sci U S A* 1999; **96:** 5177-81.

46. Florea BI, Meaney C, Junginger HE, Borchard G. Transfection efficiency and toxicity of polyethylenimine in differentiated Calu-3 and nondifferentiated COS-1 cell cultures. *AAPS PharmSci* 2002; **4:** E12.

47. Smith CA, de la Fuente J, Pelaz B, Furlani EP, Mullin M, Berry CC. The effect of static magnetic fields and tat peptides on cellular and nuclear uptake of magnetic nanoparticles. *Biomaterials* 2010; **31:** 4392-400.

48. Song HP, Yang JY, Lo SL, Wang Y, Fan WM, Tang XS, et al. Gene transfer using self-assembled ternary complexes of cationic magnetic nanoparticles, plasmid DNA and cell-penetrating Tat peptide. *Biomaterials* 2010; **31:** 769-78.

49. Murata M, Takahashi S, Kagiwada S, Suzuki A, Ohnishi S. pH-dependent membrane fusion and vesiculation of phospholipid large unilamellar vesicles induced by amphiphilic anionic and cationic peptides. *Biochemistry* 1992; **31:** 1986-92.

50. Plank C, Zatloukal K, Cotten M, Mechtler K, Wagner E. Gene transfer into hepatocytes using asialoglycoprotein receptor mediated endocytosis of DNA complexed with an artificial tetra-antennary galactose ligand. *Bioconjug Chem* 1992; **3:** 533-9.

51. Green M, Loewenstein PM. Autonomous functional domains of chemically synthesized human immunodeficiency virus tat trans-activator protein. *Cell* 1988; **55:** 1179-88.

52. Frankel AD, Bredt DS, Pabo CO. Tat protein from human immunodeficiency virus forms a metal-linked dimer. *Science* 1988; **240:** 70-3.

53. Xylourgidis N, Fornerod M. Acting out of character: regulatory roles of nuclear pore complex proteins. *Dev Cell* 2009; **17:** 617-25.

54. Xu C, Xie J, Kohler N, Walsh EG, Chin YE, Sun S. Monodisperse magnetite nanoparticles coupled with nuclear localization signal peptide for cell-nucleus targeting. *Chem Asian J* 2008; **3:** 548-52.

55. Müller RH, Maassen S, Weyhers H, Mehnert W. Phagocytic uptake and cytotoxicity of solid lipid nanoparticles (SLN) sterically stabilized with poloxamine 908 and poloxamer 407. *J Drug Target* 1996; **4:** 161-70.

56. Storm G, Belliot SO, Daemen T, Lasic DD. Surface modification of nanoparticles to oppose uptake by the mononuclear phagocyte system. *Adv Drug Deliv Rev* 1995; **17:** 31-48.

57. Jain TK, Reddy MK, Morales MA, Leslie-Pelecky DL, Labhasetwar V. Biodistribution, clearance, and biocompatibility of iron oxide magnetic nanoparticles in rats. *Mol Pharm* 2008; **5:** 316-27.

58. Mykhaylyk O, Cherchenko A, Ilkin A, Dudchenko N, Ruditsa V, Novoseletz M, et al. Glial brain tumor targeting of magnetite nanoparticles in rats. *J Magn Magn Mater* 2001; **225:** 241-47.

59. Kim JS, Yoon TJ, Yu KN, Kim BG, Park SJ, Kim HW, et al. Toxicity and tissue distribution of magnetic nanoparticles in mice. *Toxicol Sci* 2006; **89:** 338-47.

60. Lacava ZGM, Azevedo RB, Lacava LM, Martins EV, Garcia VAP, Rébula CA, et al. Toxic effects of ionic magnetic fluids in mice. *J Magn Magn Mater* 1999; **194:** 90-95.

61. Lacava LM, Garcia VAP, Kückelhaus S, Azevedo RB, Sadeghiani N, Buske N, et al. Long-term retention of dextran-coated magnetite nanoparticles in the liver and spleen. *J Magn Magn Mater* 2004; **272-276:** 2434-35.

62. Olden K, editor. Health effects from exposure to power-line frequency electric and magnetic fields [Internet]. Research triangle park (NC): National institute of environmental health sciences (US); 1999 [cited 2010 April 15]. Available from: http://www.niehs.nih.gov/health/docs/niehs-report.pdf.

63. Leszczynski D. Rapporteur report: cellular, animal and epidemiological studies of the effects of static magnetic fields relevant to human health. *Prog Biophys Mol Biol* 2005; **87:** 247-53.

64. Saunders R. Static magnetic fields: animal studies. *Prog Biophys Mol Biol* 2005; **87:** 225-39.

65. Sato K, Yamaguchi H, Miyamoto H, Kinouchi Y. Growth of human cultured cells exposed to a non-homogeneous static magnetic field generated by Sm-Co magnets. *Biochim Biophys Acta* 1992; **1136:** 231-8.

66. Nakahara T, Yaguchi H, Yoshida M, Miyakoshi J. Effects of exposure of CHO-K1 cells to a 10-T static magnetic field. *Radiology* 2002; **224:** 817-22.

67. Coletti D, Teodori L, Albertini MC, Rocchi M, Pristerà A, Fini M, et al. Static magnetic fields enhance skeletal muscle differentiation in vitro by improving myoblast alignment. *Citometry PartA* 2007; **71A:** 846-56.

68. Kotani H, Kawaguchi H, Shimoaka T, Iwasaka M, Ueno S, Ozawa H, et al. Strong static magnetic field stimulates bone formation to a definite orientation in vitro and in vivo. *J Bone Miner Res* 2002; **17:** 1814-21.

69. Sun C, Lee JS, Zhang M. Magnetic nanoparticles in MR imaging and drug delivery. *Adv Drug Deliv Rev* 2008; **60:** 1252-65.

70. Saini S, Stark DD, Hahn PF, Wittenberg J, Brady TJ, Ferrucci JT. Ferrite particles: a superparamagnetic MR contrast agent for the reticuloendothelial system. *Radiology* 1987; **162:** 211-6.

71. Saini S, Stark DD, Hahn PF, Bousquet JC, Introcasso J, Wittenberg J, et al. Ferrite particles: a superparamagnetic MR contrast agent for enhanced detection of liver carcinoma. *Radiology* 1987; **162:** 217-22.

72. Weissleder R, Stark DD. Magnetic resonance imaging of liver tumors. *Semin Ultrasound CT MR* 1989; **10:** 63-77.

73. Weissleder R, Elizondo G, Wittenberg J, Rabito CA, Bengele HH, Josephson L. Ultrasmall superparamagnetic iron oxide: characterization of a new class of contrast agents for MR imaging. *Radiology* 1990; **175:** 489-93.

74. Chertok B, David AE, Moffat BA, Yang VC. Substantiating in vivo magnetic brain tumor targeting of cationic iron oxide nanocarriers via adsorptive surface masking. *Biomaterials* 2009; **30:** 6780-7.

75. Chertok B, David AE, Huang Y, Yang VC. Glioma selectivity of magnetically targeted nanoparticles: a role of abnormal tumor hydrodynamics. *J Control Release* 2007; **122:** 315-23.

76. ClinicalTrials.gov [Internet]. Bethesda (MD): National Institutes of Health (US); 1993 - . Pre-operative staging of pancreatic cancer using superparamagnetic iron oxide magnetic resonance imaging (SPIO MRI) [cited 2010 September 12].; [about 3 p.]. Available from: http://clinicaltrials.gov/ct2/show/NCT00920023 ClinicalTrials.gov Identifier NCT0090023.

77. Jain R, Dandekar P, Patravale V. Diagnostic nanocarriers for sentinel lymph node imaging. *J Control Release* 2009; **138:** 90-102.

78. Zhu L, Loo WT, Chow LW. Circulating tumor cells in patients with breast cancer: possible predictor of micro-metastasis in bone marrow but not in sentinel lymph nodes. *Biomed Pharmacother* 2005; **59:** S355-8.

79. Cammareri P, Lombardo Y, Francipane MG, Bonventre S, Todaro M, Stassi G. Isolation and culture of colon cancer stem cells. *Methods Cell Biol* 2008; **86:** 311-24.

80. Joo KM, Nam DH. Prospective identification of cancer stem cells with the surface antigen CD133. *Methods Mol Biol* 2009; **568:** 57-71.

81. Wang GY, Li Y, Yu YM, Yu B, Zhang ZY, Liu Y, et al. Detection of disseminated tumor cells in bone marrow of gastric cancer using magnetic activated cell sorting and fluorescent activated cell sorting. *J Gastroenterol Hepatol* 2009; **24:** 299-306.

82. Multhoff G, Botzler C, Wiesnet M, Müller E, Meier T, Wilmanns W, et al. A stress-inducible 72-kDa heat-shock protein (HSP72) is expressed on the surface of human tumor cells, but not on normal cells. *Int J Cancer* 1995; **61:** 272-9.

83. Johannsen M, Gneveckow U, Eckelt L, Feussner A, Waldöfner N, Scholz R, et al. Clinical hyperthermia of prostate cancer using magnetic nanoparticles: presentation of a new interstitial technique. *Int J Hyperthermia* 2005; **21:** 637-47.

84. Maier-Hauff K, Rothe R, Scholz R, Gneveckow U, Wust P, Thiesen B, et al. Intracranial thermotherapy using magnetic nanoparticles combined with external beam radiotherapy: results of a feasibility study on patients with glioblastoma multiforme. *J Neurooncol* 2007; **81:** 53-60.

85. FDA-Approved Drugs [Internet]. Boston (MA): CenterWatch. 1995 - . FDA Approved Drugs for Oncology [cited 2010 September 14]; [about 7 p.]. Available from: http://www.centerwatch.com/drug-information/fda-approvals/drug-areas.aspx?AreaID=12.

86. Widder KJ, Morris RM, Poore GA, Howard DP, Senyei AE. Selective targeting of magnetic albumin microspheres containing low-dose doxorubicin: total remission in Yoshida sarcoma-bearing rats. *Eur J Cancer Clin Oncol* 1983; **19:** 135-9.

87. Lübbe AS, Bergemann C, Riess H, Schriever F, Reichardt P, Possinger K, et al. Clinical experiences with magnetic drug targeting: a phase I study with 4'-epidoxorubicin in 14 patients with advanced solid tumors. *Cancer Res* 1996; **56:** 4686-93.

88. Alexiou C, Arnold W, Klein RJ, Parak FG, Hulin P, Bergemann C, et al. Locoregional cancer treatment with magnetic drug targeting. *Cancer Res* 2000; **60:** 6641-8.

89. Goodwin SC, Bittner CA, Peterson CL, Wong G. Single-dose toxicity study of hepatic intra-arterial infusion of doxorubicin coupled to a novel magnetically targeted drug carrier. *Toxicol Sci* 2001; **60:** 177-83.

90. Koda J, Venook A, Walser E. A multicenter, phase I/II trial of hepatic intra-arterial delivery of doxorubicin hydrochloride adsorbed to magnetic targeted carriers in patients with hepatocellular carcinoma. *Eur J Cancer* 2002; **38:** S18.

91. Wilson MW, Kerlan RK, Fidelman NA, Venook AP, LaBerge JM, Koda J, et al. Hepatocellular carcinoma: regional therapy with a magnetic targeted carrier bound to doxorubicin in a dual MR imaging/ conventional angiography suite--initial experience with four patients. *Radiology* 2004; **230:** 287-93.

92. ClinicalTrials.gov [Internet]. Bethesda (MD): National Institutes of Health (US); 1993 - . Safety and efficacy of doxorubicin adsorbed to magnetic beads Vs. IV doxorubicin in treating liver cancer [cited 2010 May 5]; [about 2 p.]. Available from: http://clinicaltrials.gov/ct/show/NCT00034333 ClinicalTrial.gov Identifier: NCT00034333.

93. Kamensek U, Sersa G. Targeted gene therapy in radiotherapy. *Radiol Oncol* 2008; **42:** 115-35.

94. Cemazar M, Jarm T, Sersa G. Cancer electrogene therapy with interleukin-12. *Curr Gene Ther* 2010; **10:** 300-11.

95. Krötz F, Sohn HY, Gloe T, Plank C, Pohl U. Magnetofection potentiates gene delivery to cultured endothelial cells. *J Vasc Res* 2003; **40:** 425-34.

96. Krötz F, de Wit C, Sohn HY, Zahler S, Gloe T, Pohl U, et al. Magnetofection--a highly efficient tool for antisense oligonucleotide delivery in vitro and in vivo. *Mol Ther* 2003; **7:** 700-10.

97. Jahnke A, Hirschberger J, Fischer C, Brill T, Köstlin R, Plank C, et al. Intratumoral gene delivery of feIL-2, feIFN-gamma and feGM-CSF using magnetofection as a neoadjuvant treatment option for feline fibrosarcomas: a phase-I study. *J Vet Med A* 2007; **54:** 599-606.

98. Hüttinger C, Hirschberger J, Jahnke A, Köstlin R, Brill T, Plank C, et al. Neoadjuvant gene delivery of feline granulocyte-macrophage colony-stimulating factor using magnetofection for the treatment of feline fibrosarcomas: a phase I trial. *J Gene Med* 2008; **10:** 655-67.

99. Lu Y, Madu CO. Viral-based gene delivery and regulated gene expression for targeted cancer therapy. *Expert Opin Drug Deliv* 2010; **7:** 19-35.

100. Russ V, Wagner E. Cell and tissue targeting of nucleic acids for cancer gene therapy. *Pharm Res* 2007; **24:** 1047-57.

101. Wolff JA, Malone RW, Williams P, Chong W, Acsadi G, Jani A, et al. Direct gene transfer into mouse muscle in vivo. *Science* 1990; **247:** 1465-8.

102. Ardehali A, Fyfe A, Laks H, Drinkwater DC, Qiao JH, Lusis AJ. Direct gene transfer into donor hearts at the time of harvest. *J Thorac Cardiovasc Surg* 1995; **109:** 716-20.

103. Schwarz ER, Speakman MT, Patterson M, Hale SS, Isner JM, Kedes LH, et al. Evaluation of the effects of intramyocardial injection of DNA expressing vascular endothelial growth factor (VEGF) in a myocardial infarction model in the rat--angiogenesis and angioma formation. *J Am Coll Cardiol* 2000; **35:** 1323-30.

104. Mueller C, Graessmann A, Graessmann M. Mapping of early SV40-specific functions by microinjection of different early viral DNA fragments. *Cell* 1978; **15:** 579-85.

105. Neumann E, Schaefer-Ridder M, Wang Y, Hofschneider PH. Gene transfer into mouse lyoma cells by electroporation in high electric fields. *EMBO J* 1982; **1:** 841-5.

106. Sanford JC, Klein TM, Wolf ED, Allen N. Delivery of substances into cells and tissues using a particle bombardment process. *Particul Sci Technol* 1987; **5:** 27-37.

107. Bao S, Thrall BD, Miller DL. Transfection of a reporter plasmid into cultured cells by sonoporation in vitro. *Ultrasound Med Biol* 1997; **23:** 953-9.

108. Liu F, Song Y, Liu D. Hydrodynamics-based transfection in animals by systemic administration of plasmid DNA. *Gene Ther* 1999; **6:** 1258-66.

109. McKnight T, Melechko A, Griffin G, Guillorn MA, Merkulov VI, Serna F, et al. Intracellular integration of synthetic nanostructures with viable cells for controlled biochemical manipulation. *Nanotechnology* 2003; **14:** 551-6.

110. Ohlfest JR, Freese AB, Largaespada DA. Nonviral vectors for cancer gene therapy: prospects for integrating vectors and combination therapies. *Curr Gene Ther* 2005; **5:** 629-41.

111. Morishita N, Nakagami H, Morishita R, Takeda S, Mishima F, Terazono B, et al. Magnetic nanoparticles with surface modification enhanced gene delivery of HVJ-E vector. *Biochem Biophys Res Commun* 2005; **334:** 1121-6.

112. Mah C, Zolotukhin I, Fraites T, Dobson J, Batich C, Byrne B. Microsphere-mediated delivery of recombinant AAV vectors in vitro and in vivo. *Mol Ther* 2000; **1:** 239S.

113. Xenariou S, Griesenbach U, Ferrari S, Dean P, Scheule RK, Cheng SH, et al. Using magnetic forces to enhance non-viral gene transfer to airway epithelium in vivo. *Gene Ther* 2006; **13:** 1545-52.

114. Boussif O, Lezoualc'h F, Zanta MA, Mergny MD, Scherman D, Demeneix B, et al. A versatile vector for gene and oligonucleotide transfer into cells in culture and in vivo: polyethylenimine. *Proc Natl Acad Sci U S A* 1995; **92:** 7297-301.

115. Pan X, Guan J, Yoo JW, Epstein AJ, Lee LJ, Lee RJ. Cationic lipid-coated magnetic nanoparticles associated with transferrin for gene delivery. *Int J Pharm* 2008; **358:** 263-70.

116. Xiang JJ, Nie XM, Tang JQ, Wang YJ, Li Z, Gan K, et al. In vitro gene transfection by magnetic iron oxide nanoparticles and magnetic field increases transfection efficiency. *Zhonghua Zhong Liu Za Zhi* 2004; **26:** 71-4.

117. Yang SY, Sun JS, Liu CH, Tsuang YH, Chen LT, Hong CY, et al. Ex vivo magnetofection with magnetic nanoparticles: a novel platform for nonviral tissue engineering. *Artif Organs* 2008; **32:** 195-204.

118. Ino K, Kawasumi T, Ito A, Honda H. Plasmid DNA transfection using magnetite cationic liposomes for construction of multilayered gene-engineered cell sheet. *Biotechnol Bioeng* 2008; **100:** 168-76.

119. Kamau Chapman SW, Hassa PO, Koch-Schneidemann S, von Rechenberg B, Hofmann-Amtenbrink M, Steitz B, et al. Application of pulsed-magnetic field enhances non-viral gene delivery in primary cells from different origins. *J Magn Magn Mater* 2008; **320:** 1517-27.

120. Chorny M, Polyak B, Alferiev IS, Walsh K, Friedman G, Levy RJ. Magnetically driven plasmid DNA delivery with biodegradable polymeric nanoparticles. *FASEB J* 2007; **21:** 2510-9.

121. Kamau SW, Hassa PO, Steitz B, Petri-Fink A, Hofmann H, Hofmann-Amtenbrink M, et al. Enhancement of the efficiency of non-viral gene delivery by application of pulsed magnetic field. *Nucleic Acids Res* 2006; **34:** e40.

122. McBain S, Griesenbach U, Xenariou S, Keramane A, Batich CD, Alton EWFW, et al. Magnetic nanoparticles as gene delivery agents: enhanced transfection in the presence of oscillating magnet arrays. *Nanotechnology* 2008; **19:** 1-5.

123. Maass G, Schweighoffer T, Berger M, Schmidt W, Herbst E, Zatloukal K, et al. Tumor vaccines: effects and fate of IL-2 transfected murine melanoma cells in vivo. *Int J Immunopharmacol* 1995; **17:** 65-73.

124. Schmidt W, Schweighoffer T, Herbst E, Maass G, Berger M, Schilcher F, et al. Cancer vaccines: the interleukin 2 dosage effect. *Proc Natl Acad Sci U S A* 1995; **92:** 4711-4.

125. Kircheis R, Küpcü Z, Wallner G, Wagner E. Cytokine gene-modified tumor cells for prophylactic and therapeutic vaccination: IL-2, IFN-gamma, or combination IL-2 + IFN-gamma. *Cytokines Cell Mol Ther* 1998; **4:** 95-103.

research article

Role of ^{18}F-choline PET/CT in evaluation of patients with prostate carcinoma

Marina Hodolic

Department for Nuclear Medicine, University Medical Centre Ljubljana, Slovenia

Correspondence to: Marina Hodolič, MD, PhD, Department for Nuclear Medicine, University Medical Centre Ljubljana, Zaloška 7, Slovenia; Phone:+386 1 522 3548; Fax:+386 1 522 22 37; E-mail: marina.hodolic@kclj.si

Background. Choline presents a high affinity for malignant prostate tissue. It can be labelled with positron emitting ^{18}F, and used for the evaluation of patients with prostate carcinoma by PET/CT imaging. The aim of this paper is to summarise our experience with fluoromethylcholine (^{18}F-choline) PET/CT in patients with prostate cancer.

Methods. In 4 months we investigated the patients with histopathological (or cytological) confirmed prostate cancer. Two observers evaluated the early and late ^{18}F-choline PET images in correlation with corresponding localising CT images and using the semiquantitative standard uptake value (SUV) calculation.

Results. The ^{18}F-choline PET/CT was made in 50 patients with prostate cancer. There were 18 patients after radical prostatectomy and 32 without surgery. In all patients without surgery the pathological uptake was seen in the prostate. In 14 (44 %) patients of this group there was evidence of metastatic spread in local or distant lymph nodes and/or bones. In out of 18 patients after radical prostatectomy the local recurrence was detected in 6 patients (33%) and distant metastases were present in 2 patients (10%).

Conclusions. ^{18}F-choline PET/CT seems to be useful imaging modality in patients with prostate carcinoma; it can demonstrate spread of the disease preoperatively and detect the local recurrence after radical prostatectomy.

Key words: prostate carcinoma; ^{18}F-choline PET/CT; diagnosis; staging; follow-up

Introduction

Prostate carcinoma is the most common life-threatening cancer affecting men in the Western world. The mortality is around 10%. The major goals of pretherapeutic imaging are to determine the local extent of prostate carcinoma in terms of intraprostate localisation, extracapsular extension, seminal vesicle invasion, tumour infiltration into neurovascular bundles, surrounding tissues and organs in the small pelvis, detection of loco-regional metastases via the lymph nodes and detection of distant metastases. The exact pretherapeutic diagnosis and staging are essential, because the tumour treatment must be selected in strict dependence on the clinical tumour stage and risk profile.[1,2]

Both anatomic and functional molecular imaging of prostate carcinoma is important especially when there are problems with diagnosis, for example when prostate punch biopsies are negative while the suspicion of prostate carcinoma persists

(for example rising PSA). They may also be helpful in localising the carcinoma, revealing how the carcinoma relates to the surrounding intra- and extraprostatic structures and organs.

[18]F-Fluorodeoxyglucose (FDG) PET/CT is a nuclear medicine procedure currently most widely used to diagnose primary and metastatic cancers.[3] Unfortunately, not all tumours show a significant increase of metabolic activity on ^{18}F-FDG PET/CT imaging. This is particularly true for neuroendocrine tumours, hepatic tumours and prostate cancer.[4]

Choline presents a high affinity for malignant prostate tissue, even if low grade. Choline can be labelled with either ^{11}C or ^{18}F, the former being the preference due to the lower urinary excretion and patients' exposure. The latter is more useful for a possible distribution to centres lacking in on-site cyclotron. The sensitivity of ^{18}F-choline PET/CT to detect prostate cancer preoperatively is 73%, greater than with ^{18}F-FDG PET/CT (31%). Also the accu-
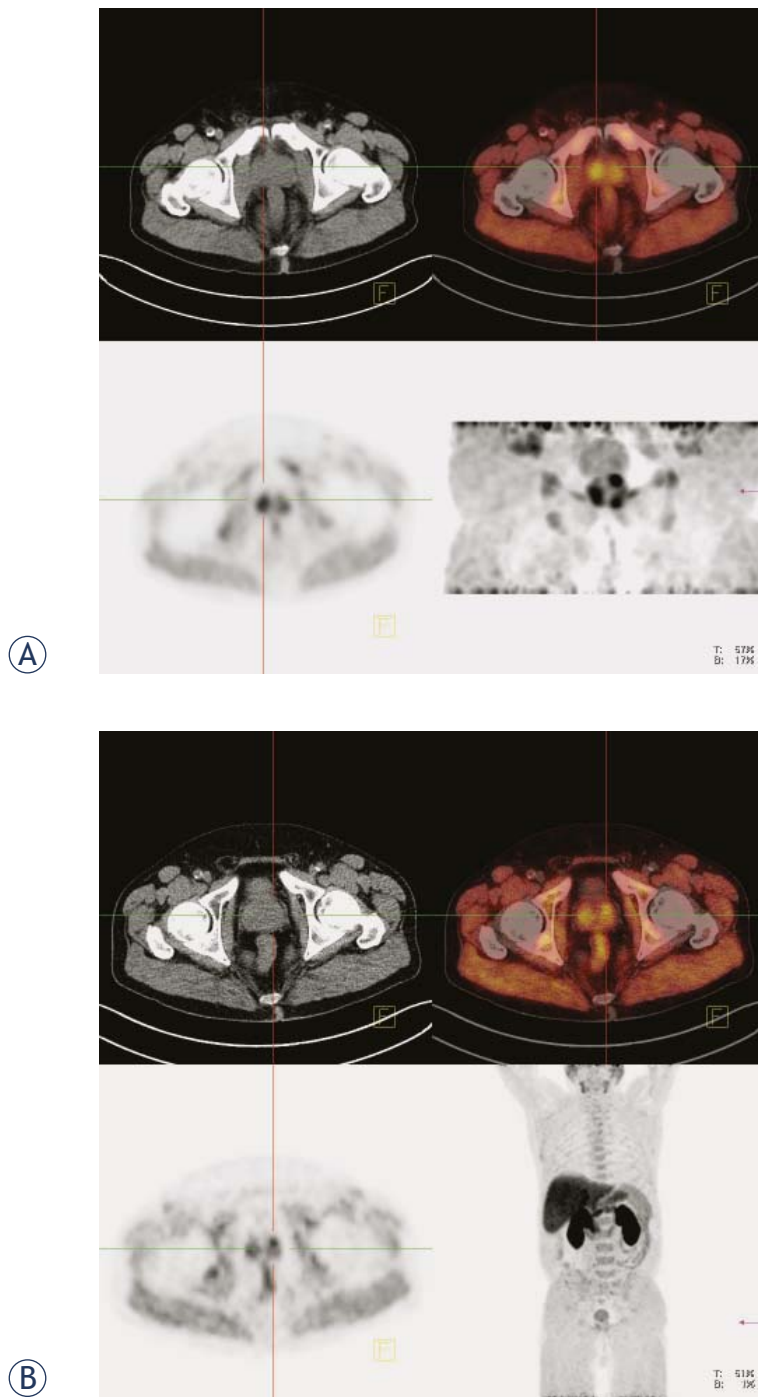
FIGURE 1. Prostate carcinoma: A prostatic bed (early images), B whole body (late images). Upper left panel: CT image. Upper right panel: fused PET/CT image. Lower left panel: PET image. Lower right panel: maximum intensity projection (MIP).

racy is greater with ^{18}F-choline PET/CT (67%) than using ^{18}F-FDG PET/CT (53%).[5] The use of ^{18}F-FDG in prostate cancer is limited to the most aggressive cancers.[6]

The aim of this paper is to summarise our experience with fluoromethylcholine (^{18}F-choline) and PET/CT in patients with prostate cancer.

Patients and methods

From 12.05.2010 to 15.09.2010 months we investigated the patients with cytological or histological confirmed prostate cancer.

The patients were fasting 6-10 hours prior the scan. ^{18}F-choline (IASOcholine® from IASON Austria) was injected *i.v.* (200 – 300 MBq, according to the weight of the patient) using the automatic radionuclide injector (Medrad). List mode acquisition over prostatic bed started immediately after the injection of the tracer and lasts for 5 minutes. After this early phase patients rested for approximately one hour. The whole body acquisition was performed thereafter, 2 min per bed position from base of the skull to midthigh (9 bed positions on average). Siemens Biograph mCT PET/CT scanner has been used.

Early images were reconstructed from the list mode acquisition study before the activity appeared in the bladder (Figure 1A). Early (0-5 min *p.i.*) images and late (60 min *p.i.*) whole body images were presented in the usual transaxial, coronal and sagital planes. Two observers evaluated the images in correlation with corresponding localising CT images and using semiquantitative standard uptake value (SUV) calculation.

Results

The ^{18}F-choline PET-CT was performed in 50 patients with prostate cancer. The mean age was 67.7 years. There were 32 patients before radical prostatectomy and 18 after surgery (Table 1.).

The early phase has been used to evaluate prostate or prostate bed. The findings corresponded to late phase images in all patients (Figures 1 A, B). In patients with bony metastases in the pelvis the pathological uptake was seen in metastases already during the first 5 min after the tracer injection (Figures 2 A, B).

In all patients without surgery the pathological uptake was seen in the prostate. In 14 (44 %) patients of this group there was evidence of metastatic spread in local or distant lymph nodes (Figure 3) and/or bones (Figure 2 B). In patients after radical prostatectomy the local recurrence was detected in 6 patients (Figure 4) (33%) and distant metastases

TABLE 1. Results of ^{18}F-choline PET/CT scans in 50 patients with prostate carcinoma

	Number of patients	Prostatic bed (positive)	Metastases (positive)
After radical prostatectomy	18	6 (33 %)	2 (10%)
No surgery	32	32 (100%)	14 (44%)
Total	50	38 (96%)	16 (33%)

were present in 2 patients one had also the local recurrence; the other one has no evidence of local recurrent disease (Table 1).

Discussion

Indications for ^{18}F-choline PET/CT imaging modality in evaluation of patients with prostate cancer cover a wide spectrum of clinical settings: localisation of intraprostatic neoplastic lesions, initial staging, detection of occult recurrences and characterisation of images on conventional imaging modalities, which are questionable or difficult to interpret. ^{18}F-choline is taken up by prostatic carcinoma as well as distant metastases very fast, already during 5 min after the injection (Figure 2).

The accurate knowledge of the normal biodistribution of ^{18}F-choline is essential for the correct interpretation of PET/CT images. CT enables the differentiation of physiological bowel activity and ^{18}F-choline excretion in the ureters. ^{18}F-choline uptake in benign pathological conditions mainly includes sites of inflammation; nevertheless, the accumulation in tumour deposits not due to prostate cancer cannot be excluded.[7]

Similarly to FDG, choline is also taken up by infection.[8] The differentiation between inflamed and metastatic lymph nodes can be achieved either by two phases PET or by appropriate antimicrobial treatment preceding ^{18}F-choline PET/CT. On dual-phase PET of the prostate, areas of malignancy consistently demonstrated the stable or increasing ^{18}F-choline uptake, whereas most areas containing benign tissue demonstrated the decreasing uptake.

Delayed or dual-phase imaging after the injection of ^{18}F-choline may improve the performance of ^{18}F-choline PET for localising malignant areas of the prostate.[9] ^{18}F-choline PET/CT showed a fast progressively increasing max. SUV in biopsy confirmed cancer lesions up to 14 min post injection while decreasing in inguinal lymph nodes interpreted as benign. Furthermore, it was very useful in differentiating local recurrences from confounding blood pool and urinary activity.[10] Although more data need to be obtained, it appears that ^{18}F-choline
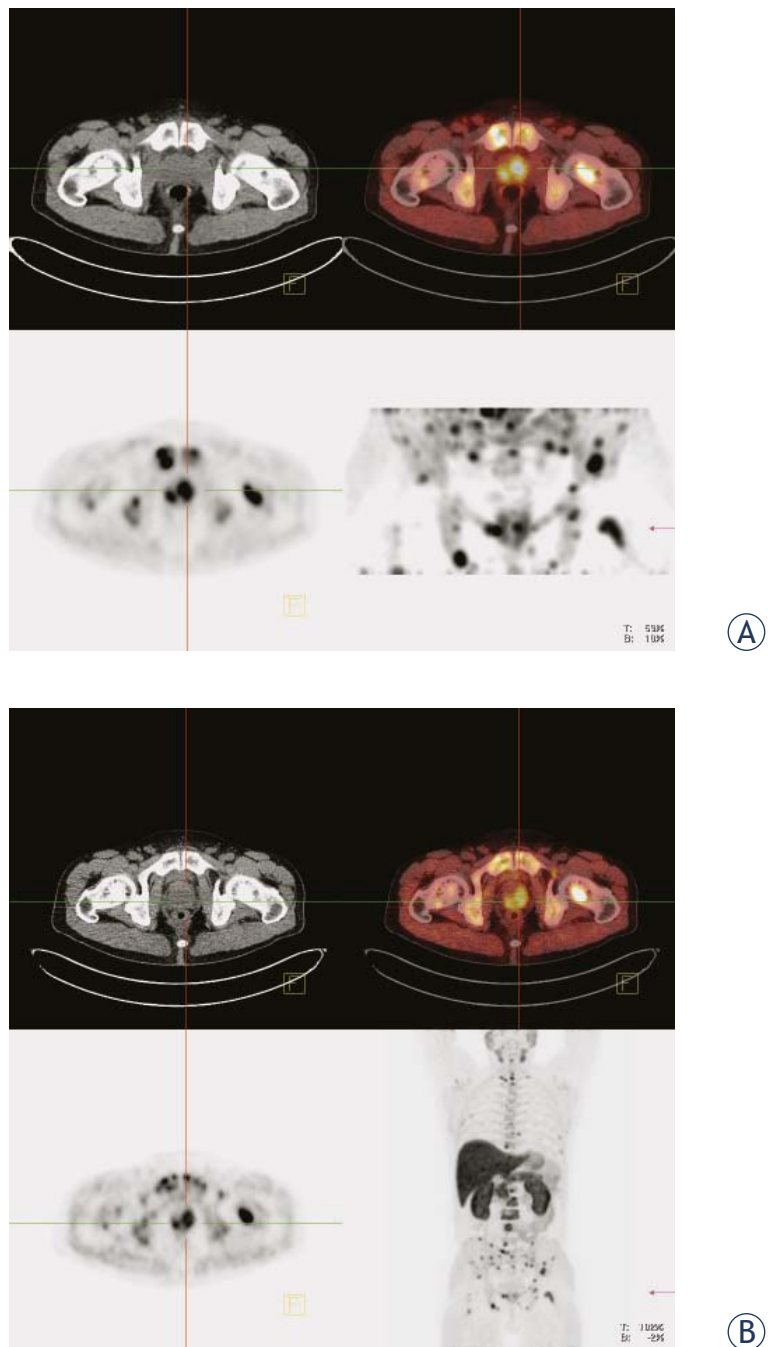
FIGURE 2. Bone metastases due to prostate cancer: A prostatic bed (early images), B whole body (late images). Upper left panel: CT image. Upper right panel: fused PET/CT image. Lower left panel: PET image. Lower right panel: maximum intensity projection (MIP).

FIGURE 3. Lymph node metastases due to prostate cancer: whole body scan (late images). Upper left panel: CT image. Upper right panel: fused PET/CT image. Lower left panel: PET image. Lower right panel: maximum intensity projection (MIP).

FIGURE 4. Relapse of prostate cancer: whole body (late images). Upper left panel: CT image. Upper right panel: fused PET/CT image. Lower left panel: PET image. Lower right panel: maximum intensity projection (MIP).
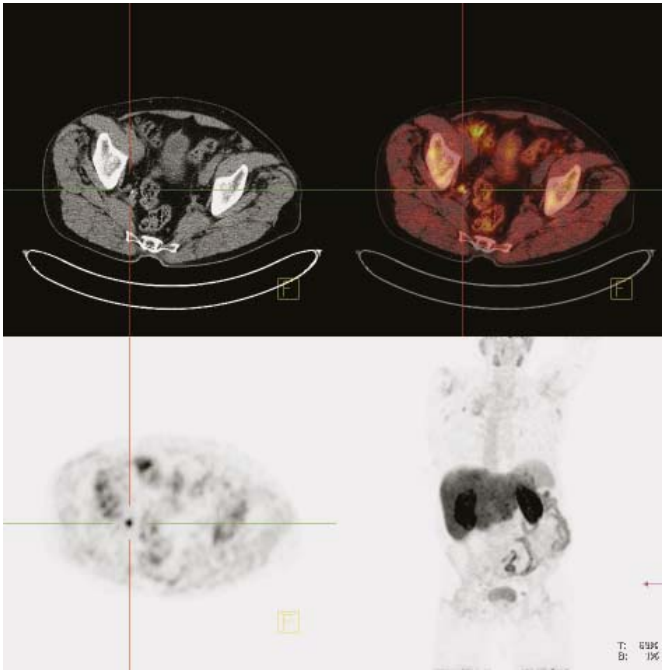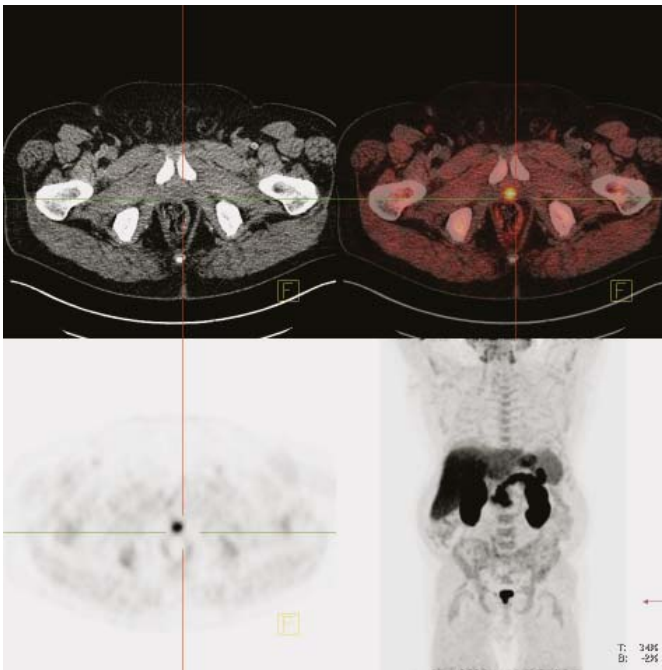
PET/CT is highly efficient in preoperative management regarding N and M staging of prostate cancer once metastatic disease is strongly suspected or documented.[11] ^{18}F-choline PET/CT could be useful in the evaluation of patients with prostate cancer who are at high risk for extracapsular disease, and it could be used to preoperatively exclude distant metastases.[12]

Patients with persistent elevated PSA and repeated negative prostate biopsy, (*i.e.* prostate being biopsied at multiple times), were investigated with ^{18}F-choline PET/CT to delineate prostate cancer and guide renewed prostate biopsy. In 25% of patients, ^{18}F-choline PET/CT allowed the identification of neoplastic prostatic zones.[13]

The sensitivity, specificity and accuracy of ^{18}F-choline PET/CT in the detection of bone metastases in prostate cancer are 74%, 99% and 85%, respectively. ^{18}F-choline PET-CT may be superior to bone scintigraphy for the early detection of metastatic bone disease due to the detection of bone marrow metastases.[13]

Out of all patients with carcinoma of the prostate undergoing therapeutic regimes with curative intent, 15-23% will ultimately relapse and 16-35% will need some sort of salvage therapy within 5 years. Of relapsing patients, 50% will have local recurrence and 50% systemic disease with or without local recurrence. Therefore, the localisation of recurrent prostate cancer is critical for selecting a local or systemic therapeutic strategy.[15] Modern fusion imaging with ^{18}F-choline PET/CT has augmented the diagnostic imaging spectrum for the assessment of relapsing prostate cancer. In 60-70% of patients with biochemical relapse, recurrent tumour can be detected and anatomically precisely localised. Imaging with ^{18}F-choline PET/CT and MRI possesses a high potential for the early localisation of recurrent prostate carcinoma.[16]

In patients with biochemical relapse after the radical treatment for prostate cancer, ^{18}F-choline PET/CT represents a single step, whole-body, non-invasive study that allows disease detection and localisation. Detection sensitivity is probably negatively correlated with serum PSA concentration. Pelosi *et al.* reported that ^{18}F-choline PET scan detected the disease relapse in 42.9% of cases (24/56). PET sensitivity was 20% in the PSA ≤ 1 ng/ml subgroup, 44% in PSA > 1 and ≤ 5, and 81.8% in PSA > 5 ng/ml subgroup, respectively.[17] According to other investigators ^{18}F-choline PET/CT is not likely to have a significant impact on the care of prostate cancer patients with biochemical recurrence until PSA increases to above 4 ng/ml. However,

in selected patients, ^{18}F-choline PET/CT helps to exclude distant metastases when the salvage local treatment is intended.[18] Most probably doubling time of serum PSA increase is more important as PSA level itself.

[18]F-choline PET/CT seems to be useful also for the evaluation of other cancers with poor FDG uptake, such as hepatocellular carcinoma.[19]

Conclusions

In future studies some of dilemmas that appear in presented study need to be solved: to correlate PET/CT results with standard prognostic factors and to determine their prognostic significance (correlation of our PET/CT results with starting PSA, clinical T stage, Gleason score in surgically treated/biopsied patients and PSA doubling time in patients with biochemical recurrence).

[18]F-choline PET/CT seems to be useful imaging modality in patients with prostate carcinoma for demonstrating the spread of the disease preoperatively and to detect local recurrent disease after radical prostatectomy.

References

1. Reske SN. Nuclear imaging of prostate cancer: current status. *Urologe A* 2007; **46:** 1485-99.

2. Kragelj B. Increased late urinary toxicity with whole pelvic radiotherapy after prostatectomy. *Radiol Oncol* 2009; **43:** 88-96.

3. Avazpour I, Roslan RE, Bayat P, Saripan MI, Nordin AJ, Abdullah RSAR. Segmenting CT images of bronchogenic carcinoma with bone metastases using PET intensity markers approach. *Radiol Oncol* 2009; **43:** 180-6.

4. Naji M, Hodolic M, El-Refai S, Khan S, Marzola MC, Rubello D, et al. Endocrine tumors: the evolving role of positron emission tomography in diagnosis and management. *J Endocrinol Invest* 2010; **33:** 54-60.

5. Watanabe H, Kanematsu M, Kondo H, Kako N, Yamamoto N, Yamada T, et al. Preoperative detection of prostate cancer: a comparison with 11C-choline PET, 18F-fluorodeoxyglucose PET and MR imaging. *J Magn Reson Imaging* 2010; **31:** 1151-6.

6. Talbot JN, Gutman F, Huchet V, Kerrou K, Balogova S, Kerrouche N, et al. [Clinical usefulness of positron emission tomography in prostate cancer]. [French]. *Presse Med* 2007; **36:** 1794-806.

7. Schillaci O, Calabria F, Tavolozza M, Ciccio C, Carlani M, Caracciolo CR, et al. 18F-choline PET/CT physiological distribution and pitfalls in image interpretation: experience in 80 patients with prostate cancer. *Nucl Med Commun* 2010; **31:** 39-4.

8. Le C, van de Weijer EP, Pos FJ, Vogel W. Active inflammation in 18F-methylcholine PET/CT. *Eur J Nucl Med Mol Imaging* 2010; **37:** 654-5.

9. Kwee SA, Wei H, Sesterhenn I, Yun D, Coel MN. Localization of primary prostate cancer with dual-phase 18F-fluorocholine PET. *J Nucl Med* 2006; **47:** 262-9.

10. Steiner Ch, Vees H, Zaidi H, Wissmeyer M, Berrebi O, Kossovsky MP, et al. Three-phase 18F-fluorocholine PET/CT in the evaluation of prostate cancer recurrence. *Nuklearmedizin* 2009; **48:** 1-9.

11. Langsteger W, Heinisch M, Fogelman I. The role of fluorodeoxyglucose, 18F-dihydroxyphenylalanine, 18F-choline, and 18F-fluoride in bone imaging with emphasis on prostate and breast. *Semin Nucl Med* 2006; **36:** 73-92.

12. Beheshti M, Imamovic L, Broinger G, Vali R, Waldenberger P, Stoiber F, et al. 18F choline PET/CT in the preoperative staging of prostate cancer in patients with intermediate or high risk of extracapsular disease: a prospective study of 130 patients. *Radiology* 2010; **254:** 925-33.

13. Igerc I, Kohlfurst S, Gallowitsch HJ, Matschnig S, Kresnik E, Gomez-Segovia I, et al. The value of 18F-choline PET/CT in patients with elevated PSA-level and negative prostate needle biopsy for localisation of prostate cancer. *Eur J Nucl Med Mol Imaging* 2008; **35:** 976-83.

14. Beheshti M, Vali R, Waldenberger P, Fitz F, Nader M, Loidl W, et al. Detection of bone metastases in patients with prostate cancer by 18F fluorocholine and 18F fluoride PET-CT: a comparative study. *Eur J Nucl Med Mol Imaging* 2008; **35:** 1766-74.

15. Horvat AG, Kovac V, Strojan P. Radiotherapy in palliative treatment of painful bone metastases. *Radiol Oncol* 2009; **43:** 213-24.

16. Reske SN; Blumstein NM; Glatting G. PET and PET/CT in relapsing prostate carcinoma. *Urologe A* 2006; **45:** 1240-50.

17. Pelosi E, Arena V, Skanjeti A, Pirro V, Douroukas A, Pupi A, et al. Role of whole-body 18F-choline PET/CT in disease detection in patients with biochemical relapse after radical treatment for prostate cancer. *Radiol Med* 2008; **113:** 895-904.

18. Cimitan M, Bortolus R, Morassut S, Canzonieri V, Garbeglio A, Baresic T, et al. [18F]fluorocholine PET/CT imaging for the detection of recurrent prostate cancer at PSA relapse: experience in 100 consecutive patients. *Eur J Nucl Med Mol Imaging* 2006; **33:** 1387-98.

19. Yamamoto Y, Nishiyama Y, Kameyama R, Okano K, Kashiwagi H, Deguchi A, et al. Detection of hepatocellular carcinoma using 11C-choline PET: comparison with 18F-FDG PET. *J Nucl Med* 2008; **49:** 1245-8.

case report

Pelvic hemangiopericytoma: the role of diffusion weighted imaging in targeting the biopsy site and in monitoring the tumour response to radiotherapy

Evangelos Perdikakis[1], Eelco de Bree[2], Elpida Giannikaki[3], Evangelia G. Chryssou[1], Christine Valatsou[1], Apostolos Karantanas[1]

[1] Department of Radiology, University of Crete, Stavrakia, Heraklion, Crete, Greece

[2] Department of Oncological Surgery, University of Crete, Stavrakia, Heraklion, Crete, Greece

[3] Crete University, Department of Pathology, Stavrakia, Heraklion, Crete, Greece

Background. Despite advances in imaging, the accurate characterization of soft tissue tumours remains a challenging task. Furthermore, the interpretation of post treatment changes and evaluation of tumour response to therapy is another complicating issue regarding soft tissue tumour imaging.

Case report. Herein, a patient with a pelvic hemangiopericytoma, by whom different diagnostic imaging methods were used, is presented.

Conclusions. Diffusion weighted imaging (DWI) might provid useful information in guiding biopsy and enabled monitoring of the radiation therapy results.

Key words: CT, MR imaging, diffusion weighted imaging; biopsy; hemangiopericytoma; pelvis; radiotherapy

Introduction

Soft-tissue tumours often require a combined therapeutical approach including surgical resection, chemotherapy and radiation therapy.[1] In selected inoperable cases, the radiation therapy and chemotherapy may be the only treatment options.[2] Although MR imaging is considered the modality of choice for the diagnosis and the follow-up of the applied therapeutic scheme, diagnostic dilemmas may rise both for the clinician and the radiologist.

The accurate assessment of a positive or negative tumour response to radiation or to chemotherapy plays an important role in the appropriate patient management.[3] Distinguishing between the normal and anticipated therapeutic results from tumour recurrence is another difficult issue in post treatment imaging.[3] The application of diffusion weighted imaging (DWI) in oncological imaging has gained enough attention and enthusiasm during the past

decade with increasing efforts of its extracerebral applications.[4,5] DWI might help in the differentiation of various benign and malignant alterations.[5,6] The basic principle and the main advantage of this rather new method is the ability to study the water movement at a cellular level.[4] Impendance in the random water motion is expressed as the diffusion restriction and the qualitative and the quantitative analysis is now feasible due to technological improvements and newer MR techniques.

We describe the radiologic findings of a pelvic hemangiopericytoma that was treated solely with the radiation therapy. Hemangiopericytoma is a rare soft tissue tumour that usually breaks out during adulthood.[7] It is considered a malignant tumour of vascular origin that commonly requires a combined therapeutical scheme.[7] In the present case report the emphasis is given on the application of DWI both prior to the diagnosis as well as in the imaging follow-up.

Case report

A 58-year-old female patient presented to the surgical oncology department with a 6-month history of abdominal discomfort, constipation and pain in her back irradiating to the right femoral and inguinal area. An increased frequency of micturition initiated at the same time period, was also reported. The laboratory examinations were within normal limits indicating only a minor sideropenic anaemia and hyperlipidemia. The physical examination of the abdomen was negative but the digital vaginal examination showed the presence of a palpable mass in the right pelvic wall. A subsequent US examination, performed elsewhere (not available), verified the presence of the lesion and characterized it as highly suspicious for malignancy.

A following multidetector computed tomography (MDCT) examination demonstrated that the lesion was located in the right ischiorectal *fossa*, invaded the obturator muscles and the right ischiopubic *ramus* and extended in the femoral anatomical compartment displacing anteriorly the right pectineus muscle (Figure 1A). The tumour was isodense to skeletal muscles in the non contrast series and showed intense enhancement in the arterial and delayed phase.

The patient was referred for additional MR imaging evaluation. MR imaging showed the tumour to exhibit low signal intensity on T1-w and high but heterogeneous signal intensity on T2-w images (Figures 1B-D). Intense and heterogenous enhancement was shown following the gadolinium injection (Figures 2A-B). The application of DWI showed areas of increased signal intensity that were indicative of a high cellular tumour (Figures 2C-D).

The patient underwent a CT-guided biopsy targeted in the intratumoural areas that corresponded to areas of the maximum diffusion restriction and the diagnosis of hemangiopericytoma was established (Figure 3). Findings, consistent with malignant biological behaviour, such as necrosis, cellular *atypia* and high mitosis count, were absent. MDCT examinations of the chest and abdomen were negative for metastatic disease.

Due to the local extent and infiltration the tumour was considered unresectable. The radical excision of the tumour should have led to hemipelvectomy, which was not justified in absence of apparent malignant features. In a multi-disciplinary meeting the initial treatment with radiotherapy was suggested. Radiotherapy consisted of 50.4 Gy (28 x 1.8 Gy, 3 fields) external beam radiation
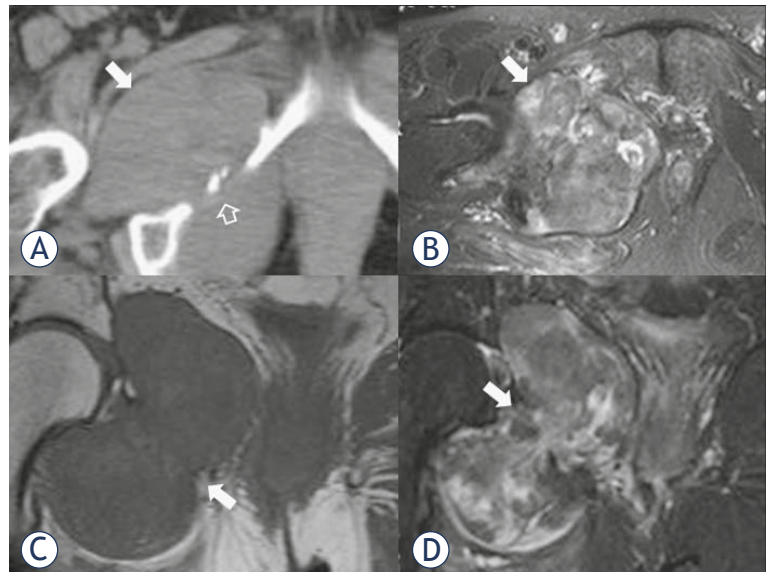
FIGURE 1. The axial (A) noncontrast multidetector computed tomography (MDCT) image shows a large isodense mass occupying the right ischiorectal fossa and extending in the femoral anatomic compartment posteriorly to the pectineus muscle (solid arrow in A). Note invasion and destruction of ischiopubic ramus (open arrow in A). The axial (B) fat suppressed T2-w MR image demonstrates a heterogeneous, with predominantly high signal intensity mass (arrow in B). The coronal (C) T1-w and the coronal (D) short tau inversion recovery (STIR) images demonstrate a large bicompartmental mass (with pelvic and femoral component) that shows an "hour-glass" configuration (arrows in C, D).
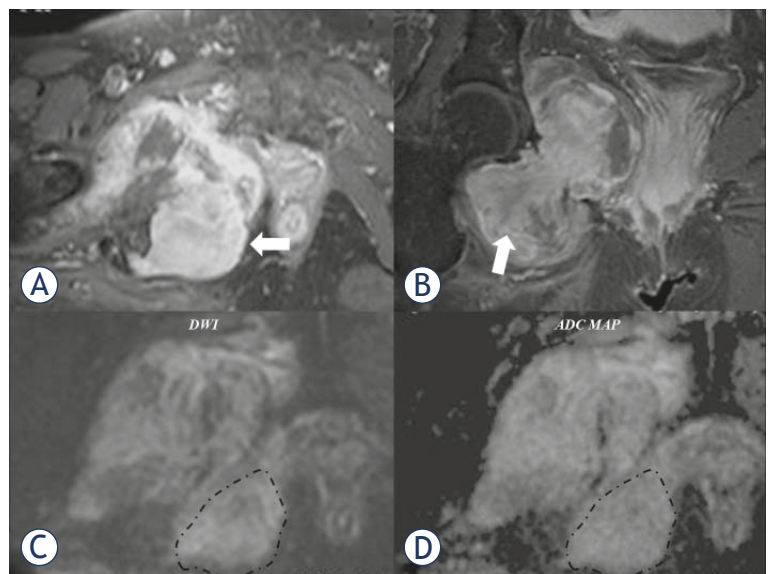
FIGURE 2. The axial (A) and coronal (B) contrast enhanced fat suppressed T1-w MR images show intense enhancement of the lesion (arrows). The diffusion weighted imaging (DWI) (C) and the corresponding apparent diffusion coefficient (ADC) map (D) demonstrate signs of increased restriction in diffusion, a finding in keeping with the high cellular nature of the tumour. Area in dashed line corresponds to the biopsy selected site.

FIGURE 3. (A) CT guided biopsy of the lesion with an 18G true cut needle. (B) Power view (H&E stain, X100) of the biopsy, showing a mesenchymal tumour with a hemangiopericytoma-like pattern, composed of spindle cells arranged in short bundles and the characteristic vascular pattern with a partial "staghorn" configuration. (C) High power view of the spindle cell areas (H&A, X400). The spindle cells show no atypia, mitosis or necrosis.

FIGURE 4. Assessment of the tumour response 6 months (upper series) and 12 months (lower series), following radiother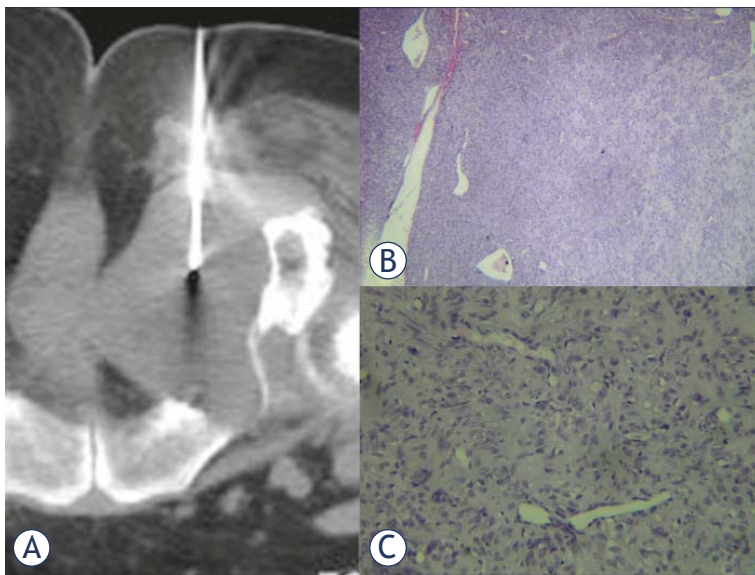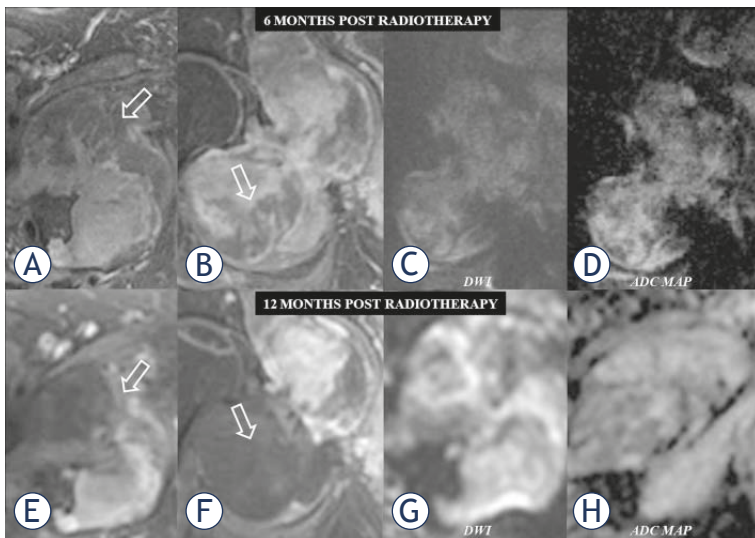apy. Fat suppressed post gadolinium T1-w MR images in the axial (A, E) and coronal plane (B, F), diffusion weighted imaging (DWI) in the coronal (C) and axial (G) plane and the corresponding apparent diffusion coefficient (ADC) maps (D, H). Note consecutive toumoral necrosis (no enhancement), which is more pronounced in the femoral compartment of the mass (open arrows). The increased signal in the femoral part of the lesion (C, G) as well as in the ADC map (D, H), represents tumour liquefaction and thus an evidence of positive response to radiotherapy. For comparison purposes the chosen DWI performed 6 and 12 months following treatment, are of the same *b* values.

with weekly intravenous administration of 20 mg Caeylix and 20 mg Cisplatin as radiation sensitizers. Unfortunately, radiotherapy was applied as a palliative radiation and not as the primary treatment, because the patient did not give her full consent in fear of the possible radiation injuries and complications. Four weeks after finishing radiotherapy the patient revisited the surgical department, with new imaging studies. The MDCT examination of the chest and abdomen was again negative for metastatic disease, while the MR imaging showed a small reduction in tumour size. Gradually, there was a complete relief of symptoms. The radiotherapist considered that there was no indication to persuade the patient to complete radiotherapy to the full therapeutic dose especially after such a long period without the treatment and preferred the remaining dose to be administered in case of the tumour growth.

Six months following treatment the patient was scheduled for a follow-up MR imaging, which verified a decrease in the lesion's enhancement characteristics post gadolinium. Intratumoural areas that did not enhance were considered to be a positive response to therapy (Figures 4A-D). Furthermore, DWI showed a slight increase in the intralesional signal intensity of the femoral component of the mass with a concomitant signal increase in the apparent diffusion coefficient (ADC) map. This finding was considered an indication of the reduction in the restriction of water molecules and correlated with the nonenhancing areas (Figures 4A-D). In other words, the mass seemed to begin to become less cellular and liquefied as a result of the radiation therapy.

The effectiveness of the therapy was further assessed and established on a follow-up MR imaging study twelve months post radiotherapy. Despite no change in the outer shape and contour of the tumour, more than 60% of its volume showed no evidence of the enhancement and at the same time DWI showed further indications of the unimpaired diffusion as a result of possible tumour necrosis and liquefaction (Figures 4E-H). One year after radiotherapy the MDCT examination of chest and abdomen remained also negative for eventual metastatic disease and the patient was free of symptoms.

Discussion

Hemangiopericytomas are rare soft tissue tumours that usually occur in adulthood during the 4th and 5th decade.[7] Various locations of the tumour

have been reported with an increased prevalence in the lower extremities and retroperitoneum.[7,8] Histopathologically the tumour arises from the Zimmerman pericytes around either capillaries and/or postcapillary venules and thus on the microscopic examination the characteristic finding is the identification of capillary channels surrounded by spindle-shaped cells.[8,9] Clinically, a usually painless mass located in the deep soft tissues may present with mass effect on adjacent organs and structures.[7-9] The surgical resection is the treatment of choice but the tumour tends to recur even after the total macroscopic resection. Local invasion or relapsing tumours may preclude the surgical treatment. Distant metastases occur in the lungs or bones and are observed in high-grade, poorly differentiated or undifferentiated tumours (grade III-IV).[10] In inoperable cases or as an adjuvant treatment, radiation therapy can be applied.[11]

In our case a bicompartmental tumour was identified (pelvic and femoral location) that initially presented due to the local mass effect and pressure on adjacent anatomical structures. The correct tumour characterization was feasible by means of CT-guided biopsy and the targeting of the biopsy site was done by using the information from the DWI sequences.

The physical basis of diffusion-weighted imaging relies on the random motion of the water molecules (Brownian motion) that was first described by Einstein in 1905.[12] The restriction of this random movement of water molecules that is present within biologic tissues (due to impendance caused by cell membranes and intracellular organelles) as well as differences between intra-extracellular spaces is the basis of DWI.[13-14] As a consequence, increased tissue cellularity that is present in highly cellular neoplasms may impede the free movement of water molecules and may reflect as the increased restriction in DWI images. On the contrary, the restoration of a less tight cellular environment (post therapy) may be imaged as an increase in the molecular diffusion.[15-17]

A quantitative analysis can be achieved with the acquisition of ADC maps from diffusion images obtained at different b values. Consequently, we used DWI in two modes. Firstly, the selection of the target site for biopsy was based on the area that demonstrated the maximal restriction in diffusion. This was chosen by correlating DWI and ADC maps. The interpretation of diffusion weighted images allows the detection of focal solid and cystic lesions.[15-17] The more cellular areas can provide better diagnostic results following CT-guided biopsies obviating thus the need for repeating an interventional procedure. This application may be of extreme value in cases of soft tissue tumours that contain areas of intratumoural necrosis. A biopsy targeted at the necrotic area would turn out to be non diagnostic and repetition would be needed, increasing thus the cost and possible complications.

Secondly, the tumour's response to radiotherapy was also assessed with DWI. We correlated the post gadolinium MR images with DWI and ADC images, both before and after the treatment. This correlation showed that non enhancing areas demonstrated the diffusion restoration on a one-year follow-up studies, a finding that was considered a positive response to the treatment. The observation of tumour necrosis, which is thought to be representative of a positive therapeutic response, is of paramount clinical importance. Hamstra *et al.* and Dudeck *et al.* have recently studied this novel application of DWI in oncology and initial results are considered encouraging in evaluating the anticancer treatment.[15,17] This role of DWI in monitoring the tumour response to radiotherapy or chemotherapy might be of extreme value in the future. Patients with contrast media allergy and inability to be studied with gadolinium infusion could have an adjuvant MR tool for the assessment of the therapeutic scheme.

In conclusion, our case suggests that DWI may be used for targeting the appropriate biopsy site and for the assessment of the radiation treatment. However, a larger series of patients is needed to confirm this application and establish a feasible and reproducible diffusion weighted MR imaging protocol for the follow-up of the oncological patient.

References

1. Espat NJ, Lewis JJ, Leung D, Woodruff JM, Antonescu CR, Shia J, et al. Conventional hemangiopericytoma. *Cancer* 2002; **95:** 1746-51.

2. Szklaruk J, Tamm EP, Choi H, Varavithya V. MR imaging of common and uncommon large pelvic masses. *RadioGraphics* 2003; **23:** 403-24.

3. Garner HW, Kransdorf MJ, Bancroft LW, Peterson JJ, Berquist TH, Murphey MD. Benign and malignant soft-tissue tumors: posttreatment MR imaging. *RadioGraphics* 2009; **29:** 119-34.

4. Qayyum A. Diffusion-weighted imaging in the abdomen and pelvis: concepts and applications. *RadioGraphics* 2003; **29:** 1797-810.

5. Inan N, Kilinc F, Sarisoy T, Gumustas S, Akansel G, Demirci A. Diffusion weighted MR imaging in the differential diagnosis of haemangiomas and metastases of the liver. *Radiol Oncol* 2010; **44:** 24-9.

6. Oztekin O, Calli C, Kitis O, Adibelli ZH, Eren CS, Apaydin M, et al. Reliability of diffusion weighted MR imaging in differentiating degenerative and infectious end plate changes. *Radiol Oncol* 2010; **44:** 97-102.

7. Dufour H, Métellus P, Fuentes S, Murracciole X, Régis J, Figarella-Branger D, et al. Meningeal hemangiopericytoma: a retrospective study of 21 patients with special review of postoperative external radiotherapy. *Neurosurgery* 2001; **48:** 756-63.

8. Kehagias D, Gouliamos A, Vlahos L. MR appearance of pelvic hemangiopericytoma. *Eur Radiol* 1999; **9:** 163-5.

9. Kothari PS, Murphy M, Howells GL, Williams DM. Hemangiopericytoma: a report of two cases arising on the lip. *Br J Oral Maxillofac Surg* 1996; **34:** 454-6.

10. Goldman SM, Davidson AJ, Neal J. Retroperitoneal and pelvic hemangiopericytomas: clinical, radiologic, and pathologic correlation. *Radiology* 1998; **168:** 13-7.

11. Bastin KT, Mehta MP. Meningeal hemangiopericytoma: defining the role for radiation therapy. *J Neurooncol* 1992; **14:** 277-87.

12. Hagmann P, Jonasson L, Maeder P, Thiran JP, Wedeen VJ, Meuli R. Understanding diffusion MR imaging techniques: from scalar diffusion-weighted imaging to diffusion tensor imaging and beyond. *RadioGraphics* 2006; **26:** S205-23.

13. Thoeny HC, De Keyzer F. Extracranial applications of diffusion-weighted magnetic resonance imaging. *Eur Radiol* 2007; **17:** 1385-93.

14. Bammer R. Basic principles of diffusion-weighted imaging. *Eur J Radiol* 2003; **45:** 169-84.

15. Hamstra DA, Rehemtulla A, Ross BD. Diffusion magnetic resonance imaging: a biomarker for treatment response in oncology. *J Clin Oncol* 2007; **25:** 4104-9.

16. deSouza NM, Reinsberg SA, Scurr ED, Brewster JM, Payne GS. Magnetic resonance imaging in prostate cancer: the value of apparent diffusion coefficients for identifying malignant nodules. *Br J Radiol* 2007; **80:** 90-5.

17. Dudeck O, Zeile M, Pink D, Pech M, Tunn PU, Reichardt P, et al. Diffusion weighted magnetic resonance imaging allows monitoring of anticancer treatment effects in patients with soft-tissue sarcomas. *J Magn Reson Imaging* 2008; **27:** 1109-13.

case report

(Mis)placed central venous catheter in the left superior intercostal vein

Ranka Stern Padovan[1], Maja Hrabak Paar[1], Igor Aurer[2]

[1] Department of Diagnostic and Interventional Radiology, University Hospital Center Zagreb, University of Zagreb, School of Medicine, Zagreb, Croatia

[2] Department of Internal Medicine, Division of Hematology, University Hospital Center Zagreb, University of Zagreb, School of Medicine, Zagreb, Croatia

Correspondence to: Dr. Maja Hrabak Paar, Department of Diagnostic and Interventional Radiology, University Hospital Center Zagreb, University of Zagreb, School of Medicine, Kispaticeva 12, HR-10000 Zagreb, Croatia. Phone: +38512388455; Fax: +38512388250; E-mail: majahrabak@gmail.com

Background. Chest X-ray is routinely performed to check the position of the central venous catheter (CVC) inserted through the internal jugular or subclavian vein, while the further evaluation of CVC malfunction is usually performed by contrast venography. In patients with superior vena cava obstruction, the tip of the catheter is often seen in collateral mediastinal venous pathways, rather than in the superior vena cava. In such cases detailed knowledge of thoracic vessel anatomy is necessary to identify the exact location of the catheter.

Case report. We report a case of 32-year-old female patient with relapsing mediastinal lymphoma and previous superior vena cava obstruction with collateral azygos-hemiazygos venous pathways. The patient had CVC inserted through the left subclavian vein and its position was detected by CT to be in the dilated left superior intercostal vein and accessory hemiazygos vein. Considering that dilated accessory hemiazygos vein can tolerate infusion, the CVC was left in place and the patient had no complaints related to CVC (mal)position. Furthermore, we present anatomical and radiological observations on the azygos-hemiazygos venous system with the special emphasis on the left superior intercostal vein.

Conclusions. Non-contrast CT scans can be a valuable imaging tool in the detection of the CVC position, especially in patients with renal insufficiency and contrast media hypersensitivity.

Key words: central venous catheterization; helical computed tomography; lymphoma, non-Hodgkin

Introduction

Chest X-ray is routinely performed to ascertain the position of the central venous catheter (CVC). The catheter should be placed in a large-calibre vein with a sufficient flow to tolerate infusion which is usually the subclavian vein, brachiocephalic vein or superior vena cava.[1] If further investigation of CVC position or malfunction is needed, contrast venography is usually performed, with intravenous contrast media administration under the fluoroscopic control using the digital subtraction angiography technique nowadays.[2] It is performed also in different vein pathologies.[3]

Radiographic and venographic features of CVC malposition in the left superior intercostal vein were previously described.[4-6] We report a case of a patient in whom CVC position was correctly detected to be in the left superior intercostal vein using non-contrast computed tomography (CT). Thus, the correct interpretation of CVC position obviated contrast venography.

Case report

A 32-year-old woman presented to our hospital with relapsing bulky mediastinal non-Hodgkin lymphoma and previous superior vena cava obstruction. A single-lumen CVC was uneventfully inserted through the left subclavian vein without imaging guidance. Aspirated blood was venous.
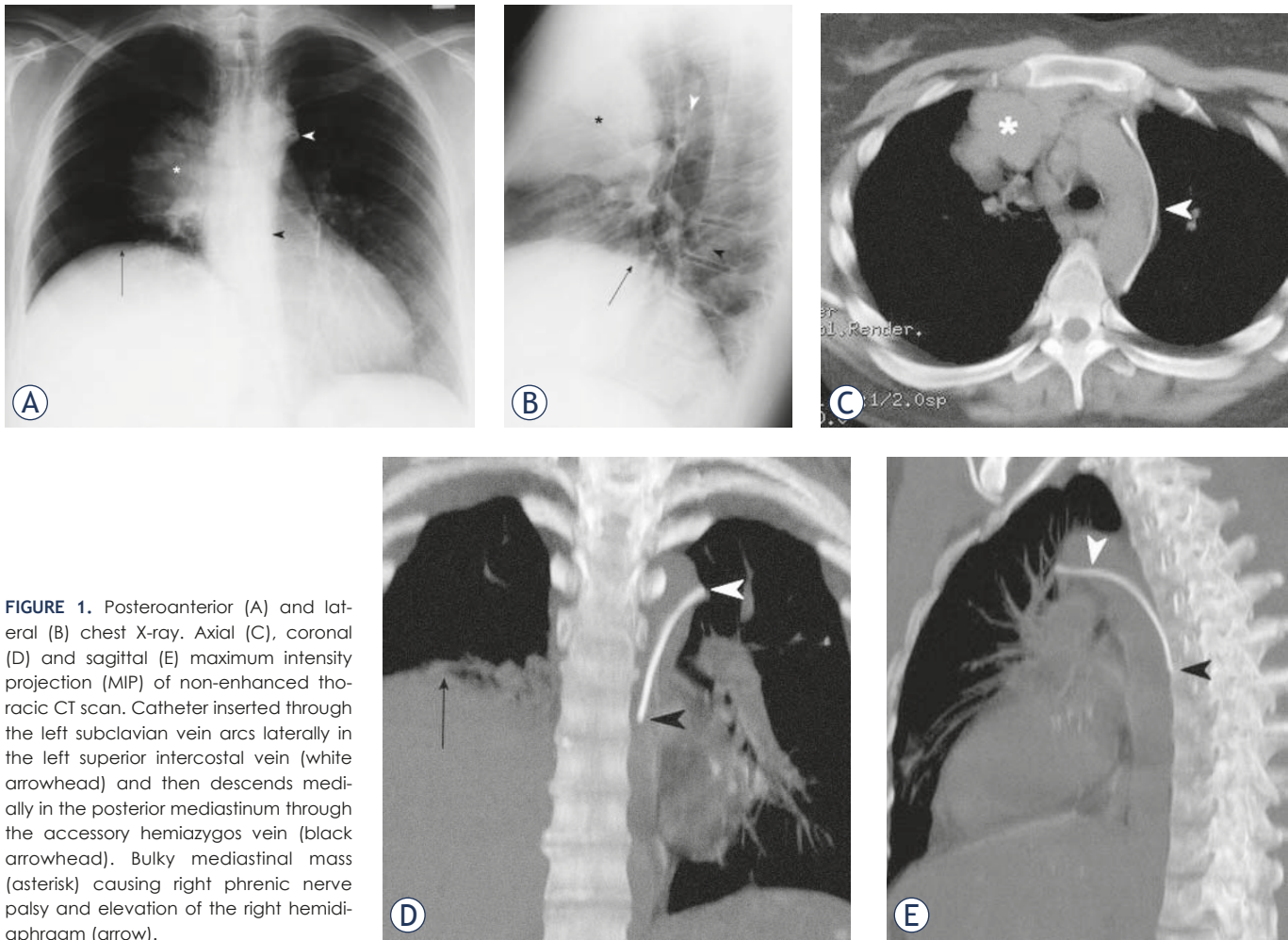
FIGURE 1. Posteroanterior (A) and lateral (B) chest X-ray. Axial (C), coronal (D) and sagittal (E) maximum intensity projection (MIP) of non-enhanced thoracic CT scan. Catheter inserted through the left subclavian vein arcs laterally in the left superior intercostal vein (white arrowhead) and then descends medially in the posterior mediastinum through the accessory hemiazygos vein (black arrowhead). Bulky mediastinal mass (asterisk) causing right phrenic nerve palsy and elevation of the right hemidiaphragm (arrow).

Routine chest X-ray was obtained to ascertain the position of the catheter (Figures 1A, B) and was interpreted as showing the catheter in the descending aorta. The right upper mediastinal mass with consequent right phrenic nerve palsy and elevation of the right hemidiaphragm was also evident.

Since hemodynamic parameters were consistent with a venous localization of the catheter, it was left in place and three hours later a non-contrast thoracic CT scan (GE LightSpeed Ultra, General Electric Healthcare, Milwaukee, USA) was performed in order to clarify its position (Figures 1C, D, E). It showed the CVC passing through the left subclavian vein, arching laterally along the aortic arch through the left superior intercostal vein and then descending medially in the posterior mediastinum through the accessory hemiazygos vein. Superior vena cava and both brachiocephalic veins were narrowed and incorporated into the bulky mediastinal mass with developed collateral pathways via the azygos-hemiazygos system.

Considering that the dilated accessory hemiazygos vein can tolerate infusion, the CVC was left in place and functioned well for three weeks. During that period the patient had no chest or back pain, nor other complaints related to CVC (mal)position.

Discussion

Malposition occurs in about one-third of CVC insertions if imaging guidance is not used, while it happens less frequently under sonographic or fluoroscopic guidance.[1] One of the rare courses of the misplaced catheter is the left superior intercostal vein, accessory hemiazygos vein and hemiazygos vein.

The left superior intercostal vein and azygos arch present a major venous loop connecting the posteriorly located azygos-hemiazygos system with the anteriorly located superior vena cava and left brachiocephalic vein.[7] They develop from the

same embryological structures – the main tract from the supracardinal vein and the terminal segment from the posterior cardinal vein.[8] The left superior intercostal vein collects blood from the left second through fourth intercostal vein, and at the level of T3 or T4 it courses anteriorly along the lateral wall of the aortic arch and empties into the left brachiocephalic vein near the venous angle. In 75% of individuals it communicates with the accessory hemiazygos vein that drains fifth through eighth left posterior intercostal veins. The accessory hemiazygos vein may communicate with the hemiazygos vein at the level T8 or T9 where hemiazygos vein crosses the midline to join the azygos vein.[9] If the left superior vena cava persists, the left superior intercostal vein becomes its tributary, analogous to the azygos arch on the right.[1]

The left superior intercostal vein can be identified on upright posteroanterior chest radiograph in 1.4%-9.5% of healthy people as a small "nipple" lateral to the aortic arch.[9,10] Diameter of the "aortic nipple" in healthy patients measures up to 4.5 mm on erect chest radiograph, and is 1-2 mm larger in supine position.[10] In case its diameter exceeds 4.5 mm, the patient should be investigated for a possible underlying venous abnormality. Dilatation of the left superior intercostal vein can be congenital or acquired. It is usually caused by superior or inferior vena caval obstruction/anomalies, congestive heart failure, portal hypertension, Budd-Chiari syndrome and left brachiocephalic vein hypoplasia.[10] In case of superior vena cava syndrome, its detection on chest X-ray can precede clinical symptoms by seven to ten weeks.[11] The course of the catheter in the left superior intercostal vein can be distinguished on chest X-ray from that of the catheter in a persistent left superior vena cava or in a pericardiophrenic vein because the latter two descend along left side of the mediastinum without arcing laterally along the aortic arch.[1]

The non-dilated left superior intercostal vein is usually too narrow for the insertion of a CVC. The insertion of the CVC tip into the narrow left superior intercostal vein irritates the vessel wall leading to catheter-related infection and thrombosis. Our patient had prior superior vena cava syndrome and thrombosis, and consequently developed collateral venous pathways, including the enlargement of the left superior intercostal vein. Enlarged collateral veins can occasionally be the site of CVC malposition. The CVC was left in place in the left superior intercostal and accessory hemiazygos vein because developed collateral venous pathways usually have a sufficient flow to tolerate infusion. The deliberate placement of CVC into the azygos-hemiazygos system with the effective long-term venous access in the patient with superior vena caval occlusion was previously reported.[12]

When oncologic patients undergo follow-up CT examinations of their underlying disease process[13], it is important to be aware of the CT findings that indicate malpositioning of the catheter.[14] Detailed knowledge of normal and anomalous venous anatomy is necessary for the correct interpretation of the CVC position. Because of the high radiation dose, CT scan cannot be recommended as a routine diagnostic procedure for the CVC position detection, but we believe that if there is any other indication for thoracic CT scanning, e.g. evaluation of mediastinal lymphadenopathy or lung disease, the position of the catheter can be precisely determined based on CT exam, making contrast venography unnecessary. The main disadvantage of the CT scan versus contrast venography is its inability to reposition the misplaced catheter. In addition, non-contrast CT scanning can be of use in patients with renal failure and contrast media hypersensitivity. Such scans are usually sufficient for the detection of CVC tip position in mediastinal veins, which are not accessible to colour Doppler imaging because of the restricted acoustic window.

Conclusions

CT can be a valuable tool in evaluation of the CVC position, especially in patients in whom diagnostic contrast venography is contraindicated due to renal failure or contrast media hypersensitivity. If the CVC tip is detected to be in the dilated left superior intercostal vein or accessory hemiazygos vein in patients with superior vena caval syndrome, the vein can usually tolerate infusion and the catheter can be left in place. Detailed knowledge of normal and anomalous venous anatomy is required for the optimal interpretation of the CVC position.

References

1. Godwin JD, Chen JTT. Thoracic venous anatomy. *AJR Am J Roentgenol* 1985; **147:** 674-84.

2. Teichgräber UK, Gebauer B, Benter T, Wagner HJ. Central venous access catheters: radiological management of complications. *Cardiovasc Intervent Radiol* 2003; **26:** 321-33.

3. Kutlu R. Obliterative hepatocavopathy - ultrasound and cavography findings. *Radiol Oncol* 2008; **42:** 181-6.

4. Smith DC, Pop PM. Malposition of a total parenteral nutrition catheter in the accessory hemiazygos vein. *JPEN J Parenter Enteral Nutr* 1983; **7:** 289-92.

5. Sarnak MJ, Levey AS. Placement of an internal jugular dialysis catheter into the superior intercostal vein. *Nephrol Dial Transplant* 1999; **14:** 2028-9.

6. Chambers NA. Left internal jugular catheter tip wedged in the left superior intercostal vein, an inferior tributary of the brachiocephalic. *Paediatr Anaesth* 2005; **15:** 1022-3.

7. Chasen MH, Charnsangavej C. Venous chest anatomy: clinical implications. *Eur J Radiol* 1998; **27:** 2-14.

8. Porzionato A, Macchi V, Parenti A, De Caro R. Unusual fibrous band on the left aspect of the aortic arch. *Clin Anat* 2005; **18:** 137-40.

9. Ball JB, Proto AV. The variable appearance of the left superior intercostal vein. *Radiology* 1982; **144:** 445-52.

10. Friedman AC, Chambers E, Sprayregen S. The normal and abnormal left superior intercostal vein. *AJR Am J Roentgenol* 1978; **131:** 599-602.

11. Carter MM, Tarr RW, Mazer MJ, Carroll FE. The "aortic nipple" as a sign of impending superior vena caval syndrome. *Chest* 1985; **87:** 775-7.

12. Meranze SG, McLean GK, Stein EJ, Jordan HA. Catheter placement in the azygos system: an unusual approach to venous access. *AJR Am J Roentgenol* 1985; **144:** 1075-6.

13. Debevec L, Jeric T, Kovac V, Bitenc M, Sok M. Is there any progress in routine management of lung cancer patients? A comparative analysis of an institution in 1996 and 2006. *Radiol Oncol* 2009; **43:** 47-53.

14. Díaz ML, Villanueva A, Herraiz MJ, Noguera JJ, Alonso-Burgos A, Bastarrika G, et al. Computed tomographic appearance of chest ports and catheters: a pictorial review for noninterventional radiologists. *Curr Probl Diagn Radiol* 2009; **38:** 99-110.

Electrogene therapy with interleukin-12 in canine mast cell tumors

Darja Pavlin[1], Maja Cemazar[2,3], Andrej Cör[3], Gregor Sersa[2], Azra Pogacnik[1], Natasa Tozon[1]

[1] University of Ljubljana, Veterinary Faculty Ljubljana, Ljubljana, Slovenia
[2] Institute of Oncology Ljubljana, Department of Experimental Oncology, Ljubljana, Slovenia
[3] University of Primorska, College of Health Care Izola, Izola, Slovenia

Background. Mast cell tumors (MCT) are the most common malignant cutaneous tumors in dogs with extremely variable biological behaviour. Different treatment approaches can be used in canine cutaneous MCT, with surgical excision being the treatment of choice. In this study, electrogene therapy (EGT) as a new therapeutic approach to canine MCTs, was established.

Materials and methods. Eight dogs with a total of eleven cutaneous MCTs were treated with intratumoral EGT using DNA plasmid encoding human interleukin-12 (IL-12). The local response to the therapy was evaluated by repeated measurements of tumor size and histological examination of treated tumors. A possible systemic response was assessed by determination of IL-12 and interferon- γ (IFN-γ) in patients' sera. The occurence of side effects was monitored with weekly clinical examinations of treated animals and by performing basic bloodwork, consisting of the complete bloodcount and determination of selected biochemistry parameters.

Results. Intratumoral EGT with *IL-12* elicits significant reduction of treated tumors' size, ranging from 13% to 83% (median 50%) of the initial tumor volume. Additionally, a change in the histological structure of treated nodules was seen. There was a reduction in number of malignant mast cells and inflammatory cell infiltration of treated tumors. Systemic release of IL-12 in four patients was detected, without any noticeable local or systemic side effects.

Conclusions. These data suggest that intratumoral EGT with plasmid encoding IL-12 may be useful in the treatment of canine MCTs, exerting a local antitumor effect.

Key words: electroporation; electrotransfection; electrogene therapy; mast cell tumors; IL-12; IFN-γ

Introduction

Mast cell tumors (MCT) are the most common malignant cutaneous tumors in dogs, accounting for around 21% of all cutaneous tumors.[1] Cutaneous MCT have extremely variable biological behavior, from low-grade tumors to highly invasive lesions with high metastatic potential, which makes proper staging and treatment of MCT very challenging.

Treatment options for canine MCT depend on prognostic factors, primarily the histological grade of the tumor and clinical stage of the disease. The treatment of choice for MCT is wide surgical excision, when possible, which results in excellent prognosis for well-differentiated MCT.[1] Poorly differentiated or anaplastic MCT carry a poor prognosis and in these tumors aggressive surgical treatment should be followed by other treatment modalities, *e.g.* radio- or chemotherapy.[1] In dogs, where it is not possible to perform surgical excision and in cases with advanced stages of disease, systemic chemotherapy is the most appropriate treatment option.[1,2]

One of the newer therapeutic approaches for local tumor control is electrochemotherapy (ECT), which has already been established as a successful treatment option for different histological types of canine tumors, including MCT.[3] It employs intralesional or systemic injection of the chemotherapeutic agent bleomycin or cisplatin, followed by local delivery of electric pulses to the tumor nodule, which significantly increase uptake and cytotox-

icity of chemotherapeutic drugs.[4-6] The procedure is based on electroporation of the cell membrane, achieving a transient increase in its permeability, thus allowing intracellular uptake of chemotherapeutic drugs from the extracellular space.[7]

The same principle can also be used for intracellular delivery of other molecules, for example plasmid DNA. Combining direct injection of plasmid DNA containing a therapeutic gene into target tissue, together with local delivery of electric pulses is called electrogene therapy (EGT).[8-10] In veterinary medicine, it has already been used for delivery of different transgenes into skeletal muscle[11-13] and intratumorally.[14,15]

IL-12 exhibits a range of biological activities, potentially important in immunotherapy of cancer. These include, for example, activation of natural killer cells, induction of IFN-γ, inhibition of angiogenesis and stimulation of nitric oxide production.[16] Gene therapy using *IL-12* has already shown remarkable antitumor activity in different tumor models at the preclinical level, and has already progressed to a number of clinical trials in both human and veterinary medicine. [17-21]

The aim of our study was to evaluate the local antitumor effect, systemic transgene release and possible side effects of EGT with the therapeutic plasmid encoding human IL-12 in canine MCT. For this purpose, a plasmid encoding human IL-12 was injected intratumorally into spontaneously occurring superficial nodules of MCT in 8 patients, followed by application of electric pulses. Local response to therapy was evaluated by regular measurements of tumor size and histological assessment of excised tumor nodules. Systemic transgene release was determined by measurements of IL-12 and IFN-γ in patients' sera. Possible side effects of the procedure were monitored by regular determination of selected hematology and biochemistry parameters.

Materials and methods

Animals

All animals in this study were referred to the Veterinary Faculty of Ljubljana in February and March 2006 for evaluation of cutaneous or subcutaneous tumor nodules. Eight patients that corresponded to inclusion criteria for the clinical study were included. The study cohort was comprised of 3 intact males and 5 spayed females of 6 different breeds (3 German boxers, and one of each: crossbreed, toy poodle, French bulldog, Siberian husky and bullterrier), their age ranging from 5 to 16

years (Table 1). Inclusion criteria for the study comprised at least one cytologically or histologically confirmed MCT, good general health status of the animal with the basic hematology and biochemistry profile within reference limits and normal renal and cardiovascular function. Animals included in the study were either ones which were planned for surgical excision of the tumor nodule as a part of standard therapeutic procedure and their owners agreed to the EGT procedure prior to surgery, or had recurrent disease in which other conventional therapy methods were already exhausted by previous treatments, or their owners refused any other type of standard treatment at the time of inclusion. Prior to inclusion, written consent for participation in the clinical study for each animal was obtained from their owners. The study was approved by the Ethical Committee at the Ministry of Agriculture, Forestry and Food of the Republic of Slovenia (approval No. 323-451/2004-9).

Clinical examination of each animal was performed before the treatment. Fine needle aspiration biopsy of tumor nodules, as well as of local lymph nodes, was taken and cytological examination of samples was performed. In all animals, staging was performed according to modified WHO staging criteria[22] with examination of thoracic radiographs, abdominal ultrasonography and basic bloodwork. Basic bloodwork consisted of a complete blood count with differential white blood cell count, which was performed using an automated laser hematology analyzer (Technicon H*1, Bayer, Germany) with species-specific software (H*1 Multi-Species V30 Software). The automated chemistry analyzer Technicon RA-XT (Bayer, Germany) was used for determination of the following biochemical parameters: blood urea nitrogen (BUN), creatinine, serum alkaline phosphatase (SAP) and alanine aminotransferase (ALT). Additionally, serum concentrations of human IL-12 and canine IFN-γ were determined using ELISA kits (Human IL-12 Quantikine ELISA Kit and Canine IFN-γ Quantikine ELISA Kit, respectively, both R&D Systems, Minneapolis, MN, USA).

A total of 11 tumor nodules were treated with EGT in the 8 patients which were included in the study. Two dogs received only one EGT, four dogs received 2 EGTs, with the second EGT session delivered one week after the first treatment, and one dog received 3 EGT sessions, each one week apart. In the remaining dog, four sessions were performed, each one month apart (Table 2).

In the patients, EGT was performed either as a single therapy (2/8 patients) or it was followed

Table 1. Summary of dogs' characteristics and histories

Pt. No.	Breed	Age (yrs)/Gender	Body weight (kg)	Duration of clin. signs (months)	Tumor location	Clinical stage	Cytology	Histology	Previous treatment	Response to previous treatment	No. of tumor nodules
1	Toy poodle	16/FS	6	3	back	I	MCT	N/A	no		1
2	Boxer	7/M	42	4	scapula	I	MCT	N/A	no		1
3	Cross-breed	10/FS	16.5	12	hind leg	II	MCT	N/A	no		1
4	Boxer	10/FS	27	6	perineum, back	II	MCT	grade II	no		2
5	Boxer	10/M	35	2	scrotum, scapula	III	MCT	grade II	no		4
6	Bullterrier	5/FS	20	>12	hind leg	II	MCT	grade II	surgery 2x chemotherapy (vincristine, CCNU)	recurrence	2
7	Siberian husky	11/FS	18	< 1	fore leg	III	MCT	grade III	no		1
8	French bull-dog	7/M	12	4	multicentric	III	MCT	grade III	surgery chemotherapy (vincristine)	recurrence PD	>10

FS, spayed female; MCT, mast cell tumor; M, male; CCNU, lomustine; PD, progressive disease

Table 2. Details of EGT treatment and response to therapy

Pt No.	Nodule	Tumor volume before EGT (cm³)	Tumor volume after EGT¹ (cm³)	No. of sessions	Dose of pIL12 per EGT session (mg)	Dose of plasmid per body weight (mg/kg)²	Post EGT therapy	Follow up after 1st EGT (months)	Response at the end of follow up	
1	1	0.25	0.1	2	0.15/0.15	0.05	/	36	SD	Euth., not related to MCT
2	1	2.3	2.0	1	0.5	0.01	Surgery	24	CR	without recurrence
3	1	3.2	1.6	2	1.0/1.0	0.12	CCNU (4 cycles)	12	SD	stable disease
4	1	0.6	0.3	2	0.5/0.2	0.06	ECT	13	CR	without recurrence
	2	1.2	0.8	2	0.5/0.4		Surgery		CR	without recurrence
5	1	2.9	0.6	2	0.5/0.5	0.03	Surgery	10	CR	without recurrence
6	1	0.03	0.005	4	0.1/0.1/0.1/0.1	0.07	/	44	SD	stable disease
	2	0.27	0.08	4	0.25/0.25/0.25/0.25		/		SD	
7	1	25.4	18.0	3	1.0/0.6/0.6	0.12	Surgery	2	PD	Euth. due to PD
8	1	0.45	0.6	1	0.2	0.025	CCNU (3 cycles)	5	PD	Euth. due to PD
	2	0.03	0.03	1	0.1					

Euth, euthanasia; MCT, mast cell tumor; CR, complete response; CCNU, lomustine; ECT, electrochemotherapy; SD, stable disease; PD, progressive disease
¹ The smallest volume of tumor nodule, achieved 1 week after the last performed EGT session
² Cumulative dose of received plasmid per kg of body weight

with one of the following therapies: standard surgical removal of MCT nodules (4/8 patients), chemotherapy (2/8 patients) or ECT (one nodule in a patient with two MCTs) (Table 2). Treated tumors were surgically removed one week after the last EGT session. In patients with systemic chemotherapy, 3 and 4 cycles of CCNU (lomustine, 60-90 mg/m², every 3 weeks) were delivered, starting two weeks after the last EGT session. ECT was performed one week after the last EGT session with intratumoral application of cisplatin (Cisplatyl, Aventis, Paris, France) at a dose 1 mg/cm³ of tumor tissue, followed by application of electric pulses (8 pulses of 100 μs duration at an amplitude of 1300 V/cm and frequency 1 Hz), using the same electric pulse generator as described below.

In animals in which histological samples of tumors were obtained either as part of the diagnostic procedure or with surgical excision after EGT, tumor samples were histologically evaluated. Histological grading was established using Patnaik's histological criteria.[22]

Plasmid preparation

The pORF-hIL-12 plasmid (InvivoGen, Toulouse, France), encoding human IL-12, was selected according to available data indicating that canine and human IL-12 share approximately 90% genetic identity based on amino acid sequence analysis.[23] It has already been shown that human IL-12 activates proliferation of canine peripheral blood mononuclear cells (PBMC) in an *in vitro* setting and triggers a number of immune responses in canine PBMC.[24] The plasmid was prepared using the Qiagen Endo-Free kit (Qiagen, Hilden, Germany), according to the manufacturer's instructions and diluted to a concentration of 1 mg/ml. Purified plasmid DNA was subjected to quality control and quantity determinations, performed by agarose gel electrophoresis and by means of spectrophotometry.

Electrogene therapy procedure

EGT was performed in animals under general anesthesia, which was induced with propofol (Propoven 10 mg/ml, Fresenius Kabi Austria GmbH, Graz, Austria) and maintained with isoflurane (Forane, Abbott Laboratories LTD, Queensborough, United Kingdom). During the anesthesia, animals received Harmann's solution (B. Braun Melsungen AG, Melsungen, Germany) at a rate of 10 ml/kg of body weight/h.

In animals under general anesthesia, hair overlying tumor nodules was removed, carefully avoiding any unnecessary manipulation of tumors which could lead to degranulation of mast cells. Each nodule was measured in three perpendicular directions (a, b, c) and the tumor volume was calculated using the formula: $V = a \times b \times c \times \pi/6$. A sterile solution of plasmid was injected into the tumor with a 1 ml syringe and 22 G needle. The dose of intratumorally injected plasmid ranged from 0.5 to 1 mg/cm³ of tumor tissue per one EGT session for tumors with volumes ranging from 0.1 cm³ to 2.5 cm³. In smaller tumors (< 0.1 cm³) and in larger tumors (> 2.5 cm³), an arbitrary dose per tumor nodule was set, being 0.1 mg for smaller and 1 mg for larger tumors (Table 2). Ten minutes after plasmid injection, electric pulses were delivered using the electric pulse generator Cliniporator™ (IGEA s.r.l., Carpi, Italy), using needle electrodes (2 arrays each composed of 4 electrodes with a 4-mm distance between them). One high voltage pulse was delivered (1 x 1200 V/cm, 100 μs), immediately followed by 8 low voltage pulses (8 x 50 ms, 140 V/cm, 2 Hz). After the electrogene procedure, all dogs received single intravenous application of carprofene (Rimadyl, Pfizer Animal Health, Dundee, United Kingdom; 4 mg/kg of bodyweight). When they fully recovered from anesthesia, they were released from hospital. Prior to release into the home environment, animals received Elizabethan collars in order to prevent any wound licking. Furthermore, treated tumor nodules were protected with suitable dressing to prevent any possible contact of humans or animals with the electroporated area.

Evaluation of response to therapy and possible side effects

Animals were examined one, two and four weeks after each EGT session and thereafter monthly. At each examination, a local as well as systemic response to the therapy was determined, along with observation for possible side effects.

The local response to therapy was evaluated with repeated measurements of tumor size as described above and calculation of tumor volumes. Additionally, in animals which underwent surgical excision of tumors, histological examination of tumor samples was performed. The systemic response to the treatment was assessed by determination of IL-12 and IFN-γ in patients' sera.

The possible occurrence of local or systemic side effects was evaluated at each follow-up with clinical examination of the animals and careful as-

sessment of the appearance of the electroporated area for any possible clinical signs, including erythema, oedema, pain, secretions, necrosis, etc. Furthermore, blood samples were taken for the same bloodwork as before the procedure.

Statistical analysis

Statistical analysis was performed using SigmaPlot software (Systat Software, Inc., Richmond CA, USA). To determine the significance of differences in tumor volumes of MCT before and after the treatment, a Friedman repeated Measures Analysis of Variance on Ranks was performed. Values of $P<0.05$ were considered significant.

Results

Response to the therapy

Before EGT, tumor volumes ranged from 0.03 to 25.4 cm³. Treated nodules reached the smallest volume one to two weeks after the last EGT procedure (Table 2), with their volumes ranging from 0.005 to 18 cm³, which was statistically significantly smaller compared to the volumes before EGT. One week after the last EGT session and before induction of any other therapeutic procedure, the tumor volume was reduced in 9/11 treated tumors, it had not changed in 1/11 treated tumors and progressed in 1/11 treated tumors. In nodules where reduction of tumor volume was achieved, it ranged from 13% and up to 83% of the initial value (median 50%).

In two patients (#1 and #6) with a total of three tumor nodules, EGT with *IL-12* was not followed by any other treatment (Table 2). In both patients, the tumor nodules reduced in size and treated patients responded to therapy with stable disease throughout the very long observation period (36 and 44 months).

Two patients (#3 and #8) received systemic chemotherapy with CCNU (Table 2). In one of these patients (#3) with stage II disease (regional lymph node involvement), stable disease with reduction in tumor volume by 50% was achieved with regression of detectable mast cell infiltration of lymph nodes and without any signs of distant metastases throughout the 12-month observation period. The second patient, (#8), treated with a combination of EGT and systemic chemotherapy had recurrent stage III disease, unresponsive to any treatment and was euthanized 5 months after EGT due to progress of the disease with systemic clinical signs.

In one patient (#4) with two tumor nodules, EGT in one nodule was followed by surgical removal of the tumor and in the other, due to its location in the perineum, EGT was followed by ECT, achieving a complete response in the treated nodule (Table 2).

In four patients (#2, #4, #5 and #7), surgical removal of 4 grade II and one grade III tumor nodules was performed one week post-EGT (Table 2). After surgery, three had a complete response to therapy without any signs of local recurrence or metastatic disease in over a 1-year observation period. The remaining one (#7), with stage III disease, had progression of clinical signs and was euthanized 2 months after EGT.

Histology of the tumors

All surgically removed tumors underwent histological examination. The control group represented MCT samples taken with a biopsy from the same tumor nodule during the diagnostic workup before inclusion into the clinical study or from untreated tumor nodules which were simultaneously removed in patients with multiple nodules.

Histological analysis of MCT prior to *IL-12* EGT showed nonencapsulated dermal and/or subcutaneous infiltrative growing masses composed of round cells arranged in densely packed cords. Most malignant mast cells were recognized in H&E stained slides by their cytoplasmic light gray-blue granules. Granules stained metachromatically with cationic dyes (toluidine blue staining). Most cells had a single nucleus, however same binucleated mast cells were also found. Among mast cell cords, variable numbers of diffusely distributed or aggregated eosinophils were seen. After the treatment, the distributions of viable malignant mast cells were reduced in comparison to the pretreatment samples (Figure 1A, B). Instead of mast cells in the dermis and subcutis, clusters of leukocyte infiltration were found. Large areas of mostly lymphocytes and plasma cells with eosinophilic cytoplasm and perinuclear halos were seen (Figure 1C, D). No similar infiltrates were found in samples of untreated lesions. Among immune cells, some degranulated mast cells were noticed without prominent neutrophils or eosinophils.

Hematology and systemic release of cytokines

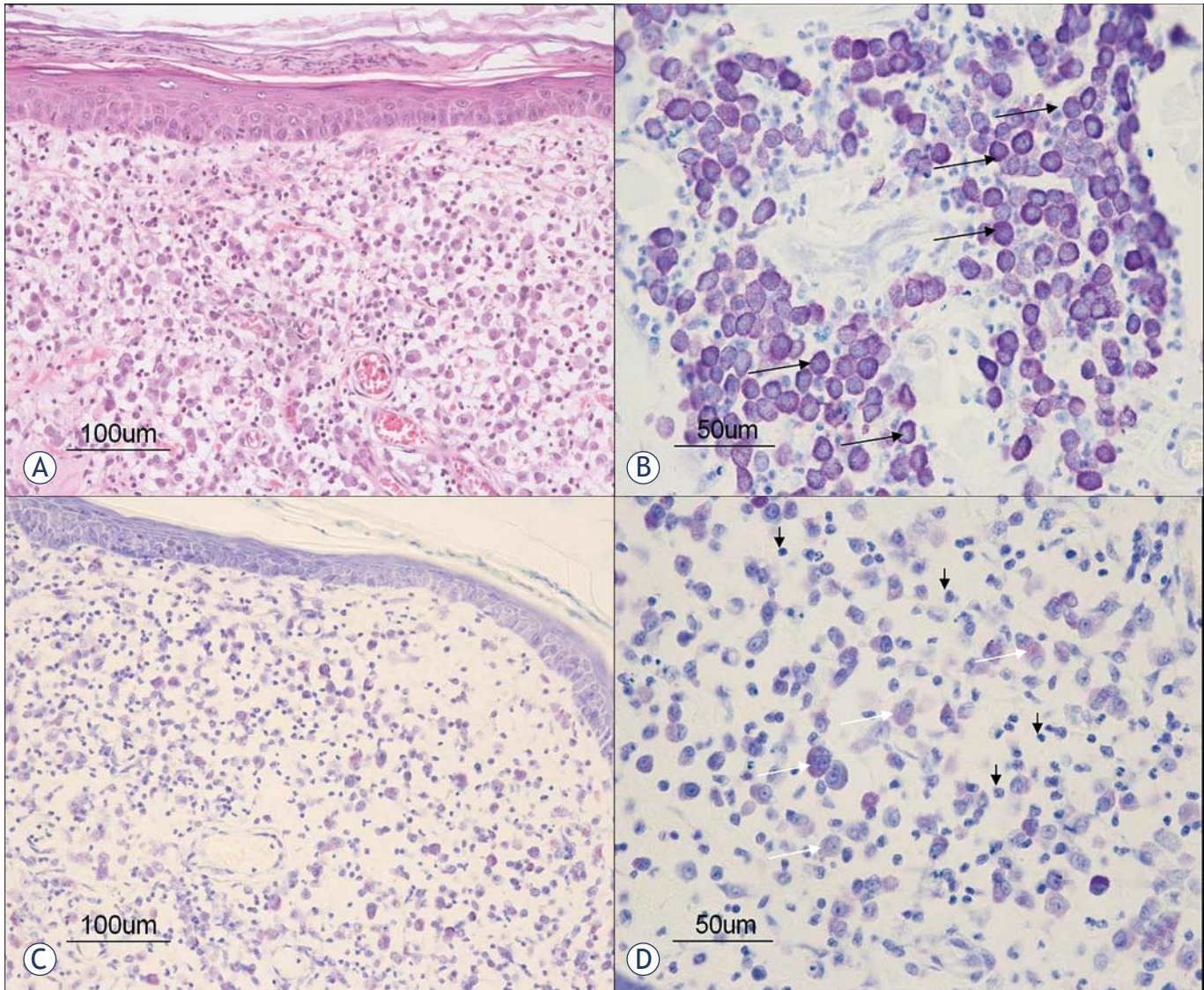In order to evaluate any possible systemic effects of the therapy, serum concentrations of human IL-12

FIGURE 1. Histological pictures of MCTs before (A and B) and after (C and D) EGT. A. Tumor mast cells are loosely arranged in the dermis without epidermal invasion (haematoxylin and eosin staining). B. Tumor mast cells (arrow) have a well granulated metachromatic cytoplasm (toluidine blue staining). C. Decreased number of mast cells in the dermis after the treatement (toluidine blue staining). D. Note the degranulated tumor mast cells with metachromatically weakly stained cytoplasm (white arrows) intermingled with numerous inflammatory cells (black arrows) (toluidine blue staining).

and canine IFN-γ were measured at regular time-points after the procedure.

IL-12 was detected in 5 samples from 3 patients, with serum concentrations ranging from 1 to 12.2 pg/ml. IFN-γ was detected in 5 samples from 2 patients, with concentrations ranging from 123.0 to 815.6 pg/ml. IL-12 and/or IFN-γ were detected in a total of 4 patients. All positive samples were collected after the EGT procedure; in samples, taken before the procedure, neither of the cytokines was detected. The highest systemic concentrations of transgene products were detected in patient #3. In this dog, all 3 post-EGT samples were positive for

both IL-12 (2.3 pg/ml to 12.2 pg/ml) and IFN-γ (170 pg/ml to 388.1 pg/ml) (Table 3).

In order to evaluate possible side effects of the procedure, clinical examinations of patients were carried out on a regular basis, with careful examination of the electroporated area and selected bloodwork.

We did not detect any evident side effects, either locally or systemically. All patients, which responded to treatment remained in good clinical condition throughout the observation period, without any additional clinical signs of disease. All analyzed blood parameters remained within

Table 3. Haematology and biochemistry profile of patient No. 3 with the highest number of serum samples, positive to IL-12 and IFN-γ

		DAY 0	DAY 7	DAY 14	DAY 28	REFERENCE VALUES
Cytokine conc.	IL-12 (pg/ml)	0	2.3	6.1	12.2	N/A
	IFN-γ (pg/ml)	0	388.1	179.6	164.3	N/A
Haematology	WBC (x10^9/l)	4.75	6.14	5.98	6.3	6-17
	RBC (x 10^{12}/l)	5.41	5.38	8.1	7.97	5.5-8.5
	HCT (L/L)	0.38	0.36	0.58	0.57	0.37-0.55
	PLT (x 10^9/l)	287	283	303	224	200-500
Biochemistry panel	BUN (mmol/l)	3.28	4.2	3.94	N/D	2.5-9.6
	Crea (μmol/l)	74.54	75.7	71.23	N/D	44.2-132.6
	SAP (U/l)	47.3	27.5	23.8	47.1	20-156
	ALT (U/l)	21.8	64.0	58.6	217.6	21-102

WBC, white blood cells; RBC, red blood cells; HCT, haematocrit; PLT, platelets; BUN, blood urea nitrogen, Crea, creatinine; SAP, serum alkaline phosphatase; ALT, alanin aminotransferase; N/D, not detected

the normal reference range. The few alterations in bloodwork parameters which occurred were only minimal and clinically irrelevant (for example, mild haemoconcentration in two samples). In two patients, slight elevations of SAP and/or ALT were detected in samples, obtained 1 and 2 months after the procedure, but they were considered side effects of CCNU chemotherapy, which was started 2 weeks after EGT. One of these two patients was euthanized due to progressive disease, unresponsive to all therapies whilst in the other, serum concentrations of both SAP and ALT returned within the reference range after discontinuation of chemotherapy. Details of hematology and the biochemistry profile in patient # 3, in which the best systemic response to treatment with the highest number of serum samples positive to IL-12 and IFN-γ was achieved, are summarized in Table 3.

Discussion

Our study demonstrates that intratumoral EGT with *IL-12* in canine MCT elicits good local antitumor effects in treated animals without any noticeable side effects. Local antitumor effects of this therapy can be seen as significant reduction in tumor size (median reduction of the pretreatment tumor volumes was 50%) and change in histological structure with reduction in the number of malignant mast cells coupled with infiltration of inflammatory cells in treated tumors. We also demonstrated that systemic release of the transgene product is possible after intratumoral EGT.

EGT is a novel treatment in medicine which has already entered the clinical stage of research in hu-

man oncology[20], and is also gaining some interest in veterinary medicine.[11-15,25] The results of EGT with various therapeutic genes including plasmid encoding IL-12 in the treatment of tumors are promising.[21] In a recent human clinical study, EGT with *IL-12* plasmid in the treatment of melanoma patients showed local as well as systemic antitumor effects with regression of tumor nodules and with minimal systemic toxicity.[20]

In our study, we treated spontaneously occurring cutaneous nodules of MCT in eight canine patients utilizing locally applied EGT with a therapeutic gene encoding human IL-12. The majority of treated nodules regressed in size after the EGT procedure by 50% (median) around 1-2 weeks after the last EGT session. These results can be compared to published results by Rakhmilevich *et al.* on growth delay of murine P815 mastocytoma[26] after bioballistic *IL-12* gene therapy and Heinzerling *et al.*[17], who utilized a similar approach for treatment of melanoma in horses with direct intratumoral application of plasmid DNA encoding human IL-12 without subsequent electroporation. In the murine mastocytoma model, a 60% reduction in volume was achieved three weeks after therapy. In equine melanomas, the mean reduction in size was 69% of the initial volume. It is possible that in dogs more repetitions of treatment sessions would result in even more pronounced tumor regression, since in the murine MCT model 6 repetitions whilst in horses up to 3 repetitions of treatment were necessary to reach a significant reduction in tumor size.

Histological analysis revealed a noticeable change in tumor morphology after EGT with *IL-12*. Beside reduction in the number of malignant mast cells, the most prominent feature of treated tumors

was diffuse infiltration of tumor tissue with lymphocytes and plasma cells as well as degranulation of remaining mast cells. These histological changes are in accordance with other studies employing intratumoral *IL-12* gene therapy with different delivery systems, where intra- and peritumoral lymphocytic infiltration was found to be a major contribution to histological changes in treated nodules.[17,20,27] The importance of lymphocytic infiltration of treated tumors after intratumoral *IL-12* EGT was shown in a variety of preclinical studies.[27,28] It was established that this mode of therapy does not elicit any antitumor effect in athymic mice deficient in T cells in contrast to immunocompetent mice, indicating the vital role of T lymphocytes in the antitumor activity of local *IL-12* EGT.[27,28] In our study, intratumoral *IL-12* EGT resulted in an immunological response with lymphocytic infiltration of treated tumors, which can be further indication that plasmid encoding human IL-12 is biologically active in dogs *in vivo*, as it was proposed to be in *in vitro* settings.[24]

The importance of the systemic action of IL-12 after local delivery in addition to local intratumoral accumulation of IL-12 has already been shown, demonstrating that circulating IL-12 is responsible for systemic antitumor effects, *e.g.* an antitumor effect on distant untreated tumors and prevention of distant metastases.[29-32] Therefore, systemic release of the transgene product would be extremely favorable in clinical settings, expanding local antitumor therapy into systemic treatment. In our study, systemic release of human IL-12 was detected in only three patients. Even though at the preclinical level there is contradictory data on the possibility of systemic transgene release after intratumoral *IL-12* EGT, in two studies on induced transmissible veneral tumors in dogs[14,15], similar concentrations of human IL-12 as in our three patients were detected. Therefore, further investigations are warranted to determine conditions for achieving systemic effects of intratumoral EGT with *IL-12* in dogs, since some release of IL-12 from treated tumors is clearly possible.

In treated patients we paid attention to two possible groups of adverse side effects. *IL-12*-based intratumoral EGT could lead to degranulation of mast cells, causing histamine release from granules, which is one of the major concerns of any mechanical manipulation of MCT. It can result in either local side effects, demonstrated as peritumoral swelling, edema and erythema, or in systemic clinical signs, for example, gastrointestinal ulceration, or even life-threatening hypotension, arrhythmias and bronchospasm. We did not observe any of these side effects, even though moderate mechanical manipulation of tumors could not be avoided since penetrating needle electrodes, which had to be inserted intratumorally, were used for EGT.

The second group of possible side effects is connected to systemic IL-12 toxicity. It has been shown that systemic administration of recombinant protein IL-12 is associated with multiple serious adverse side effects, including renal and systemic toxicity. High-dose levels were also linked to temporary immune suppression, which would not be favorable for effective immunotherapy.[33] Local intratumoral *IL-12* EGT was associated with significantly less adverse effects, while exhibiting a pronounced antitumor effect, as demonstrated by Heller *et al.* on a mouse melanoma model.[34] Even so, monitoring renal function with selected laboratory parameters (*e.g.* serum concentrations of BUN, creatinine) was recommended in any IL-12-based therapy.[34] In our study, all monitored hematological and biochemical parameters in blood samples remained within reference limits throughout the whole observation period with only few transient clinically nonsignificant and nonspecific alterations, which could be attributed to other factors. The clinical status of all animals that responded to therapy remained unaltered and they didn't show any changes in appetite, water intake and general behavior.

In conclusion, the results of our study demonstrate that intratumoral *IL-12* EGT in canine MCT is a feasible, simple and safe therapeutic procedure, which exerts local transgene expression with systemic release of the encoded protein, making it a promising treatment for canine patients with MCT. However, further refinement for effective use of this method in treatment of MCT is needed, with emphasis on optimization of the treatment protocol, including determination of appropriate dosage of the plasmid used, as well as the best possible number of EGT repetitions and optimal time interval between them.

Acknowledgements

References

1. Thamm DH, Vail DM. Mast Cell Tumors. In: Withrow SJ, Wail DM, editors. *Withrow and MacEwen's small animal clinical oncology, 4th edn*. St. Louis: Saunders; 2007. p. 402-16.

2. Maureen C, XinRu T, Benett P. Combination CCNU and Vinblastine chemotherapy for canine mast cell tumors: 57 cases. *Vet Comp Onc* 2009; **7:** 196-206.

3. Cemazar M, Tamzali Y, Sersa G, Tozon N. Mir LM, Miklavcic D, et al. Electrochemotherapy in veterinary oncology. *J Vet Intern Med* 2008; **22:** 826-31.

4. Mir LM, Glass LF, Sersa G, Teissie J, Domenge C, Miklavcic D, et al. Effective treatment of cutaneous and subcutaneous malignant tumors by electro-chemotherapy. *Br J Cancer* 1998; **77:** 2336-42.

5. Sersa G, Miklavcic D, Cemazar M, Rudolf Z, Pucihar G, Snoj M. Electrochemotherapy in treatment of tumors. *Eur J Surg Oncol* 2008; **34:** 232-40.

6. Gothelf A, Mir LM, Gehl J. Electrochemotherapy: results of cancer treatment using enhanced delivery of bleomycin by electroporation. *Cancer Treat Rev* 2003; **29:** 371-87.

7. Neumann E, Schaefer-Ridder M, Wang Y, Hofschneider PH. Gene transfer into mouse lyoma cells by electroporation in high electric fields. *EMBO J* 1982; **1:** 841-5.

8. Mir LM. Nucleic acids electrotransfer-based gene therapy (electrogene-therapy): past, current, and future. *Mol Biotechnol* 2009; **43:** 167-76.

9. Cemazar M, Golzio M, Sersa G, Rols MP, Teissié J. Electrically-assisted nucleic acids delivery to tissues in vivo: where do we stand? *Curr Pharm Des* 2006; **12:** 3817-25.

10. Heller LC, Heller R. In vivo electroporation for gene therapy. *Hum Gene Ther* 2006; **17:** 890-7.

11. Fewell JG, MacLaughlin F, Mehta V, Gondo M, Nicol F, Wilson E, et al. Gene therapy for the treatment of hemophilia B using PINC-formulated plasmid delivered to muscle with electroporation. *Mol Ther* 2001; **3:** 574-83.

12. Draghia-Akli R, Hahn KA, King GK, Cummings KK, Carpenter RH. Effects of plasmid-mediated growth hormone-releasing hormone in severely debilitated dogs with cancer. *Mol Ther* 2002; **6:** 830-6.

13. Pavlin D, Tozon N, Sersa G, Pogacnik A, Cemazar M. Efficient electrotransfection into canine muscle. *Technol Cancer Res Treat* 2008; **7:** 45-54.

14. Chou PC, Chuang TF, Jan TR, Gion HC, Huang YC, Lei HJ, et al. Effects of immunotherapy of IL-6 and IL-5 plasmids on transmissible veneral tumor in beagles. *Vet Immunol Immunopathol* 2009; **130:** 25-34.

15. Chuang, TF, Lee SC, Liao KW, Hsiao YW, Lo CH, Chiang BL, et al. Electroporation-mediated IL-12 gene therapy in a transplantable canine cancer model. *Int J Cancer* 2009; **125:** 698-707.

16. DelVecchio M, Bajetta E, Canova S, Lotze MT, Wesa A, Parmiani G, et al. Interleukin-12: biological properties and clinical application. *Clin Cancer Res* 2007; **13:** 4677-85.

17. Heinzerling LM, Feige K, Rieder S, Akens MK, Dummer R, Stranzinger G, et al. Tumor regression induced by intratumoral injection of DNA coding for human interleukin 12 into melanoma metastases in gray horses. *J Mol Med* 2001; **78:** 692-702.

18. Siddiqui F, Li C-Y, LaRue SM, Poulson JM, Avery PR, Pruitt AF, et al. A phase I trial of hyperthermia-induced interleukin-12 gene therapy in spontaneously arising feline soft tissue sarcomas. *Mol Cancer Ther* 2007; **6:** 380-9.

19. Kamensek U, Sersa G. Targeted gene therapy in radiotherapy. *Radiol Oncol* 2008; **42:** 115-35.

20. Daud AI, DeConti RC, Andrews S, Urbas P, Riker AI, Sondak VK, et al. Phase I trial of interleukin-12 plasmid electroporation in patients with metastatic melanoma. *J Clin Oncol* 2008; **26:** 5896-903.

21. Cemazar M, Jarm T, Sersa G. Cancer Electrogene Therapy with Interleukin-12. *Cur Gene Ther* 2010; **10:** 300-11.

22. Patnaik AK, Ehler WY, MacEwen EG. Canine cutaneous mast cell tumors: morphological grading and survival in 83 dogs. *Vet Pathol* 1984; **21:** 469-74.

23. Buettner M, Belke-Louis G, Rziha HJ, McInnes C, Kaaden OR. Detection, cDNA cloning and sequencing of canine interleukin 12. *Cytokine* 1998; **10:** 241-8.

24. Phillips BS, Padilla ML, Dickerson EB, Lindstrom MJ, Helfand SC. Immunostimulatory effects of human recombinant interleukin-12 on peripheral blood mononuclear cells from normal dogs. *Vet Immunol Immunopathol* 1999; **70:** 189-201.

25. Tamzali Y, Couderc B, Rols MP, Golzio M, Teissie J. Equine cutaneous tumors treatment by electro-chemo-immuno-therapy. In: Jarm T, Kramar P, Zupanic A, editors. *IFBME proceedings*, vol 16. New York: Springer; 2007. p. 610-3.

26. Rakhmilevich AL, Timmins JG, Janssen K, Pohlmann EL, Sheehy MJ, Yang NS. Gene gun-mediated IL-12 gene therapy induces antitumor effects in the absence of toxicity: a direct comparison with systemic IL-12 protein therapy. *J Immunother* 1999; **22:** 135-44.

27. Li S, Zhang L, Torrero M, Cannon M, Barret R. Administration route- and immune cell activation-dependant tumor eradication by IL-12 electrotransfer. *Mol Ther* 2005; **12:** 942-9.

28. Lucas ML, Heller L, Coppola D, Heller R. IL-12 plasmid delivery by in vivo electroporation for the successful treatment of established subcutaneous B16.F10 melanoma. *Mol Ther* 2002; **5:** 668-75.

29. Pavlin D, Cemazar M, Kamensek U, Tozon N, Pogacnik A, Sersa G. Local and systemic antitumor effect of intratumoral and peritumoral IL-12 electrogene therapy on murine sarcoma. *Cancer Biol Ther* 2009; **8:** 2114-22.

30. Tevz G, Kranjc S, Cemazar M, Kamensek U, Coer A, Krizan M, et al. Controlled systemic release of interleukin-12 after gene electrotransfer to muscle for cancer gene therapy alone or in combination with ionizing radiation in murine sarcomas. *J Gene Med* 2009; **11:** 1125-37.

31. Lucas ML, Heller R. IL-12 gene therapy using an electrically mediated nonviral approach reduces metastatic growth of melanoma. *DNA Cell Biol* 2003; **22:** 755-63.

32. Lee SC, Wu CJ, Wu PY, Huang YL, Wu CW, Tao MH. Inhibition of established subcutaneous and metastatic murine tumors by intramuscular electroporation of the interleukin-12 gene. *J Biomed Sci* 2003; **10:** 73-86.

33. Leonard JP, Sherman ML, Fisher GL, Buchanan LJ, Larsen G, Atkins MB, et al. Effects of single dose interleukin 12 exposure on interleukin-12 associated toxicity and interferon-gamma production. *Blood* 1997; **90:** 2541-8.

34. Heller L, Merkler K, Westover J, Cruz Y, Coppola D, Benson K, et al. Evaluation of toxicity following electrically mediated interleukin-12 gene delivery in a B16 mouse melanoma model. *Clin Cancer Res* 2006; **12:** 3177-83.

research article

Image cytometric nuclear texture features in inoperable head and neck cancer: a pilot study

Margareta Strojan-Flezar[1], Jaka Lavrencak[2], Mario Zganec[3], Primoz Strojan[4]

[1] Institute of Pathology, Faculty of Medicine, University of Ljubljana, Ljubljana, Slovenia

[2] Department of Cytopathology, Institute of Oncology Ljubljana, Ljubljana, Slovenia

[3] Alpineon d.o.o., Ljubljana, Slovenia

[4] Department of Radiation Oncology, Institute of Oncology Ljubljana, Ljubljana, Slovenia

Corespondence to: Prof. Primož Strojan, M.D., Ph.D., Department of Radiation Oncology, Institute of Oncology Ljubljana, Zaloška 2, SI-1000 Ljubljana, Slovenia. Phone: +386 1 5879 110; Fax: +386 1 5879 400; E-mail: pstrojan@onko-i.si

Background. Image cytometry can measure numerous nuclear features which could be considered a surrogate end-point marker of molecular genetic changes in a nucleus. The aim of the study was to analyze image cytometric nuclear features in paired samples of primary tumor and neck metastasis in patients with inoperable carcinoma of the head and neck.

Materials and methods. Image cytometric analysis of cell suspensions prepared from primary tumor tissue and fine needle aspiration biopsy cell samples of neck metastases from 21 patients treated with concomitant radiochemotherapy was performed. Nuclear features were correlated with clinical characteristics and response to therapy.

Results. Manifestation of distant metastases and new primaries was associated (p<0.05) with several chromatin characteristics from primary tumor cells, whereas the origin of index cancer and disease response in the neck was related to those in the cells from metastases. Many nuclear features of primary tumors and metastases correlated with the TNM stage.

Conclusions. A specific pattern of correlation between well-established prognostic indicators and nuclear features of samples from primary tumors and those from neck metastases was observed. Image cytometric nuclear features represent a promising candidate marker for recognition of biologically different tumor subgroups.

Key words: head and neck cancer; image cytometry; nuclear features; prognosis

Introduction

Various tumor variables related to DNA content were found predictive for the response of different tumor types to applied therapy; they also contain prognostic information on patients' survival.[1-3] Image or flow cytometry can be used as a fast and effective method for the measurements of DNA content and S-phase to evaluate the occurrence and to quantify genetic changes in different malignancies. In addition, image cytometry can measure numerous nuclear features and the foremost nuclear texture features on a two-dimensional snapshot of chromatin structure and organization. Accordingly, nuclear texture features could be considered a surrogate end-point marker of molecu-

lar genetic changes in a nucleus.[4] In the head and neck region, image cytometry has principally been used to detect and assess premalignant changes.[5-8] However, a recent study reported that image cytometric DNA content and nuclear morphometric features were significantly associated with the radiosensitivity of nasopharyngeal carcinoma and outcome of the disease.[9]

In the present study we aimed to analyze image cytometric nuclear features (foremost nuclear texture features) in paired tissue samples of primary tumors and regional metastases from the neck in a group of patients with inoperable squamous cell carcinoma of the head and neck (SCCHN) treated with concomitant chemoradiotherapy with myto-mycin C and cisplatin. We hypothesized that chro-

matin characteristics as determined by image cytometry could improve assessment of the biological potential of SCCHN reflected in the response to treatment and course of the disease.

Materials and methods

Patients

The study group comprised 21 patients with inoperable SCCHN who entered the phase I/II clinical study between 2002 and 2004.[10] Their median age was 57 years (range, 38–68). TNM stage was IVA in 6 patients and IVB in 15 patients. Details on patients and their tumors are presented in Table 1. All patients were treated with curative intent using a uniform protocol of concomitant chemoradiotherapy consisting of conventional radiotherapy (70 Gy in 35 fractions) and concomitant Mitomycin C, bioreductive agent, selectively toxic for hypoxic cells, applied I.V. in a dose of 15 mg/m^2 after the delivery of 10 Gy. Additionally, Cisplatin at a dose of 10 mg/m^2/day (6 patients) or 14 mg/m^2/day (15 patients) I.V., was applied during the last 10 fractions of irradiation to counteract the accelerated repopulation of surviving tumor clonogens ("chemoboost"). The details on treatment protocol were published elsewhere.[10]

The study protocol was approved by the National Medical Ethics Committee of the Republic of Slovenia, and informed consent was obtained from all patients participating in the study.

Preparation of tissue samples

Fifty-micron sections were cut from the formalin-fixed paraffin-embedded tissue blocks of primary tumors biopsied during diagnostic assessment. Single-cell suspensions were prepared according to the standard procedures.[11,12] For image cytometric analysis, the cell suspension was filtered through a membrane filter system and the filter was gently imprinted onto two parallel glass slides. Cell preparations were immediately immersed in Delaunay fixative (ethanol:acetone 1:1 with 0.5 ml/l trichloracetic acid).

Cell samples of neck metastases were obtained during diagnostic procedures before treatment by fine needle aspiration biopsy (FNAB) using a 20-gauge (0.7 mm diameter) needle. A direct smear was prepared from each aspirate, air-dried and stained according to Giemsa for diagnostic light microscopy evaluation. The needle and syringe were then washed in cell medium (containing 4.5%

TABLE 1. Characteristics of patients and their tumors

Patients					
Gender	female – 1, male – 20				
Age	57 (38–68)[a]				
Primary tumor site					
Oropharynx	12				
Hypopharynx	7				
Larynx	2				
Histopatological grade					
Grade 2	15				
Grade 3	6				
UICC TNM classification					
	N1	N2A	N2B	N2C	N3	Total
T1					1	1
T2					3	3
T3					2	2
T4A			3	2	5	11
T4B	1		1	2	1	4
Total	1	0	4	4	12	21
Overall UICC-TNM stage					
Stage IVA	6				
Stage IVB	15				

[a]Median (range), in years

bovine serum albumin, 0.45% EDTA in PBS with 1 IU/1ml penicillin and stored at 4°C). This resulted in cell suspension that was used to prepare several cytospins in a Shandon cytospin 4 cytocentrifuge (Thermo Shandon Inc, Pittsburgh, Pennsylvania, U.S.A.). Cytospins were fixed in Delauney fixative. For image cytometric measurements, the slides prepared from cell suspensions of primary tumors and metastases were stained stoichiometrically with thionin according to the Feulgen method.[13]

Image cytometric analysis

Image cytometric analysis was performed using an automated high resolution image cytometer, Cyto-Savant™ (Oncometrics Imaging Corp., Vancouver, BC, Canada).[14] The slides were automatically scanned with the software program Acquire (Oncometrics Imaging Corp., Vancouver, BC, Canada), incorporated into the system. More than 100 nuclear features were calculated from each of the nuclear images (Table 2). The nuclear features included common morphometric features (area, diameter, shape features, etc.), descriptive statistics of chromatin distribution (integrated optical density

TABLE 2. Image cytometric nuclear features

Nuclear Feature Group	Specific Nuclear Feature
Morphometric nuclear features	area, mean radius, variance of radius, sphericity, eccentricity, elongation
Photometric Nuclear Features (descriptvive statistics of chromatin distribution)	DNA Amount, DNA Index , variance of DNA intensity, mean DNA intensity, OD mean, OD maximum, OD variance, OD scewness, OD curtosis
Discrete Nuclear Texture Features	low density DNA area, medium density DNA area, high density DNA area, low density DNA amount, medium density DNA amount, high density DNA amount, low density DNA compactness, medium density DNA compactness, high density DNA compactness, medium/high density DNA compactness, low density - average distance, medium density - average distance, medium/high density average distance, low density objects, medium density objects
Markovian Nuclear Texture Features	entropy, energy, contrast, correlation, homogeniety, cluster shade, cluster prominence
Non-Markovian Nuclear Texture Features (local extreme features)	density light spot, density dark spot, range average, range extreme, center of gravity
Fractal Nuclear Texture Features	fractal1 area, fractal2 area, fractal dimension
Run Length Nuclear Texture Features	average long runs, average run length, short run emphasis, long run emphasis, grey level nonuniformity

[IOD], variance of optical density [OD], OD skewness and kurtosis, etc.) and nuclear texture features, represented by discrete chromatin distribution (area and shape of high, medium and low density chromatin components, average distance between chromatin components of the same optical densities, etc.), fractal texture features, Markovian texture features (entropy, energy, correlation, homogeneity, cluster shade, etc.), non-Markovian local extreme features (number of local minima and maxima in the image, etc.) and the length of texture features' run (short run emphasis, long run emphasis, gray level nonuniformity, etc.). The formulas and nuclear feature descriptions can be found elsewhere.[15]

Statistics

Probability density functions were calculated for each nuclear feature in each tumor and metastasis, respectively.[16] Differences between the study groups were evaluated with analysis of variance. Differences were considered statistically significant at p<0.05.

Results

Patients, image analysis, therapy and outcome

In 21 patients, after interactive removal of artifacts and double or multiple nuclei, an average of 2851 well-preserved nuclear images per slide (range, 91–8158) were available for image cytometric analysis of tissue samples of primary tumors, and an average of 1880 nuclear images per slide (range, 50–8563) in the FNAB samples of neck metastases.

The median follow-up time was 49 months (range, 38–63). At 8–12 weeks post therapy, complete response to treatment at the primary site and in the neck disease was observed in 19 (90.5%) and 16 (76.2%) patients, respectively. The disease reappeared locally in 2/19 patients and regionally in 5/16 patients who obtained a complete response at the primary site and in the neck, respectively. Six (28.6%) patients were diagnosed with distant metastases, and new primary tumors developed in six (28.6%) patients, 3–46 months (median, 18 months) post diagnosis of index head and neck carcinoma.

Nuclear features

Differences in nuclear features in relation to various clinical parameters and treatment outcome are summarized in Table 3, showing a specific pattern of correlation between individual prognostic indicators and nuclear features of samples from primary tumors and those from neck metastases.

Direct comparison of nuclear texture features between the primary tumors and metastases was not prudent due to initial differences in primary fixation procedures of the two sample types.[17]

Primary tumor

In regard to the primary tumor site, image cytometric analysis of nuclear features showed no differences when primary tumor samples were analyzed. Considering the TNM stage of the disease, differences were found in some of the nuclear features, namely photometric, Markovian and non-Markovian. Only one of the studied nuclear texture features (non-Markovian) was predictive

TABLE 3. Differences in nuclear features determined in tissue samples from primary tumors and neck metastases, according to clinical characteristics and treatment outcome. Differences at p<0.05 are marked with +

Nuclear features	Clinical characteristics of patients											
	Primary tumor site		TNM stage		Regional response¹		Regional recurrence		Distant metastases		New primary tumor	
	PT	NM	PT	NM	PT	NM	PT	NM	PT	NM	PT	NM
Morphometric		+				+			+		+	
Photometric			+			+			+	+		
Discrete		+		+		+			+		+	
Markovian			+						+			
Non-Markovian		+	+	+			+		+		+	
Fractal						+			+		+	
Run-length		+				+						

PT, Primary tumor; NM, Neck metastasis
¹At 8–12 weeks post-therapy

of regional recurrence by analyzing the primary tumor but none of them forecasting nodal response to therapy. The nuclear features of primary tumors belonging to all groups of nuclear morphometric and texture features differed between the patients who developed distant metastases and those who didn't. Also, some nuclear texture features of primary tumors were different for the patients who developed new primary tumors.

Neck metastasis

Differences between several nuclear morphometric and texture features (discrete, non-Markovian and run length) were found in the samples from metastases when patients were grouped according to the primary tumor site (Figure 1). When analyzing samples from patients with disease TNM stage IVA and stage IVB, the differences were also found for some nuclear texture features (discrete, non-Markovian). Variations in regional response to treatment at 8–12 weeks post therapy were associated with some morphometric and other nuclear features (photometric, discrete, fractal and run length) of metastases. Only one nuclear photometric feature was predictive for systemic dissemination of the disease, while no differences were observed in any feature of metastases in regard to regional recurrence or occurrence of new primary tumor.

Discussion

In the present study we aimed to evaluate the predictive and prognostic value of image cytometric nuclear features, characterizing different details of
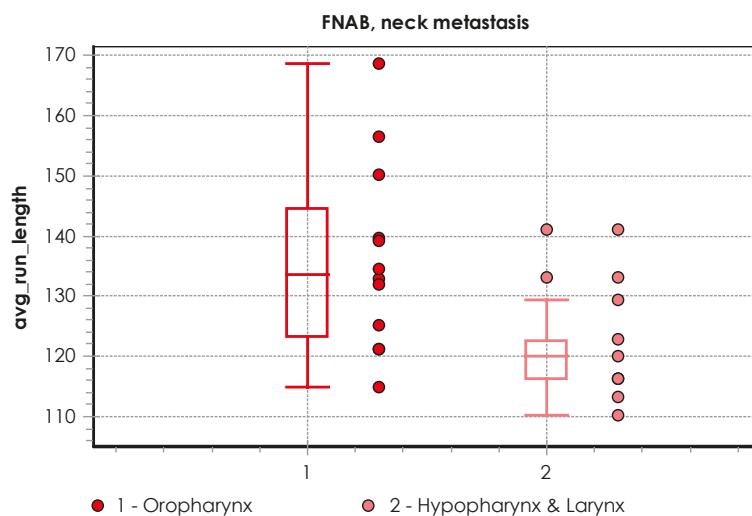
FIGURE 1. Example of box plot of different values of one nuclear texture feature (avg_run_length) for primary tumor site as analyzed in FNAB samples from neck metastases.

nuclear size, chromatin structure and its organization, in matched pairs of primary SCCHN and neck metastasis in a homogenous group of patients, in regard to the tumor extent and therapy.[10] The main finding would be that nuclear features as determined in primary tumor samples suggest the tendency for distant dissemination and occurrence of new primary tumors. On the other hand, the nuclear features of neck metastases determined regional response of the neck disease to applied radiochemotherapy and indicated primary tumor origin.

To the best of our knowledge, our study is the first to analyze the clinical applicability of image cytometric assessment of nuclear features, including texture features, in advanced SCCHN. Other

research on head and neck lesions has focused on the difference between malignant and non-malignant tissue characteristics, aiming to recognize a pattern predictive of the malignant transformation of clinically normal appearing mucosa or pre-malignant changes.[5-7] The results of these studies suggested that nuclear features could discriminate between benign and malignant mucosal changes, but further studies on their potential to predict the probability of malignant transformation of benign lesions were not conducted. Furthermore, malignancy-associated changes recognized by image cytometric analysis of non-malignant buccal mucosa cells could be used to identify high-risk individuals for invasive cancer, including SCCHN.[18,19]

Our study revealed various associations with clinically well-established prognostic factors. It is of interest that an individual prognosticator correlated with the nuclear features of a particular sample type, *i.e.* either primary tumor biopsy samples or regional metastasis FNAB samples. Although sharing many characteristics, various factors from local environment, which differed between primary tumor site and the neck, most probably critically and distinctly influence tumor cells forming primary tumor and nodal metastasis.[20] Thus, it sounds reasonable that FNAB cell samples obtained directly from metastatic nodes are more representative than biopsy specimens from primary tumors for characterizing nodal disease and vice versa. The lack of effect of T-stage on the risk of nodal failure[21] and, conversely, the observation that nodal disease at presentation does not add any significant contribution to the risk of local failure[22] corroborate this assumption.

We observed that manifestation of distant metastases and new primary tumors was significantly dependent on several nuclear chromatin features from primary tumor cells. It seems that the biological potential of cells from primary tumors characterize the clinical aggressiveness of the disease and dictate its course in an individual patient. On the other hand, the origin of index cancer and disease response to treatment in the neck at 8–12 weeks post therapy were related to nuclear features as characterized in the cells from neck metastases. Obviously, the nuclear chromatin characteristics of tumor cells from regional metastases reflect their origin, as well as susceptibility to chemoradiation. In our previous study we found FNAB sampling of neck metastases of SCCHN supplemented with immunocytochemical determination of cyclin D1 and Ki-67 a valuable method for radiosensitivity testing to predict regional response to radiotherapy.[23]

Likewise, Cabanillas *et al*. reported on a significant correlation between p53 expression in the primary SCCs of the supraglottic larynx and the matched lymph node metastases, although only p53 over-expression in the lymph nodes was predictive for regional recurrence.[24] To the contrary, Huang *et al*. found nuclear morphometry of primary tumor cells in patients with nasopharyngeal carcinoma assessed by image cytometric analysis to be predictive for the response of the primary tumor and regional metastases to radiotherapy.[9]

None of the nuclear features tested correlated with the progression of regional disease in our patients; the putative explanation would be that in the original samples taken before therapy, small clones of resistant cells surviving the treatment were not sampled and, consequently, not analyzed. This assumption goes into the context of the extremely advanced disease stages in our patients (T4 – 71.4%, N3 – 57.1%; all patients had stage IV disease), which increases the probability of under-representative samples (*i.e.* with an insufficient number of representative cells). Furthermore, disease curability could be also influenced by tumor burden and radiotherapy related factors *i.e.* technique and dose. On the other hand, many nuclear features of both primary tumors and metastases correlated with the stage of the disease, reflecting the fact that both contribute to the TNM-stage grouping.

One important advantage of image cytometric analysis is that data on nuclear features can be obtained before treatment, so they could be used for its planning. Because in SCCHN there are no markers identified so far to reliably predict the course of the disease, its response to therapy or patients' survival, our findings suggest image cytometric evaluation of the primary tumor and/or its metastases as a plausible prognostic tool. Showing the potential to be able to discriminate between different forms of the disease in respect to its aggressiveness, the nuclear features assessed by image cytometry emerge as a valuable method for tailoring treatment accordingly.

When evaluating the clinical relevance of the presented results, one must be aware of existing drawbacks of the present study. First, the number of patients is small, which precluded more detailed statistics. Furthermore, although being homogenous regarding disease stage and therapy, the patients differed significantly in respect to primary tumor origin, which could be of prognostic significance.[25] And finally, using pairs of cell samples obtained from primary tumors and their regional metastases, we gained a unique opportunity to com-

pare chromatin characteristics between the cells of index cancers and their metastases. Unfortunately, due to the differences in primary fixation procedures, which influence the nuclear features of the two sample types, as we already proven previously, this was inappropriate in the present study.[17]

In conclusion, a specific pattern of correlation between well-established prognostic indicators and nuclear features of samples from primary tumors and those from neck metastases was observed. According to our results, image cytometric nuclear features represent a promising candidate marker for the recognition of biologically more aggressive tumors and could add to a more individualized treatment of SCCHN patients. However, the study should be considered as the hypothesis generated; it was designed as a pilot series, asking for, on the basis of favorable results, confirmation in a large-scale prospective clinical trial.

Acknowledgement

References

1. Merkel DE, McGuire WL. Ploidy, proliferative activity and prognosis. DNA flow cytometry of solid tumors. *Cancer* 1990; **65:** 1194-205.

2. Böcking A, Striepecke E, Auer H. Static DNA cytometry. Biological background, technique and diagnostic interpretation. In: Wied GL, Bartels PH, Rosenthal D, Schenk U, editors. *Compendium on computerized cytology and histology laboratory.* Chicago: Tutorials of cytology; 1994. p. 107-28.

3. Shankey TV, Rabinovitch PS, Bagwell B, Bauer KD, Duque RE, Hedley DW, et al. Guidelines for implementation of clinical DNA cytometry. *Cytometry* 1993; **14:** 472-7.

4. Palcic B. Nuclear texture: can it be used as a surrogate endpoint marker? *J Cell Biochem* 1994; **19:** 40-6.

5. Dreyer T, Knoblauch I, Doudkine A, MacAulay CE, Garner D, Palcic B, et al. Nuclear texture features for classifying benign vs. dysplastic or malignant squamous epithelium of the larynx. *Anal Quant Cytol Histol* 2001; **3:** 193-200.

6. Maraki D, Becker J, Böcking A. Cytologic and DNA-cytometric very early diagnosis of oral cancer. *J Oral Pathol Med* 2004; **33:** 398-404.

7. Rode M, Strojan Flezar M, Kogoj Rode M, Us Krasovec M. Image cytometric evaluation of nuclear texture features and DNA content of the reticular form of oral lichen planus. *Anal Quant Cytol Histol* 2006; **28:** 262-8.

8. Torres-Rendon A, Stewart R, Craig GT, Wells M, Speight PM. DNA ploidy analysis by image cytometry helps to identify oral epithelial dysplasias with a high risk of malignant progression. *Oral Oncol* 2009; **45:** 468-73.

9. Huang T, Chen M, Wu M, Wu X. Image analysis of DNA content and nuclear morphometry for predicting radiosensitivity of nasopharyngeal carcinoma. *Anal Quant Cytol Histol* 2008; **30:** 169-74.

10. Strojan P, Karner K, Smid L, Soba E, Fajdiga I, Jancar B, et al. Concomitant chemoradiotherapy with mitomycin C and cisplatin in advanced unresectable carcinoma of the head and neck: phase I-II clinical study. *Int J Radiat Oncol Biol Phys* 2008; **72:** 365-72.

11. Hedley DW, Friedlander ML, Taylor IW, Rugg CA, Musgrove EA. Method of analysis of cellular DNA content of paraffin-embedded pathological material using flow-cytometry. *J Histochem Cytochem* 1983; **31:** 1333-5.

12. Reith A, Danielsen H. Assessment of DNA ploidy in tumor material. Preparation and measurement by image cytometry. In: Weid GL, Bartels PH, Rosenthal D, Schenk U, editors. *Compendium on the computerized cytology and histology laboratory.* Chicago: Tutorials of cytology; 1994. p. 185-93.

13. Kjellstrand P. Mechanisms of the Feulgen acid hydrolysis. *J Microsc* 1980; **119:** 391-6.

14. Jaggi B, Poon S, Pontifex B, Fengler J, Palcic B. A quantitative microscope for image cytometry. *J SPIE* 1991; **1448:** 89-97.

15. Doudkine A, MacAulay C, Poulin N, Palcic B. Nuclear texture measurements in image cytometry. *Pathologica* 1995; **87:** 286-99.

16. Žganec M. *Pattern recognition and data presentation in image cytometry.* [Thesis]. Ljubljana: University of Ljubljana, Faculty of Medicine; 2003.

17. Flezar M, Doudkine A, Us-Krasovec M. The effect of primary fixation with standard postfixation and the duration of hydrolysis on nuclear features in image cytometry. *Anal Cell Pathol* 1998; **17:** 131-44.

18. Burger G, Aubele M, Clasen B, Juetting U, Gais P, Rodenacker K. Malignancy associated changes in squamous epithelium of the head and neck region. *Anal Cell Pathol* 1994; **7:** 181-93.

19. Us-Krasovec M, Erzen J, Zganec M, Strojan-Flezar M, Lavrencak J, Garner D, et al. Malignancy associated changes in epithelial cells of buccal mucosa. A potential cancer detection test. *Anal Quant Cytol Histol* 2005; **27:** 254-62.

20. Joyce JA, Pollard JW. Microenvironmental regulation of metastasis *Nat Rev Cancer* 2009; **9:** 239-52.

21. Ataman ÖU, Bentzen SM, Wilson GD, Daley FM, Richman PI, Saunders MI, et al. Molecular biomarkers and site of first recurrence after radiotherapy for head and neck cancer. *Eur J Cancer* 2004; **40:** 2734-41.

22. Benzen SM, Johansen LV, Overgaard J, Thames HD. Clinical radiobiology of squamous cell carcinoma of the oropharynx. *Int J Radiat Oncol Biol Phys* 1991; **20:** 1197-206.

23. Strojan Flezar M, Srebotnik Kirbis I, Surlan Popovic K, Strojan P. Radiosensitivity of squamous cell carcinoma metastases to the neck assessed by immunocytochemical profiling of fine-needle aspiration biopsy cell specimens: a pilot study. *Radiother Oncol* 2009; **93:** 575-80.

24. Cabanillas R, Rodrigo JP, Astudillo A, Domínguez F, Suárez C, Chiara MD. P53 expression in squamous cell carcinoma of the supraglottic larynx and its lymph node metastases: new results for an old question. *Cancer* 2007; **109:** 1791-8.

25. Forastiere A, Koch W, Trotti A, Sidransky D. Head and neck cancer. *N Engl J Med* 2001; **45;** 1890-900.

research article

Triple negative breast cancer – prognostic factors and survival

Tanja Ovcaricek, Snjezana Grazio Frkovic, Erika Matos, Barbara Mozina, Simona Borstnar

Institute of Oncology Ljubljana, Ljubljana, Slovenia

Correspondence to: Tanja Ovčariček, MD; Department of Medical Oncology, Institute of Oncology Ljubljana, Zaloška 2, SI-1000 Ljubljana. Phone: +386 1 5879220; Fax: +386 1 5879400; E-mail: tovcaricek@onko-i.si

Background. Triple negative breast cancer (TNBC) is defined by a lack of expression of both estrogen (ER) and progesteron (PgR) receptors as well as human epidermal growth factor receptor 2 (HER2). Our retrospective analysis addressed prognostic factors for short- and long-term outcomes of patients (pts) with TNBC pts treated in routine clinical practice.

Patient and methods. Our retrospective study included 269 TNBC treated at Institute of Oncology Ljubljana between March 2000 and December 2006. The collected data included patients', tumours' and treatments' characteristics. The survival analyses were performed using the Kaplan-Meier method. The Cox proportional hazard model was used in the multivariate analysis.

Results. The median age of our patients was 55.3 yrs (23-88.5) and the median follow-up was 5.9 yrs (0.3-9.6). Six (2%) pts experienced local only, 79 (92%) pts distal recurrence and 66 (24%) died. The predominant localisation of the first relapse was in visceral organs (70.4%). The 5-year disease-free survival (DFS) for the entire group was 68.2% and the 5-year overall survival (OS) was 74.5%. We found a pattern of high recurrence rate in the first 3 years following the diagnosis and a clear decline in recurrence rate over the next 3 years. In the univariate analysis age, nodal status, size and lymphovascular invasion (LVI) were found to have a significant impact on DFS as well as on OS. In the multivariate analysis only age (HR=1.79; 95%CI=1.14-2.82; p=0.012) and nodal status (HR=2.71; 95%CI=1.64-4.46; p<0.001) retained their independent prognostic value for DFS and for OS only the nodal status (HR=2.96; 95%CI=1.51-5.82; p=0.002).

Conclusions. In our series of TNBC pts nodal status and age (older than 65 yrs) were found to be independent prognostic factors for DFS, whereas for OS only the nodal status. We found a pattern of a high recurrence rate in the first 3 years following the diagnosis and a decline in the recurrence rate over the next 3 yrs with higher rate of distal versus local recurrence and a predominant localization of distal metastases in visceral organs.

Key words: triple negative breast cancer; prognostic factors; treatment outcome

Introduction

Breast cancer is the most common female cancer worldwide. It is a heterogeneous disease with regard to biological behaviour, responses to treatment and prognosis.[1,2]

Seventy to 80% of all breast cancers are positive for estrogene (ER) or progesterone receptors (PgR). In contrast, the human epidermal growth factor receptor (HER2) protein overexpression and/or HER2 gene are overexpressed and/or amplified, respectively, in approximately 15-20% of the patients only, with around half of these coexpressing hormone receptors. The remaining 10-15% of breast cancers is negative for ER, PgR and HER2. These are defined as triple negative breast cancer (TNBC).[3]

Among all the breast cancer subtypes, TNBC is associated with a worse prognosis. It has a characteristic recurrence pattern with the peak risk of recurrence and the majority of deaths occurring in the first 3 and 5 years after the initial treatment, respectively. Comparing to endocrine sensitive tumours, the risk for the late recurrence (beyond 5 years after the diagnosis) decreases by 50%.

Over the past decade, the landscape of breast cancer has changed. Steroid hormone receptors such as ER and PgR in concert with the HER2 still remain critical determinants of breast cancer subtypes and the treatment decision in daily clinical

practice. But the development of microarray techniques evidenced inhomogeneous gene expression profiles and further divided breast cancer into several subtypes: luminal A, luminal B, HER2-enriched, and »basal-like« subtype. Both luminal A and B are clinically characterized by the expression of hormone receptor-related genes, whereas both HER2-enriched and the »basal-like« subtypes (BLBC) are less likely to express either ER or PgR. Moreover, the BLBC subtype is more commonly negative for all three markers. Subtypes vary in prognosis, with worse outcomes traditionally seen among the two hormone receptor negative subgroups compared to luminal subgroups.

Although frequently referred to interchangeably, the terms TNBC and »basal-like« are not completely synonymous. The term TNBC, namely, refers to the immunohistochemical classification of breast tumours lacking ER, PgR, and HER2 protein expression, whereas the »basal-like« subtype is defined via the gene expression microarray analysis. BLBC is, thus, characterized by the lack of expression of ER, PgR and HER2 (triple negative) as well as the increased expression of basal cytokeratins such as CK 5/6 and CK17. Although most BLBC do not express ER, PgR, HER2, a small number do and, therefore, the overlap between BLBC and TNBC is not complete. However, the triple negative phenotype currently serves as a reliable surrogate in the clinical practice.[4] The heterogeneous nature of breast cancer has implications for physicians and their patients. Increasingly treatments are targeted toward molecular markers.

Because of the lack of expression of hormonal receptors and HER2, chemotherapy (ChT) remains the only systemic therapeutic option in the adjuvant and metastatic setting of this disease. Currently, no specific targeted approach is available for TNBC outside clinical trials.

The aim of our retrospective study was to analyse the clinicopathological characteristics and prognostic significance of putative prognostic factors in breast cancer as well as to determine short- and long-term outcomes in a group of consecutively treated patients with TNBC at the Institute of Oncology Ljubljana.

Patients and methods

Patients

In our retrospective analysis, we included 296 consecutively treated patients with TNBC treat-ed from March 2000 until December 2006 at the Institute of Oncology Ljubljana. Patients with TNBC were identified from the database of the Department of Pathology. The established clinical and histomorphological factors such as menopausal status, pathological tumour size, tumour type, tumour grade, nodal status and hormonal receptor and HER-2 status as well as LVI were determined.

Methods

We retrieved information on tumour characteristics from the pathology reports in the medical records of patients at the Institute of Oncology Ljubljana.

Tumour type was determined according to the UICC-WHO criteria and tumour grading was performed according to the Nottingham scheme.[5] The steroid hormone receptor status was assessed by immunohistochemistry (IHC), using monoclonal rabbit ER antibody Clone SP1 (Neomarker) and monoclonal mouse anti-human PR antibody, Clone PgR 636 (Dako). Tumours were categorized as ER or PR positive if nuclear staining was observed in at least 10% of nuclei. The HER2 protein expression was determined by IHC using FDA approved HercepTest™ K5206 (DAKO) according to the recommended protocol. The membrane staining intensity and the pattern of the invasive component was evaluated according to Dako Cytomation's 'Atlas for Interpretation of HercepTest™'. Tumours were classified as IHC score 0 (negative) if no membrane staining or staining in less than 10% of the tumour cells was observed, an IHC score 1+ (negative) if a faint or barely perceptible partial membrane staining was detected in more than 10% of tumour cells, an IHC score 2+ (weakly positive) if weak or moderate complete membrane staining was observed in more than 10% of tumour cells and an IHC score 3+ (strongly positive) if complete strong membrane staining was observed in more than 10% of tumour cells.

The HER2 gene amplification was determined by dual-colour fluorescence *in situ* hybridisation (FISH) using FDA approved PathVysion® HER2 DNA probe kit and Paraffin pretreatment kit (both Abbot-Vysis). After whole slides were screened, HER2 gene and chromosome 17 centromere signals were counted in at least 20 nuclei and gene/centromere ratio was calculated. If the ratio was borderline (between 1.7-2.3), signals were counted in additional 40 nuclei and ratio was calculated

again. Tumours were classified as 'not amplified' (FISH-) if the calculated ratio was less than 2 and 'amplified' (FISH+) if the ratio was 2 or greater. The tumour was characterized as triple negative if hormone receptor status as well as HER2 status were both negative.

For urokinase plasminogen activator (uPA) and plasminogen activator inhibitor (PAI-1) determination, the tumour specimens were obtained by surgery and stored in liquid nitrogen until the extraction. The frozen tumour tissue samples were pulverized using a micro-dismembrator. The tumour powder was suspended in buffer (pH 8.5) containing 0.02 M Tris-HCl, 0.125 M NaCl and 2% Triton X-100 and shaken for 3 hours at 4ºC. The obtained suspension was then centrifuged for 30 min at 100000 x g. Protein content was determined according to the Pierce assay. Both biological markers were determined in tumour detergent extracts by commercially available enzyme-linked immunosorbent assays (American Diagnostica Inc., Greenwich, CT). Statistically optimized cut-off values were assigned for uPA (3 ng/mg protein) and PAI-1 (14 ng/mg protein).

Treatment decisions regarding the primary surgery and the adjuvant systemic therapy were based primarily on consensus recommendations at the time. After the completion of the primary treatment, patients underwent regular follow-up examinations at our institute.

All the procedures were in accordance with the ethical standards of our institute's Ethical Committee.

Statistical methods

The endpoints in this study were disease-free survival (DFS) and overall survival (OS). DFS was calculated from the date of the start of the primary therapy to the date of the breast cancer recurrence, the date of death from any cause, or the date of the last follow-up. OS was calculated from the date of the start of the primary therapy and death of any cause. DFS and OS as a function of the markers studied were estimated by the Kaplan-Meier method and the log-rank test was used to test for differences. The Cox multivariate hazards models were used to calculate the hazard ratios (HR) and their 95% confidence intervals (95% CI) in the analysis of DFS and OS. Computations were performed with the use of the SPSS 18 statistical package. The differences in the treatment between age groups were calculated using Pearson Chi-Square test. All reported p values are two tailed.

TABLE 1. Patient and tumour characteristics

Characteristic	Number	% (of known)
Age (median, range)	55 (23-88.5)	
Menopausal status		
pre/perimenopausal	104	39.7
postmenopausal	158	60.3
unknown	7	
Tumour type		
invasive ductal	244	90.7
invasive lobular	10	3.7
other invasive	15	5.6
Size		
≤ 2 cm	107	41.0
>2cm	154	59.0
unknown	8	
LVI		
no	189	75.3
yes	62	24.7
unknown	18	
Grade		
I	7	2.7
II	39	14.8
III	217	82.5
unknown	6	
Nodal status		
positive	123	46.1
negative	144	53.9
unknown	2	
uPA		
<3 ng/mg protein	44	23.8
≥ 3 ng/mg protein	141	76.2
unknown	84	
PAI-1		
<14 ng/mg protein	73	39.5
≥ 14 ng/mg protein	112	60.5
unknown	84	
Chemotherapy regimen (adjuvant or neoadjuvant)		
without chemotherapy	53	19.7
anthracycline based	129	48
CMF	31	11.5
anthracyclines and taxanes	53	19.7
other	3	1.1
Localisation of first relapse (N=85)		
local relapse only	6	7.1
visceral ± other localisations	57	67.1
soft tissues and bones	3	3.5
soft tissues only	7	8.2
bones only	12	14.1

LVI = lymphovascular invasion; uPA = urokinase plasminogen activator; PAI-1 = plasminogen activator inhibitor; CMF = cyclophosphamide, methotrexate and 5-fluoracil

Results

Patients

At the time of the primary treatment, none of the patients had any evidence of distant metastases. The tumour's, patient's and treatment characteristics are presented in Table 1. The median age of the patients was 55 years (range, 23-88.5). The majority

of women were postmenopausal at the presentation (60.3%).

Patients were more likely to have grade III tumours (82.5%), tumour size was larger than 2 cm in almost two thirds (59%). At least one axillary lymph node was positive in 46.1% of patients. One third of the tumours were positive for lymphovascular invasion (LVI). Of 185 patients with determined uPA and PAI-1 value, 141 had uPA ≥3 ng/mg and 112 patients PAI-1 ≥ 14 ng/mg.

All the patients underwent the radical local treatment. Most of the patients (80%) were treated with some kind of ChT.

Follow-up

The median follow-up was 5.9 years (range 0.3 –9.6 years). Six (7.1%) patients experienced local, 79 (92%) patients distal recurrence and 66 (24%) died. After 5 years of follow-up the relapse developed only in 6 patients and only 4 died.

Survival plots

The 5-year DFS was 68.2% and the 5-year OS was 74.5%. Survival curves are shown in the Figures 1 and 2.

Univariate and multivariate survival analysis

In the univariate analysis age, nodal status, size, and LVI were found to have significant impact on DFS as well as on OS while the menopausal status, tumour grade, uPA and PAI-2 had none.

In the multivariate analysis (Cox model) for DFS, age and nodal status retained its independent prognostic value. The patients with positive lymph nodes had a 2.71-fold higher risk of relapse (95%CI = 1.64-4.46). The risk of relapse was 1.79-fold higher in patients younger than 65 years compared with older patients (95%CI = 1.14-2.82). For OS only nodal status was an independent prognostic factor. The risk of death was 2.96 higher in patients with positive lymph nodes (95%CI = 1.51-5.82) (Table 2).

Discussion

Emerging data on the clinical implication of the triple-negative phenotype indicate an aggressive course of this disease. Despite the widespread acknowledgment of the poor clinical outcome of TNBC, the prognostic value of specific morpholog-
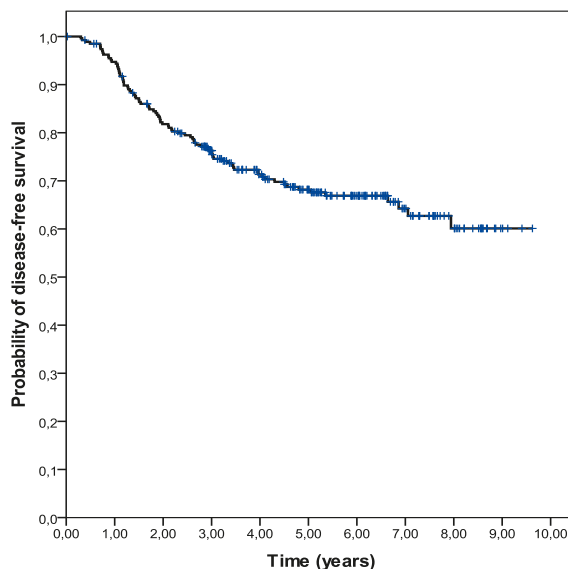
FIGURE 1. Disease-free survival (DFS) in 269 triple negative breast cancer (TNBC) patients.
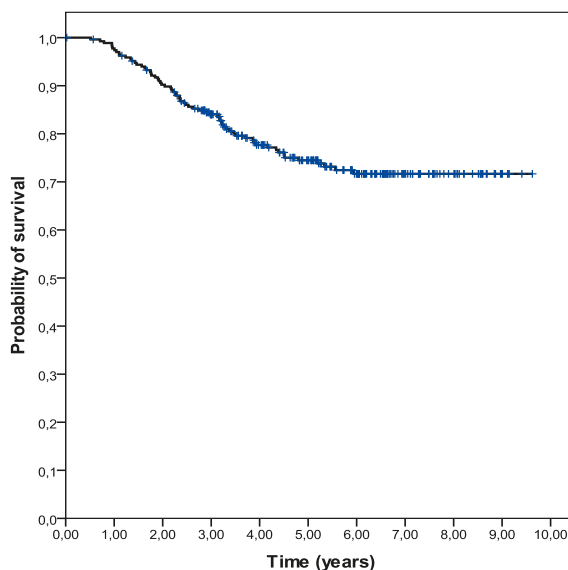
FIGURE 2. Overall survival (OS) in 269 triple negative breast cancer (TNBC) patients.

ical and biological features of these tumours continues to raise a substantial degree of uncertainty and controversy.

To date, studies on patients with TNBC have been limited mostly by the small sample sizes and short follow-up times. Our retrospective analysis was conducted in a relatively large number of consecutive patients (296) treated in the routine clinical practice with the median follow-up time of almost 6 years.

The majority of our TNBC patients had relatively large tumours at presentation (>2cm in 59% of patients), predominant type of tumour was inva-

TABLE 2. Univariate and multivariate analysis (Cox model) for 269 TNBC patients

	PFS			OS		
	univariate	multivariate		univariate	multivariate	
Characteristic	p	p	HR (95%CI)	p	p	HR (95%CI)
Menopausal status (pre/peri vs. postmenopausal)	0.172	-	-	0.278	-	-
Age (≥65yrs vs <65 yrs)	0.009	0.012	1.79 (1.14-2.82)	0.035	ns	-
Nodal status (positive vs. negative)	<0.001	<0.001	2.71 (1.64-4.46)	0.001	0.002	2.96 (1.51-5.82)
Size (>2cm vs. ≤ 2 cm)	0.004	ns	-	0.002	ns	-
Grade (III vs. I+II)	0.315	-	-	0.917	-	-
LVI (yes vs .no)	<0.001	ns	-	0.006	ns	-
uPA (≥ 3 ng/mg prot vs. <3)	0.827	-	-	0.732	-	-
PAI-1 (≥ 14 ng/mg prot vs. <14)	0.487	-	-	0.632	-	-
ChT regimen (anthracycline based vs. anthracycline + taxanes vs. CMF)	0.234	-	-	0.071	-	-

LVI = lymphovascular invasion; uPA = urokinase plasminogen activator; PAI-1 = plasminogen activator inhibitor; ChT = chemotherapy; CMF = cyclophosphamide, methotrexate and 5-fluoracil

sive ductal carcinoma (90.7%), the majority of tumours were poorly differentiated (82.5%), almost half of patients had positive axillary lymph nodes at presentation (Table 1). Also in some previous reports triple-negative tumours were described as relatively large tumours (>2cm) with a high rate of node positivity.[1,3,5] Similar to our study also other investigators found that characteristically TNBC exhibit an invasive ductal histology and a high histologic grade, present with high mitotic index, frequent apoptotic cells and carry central necrotic zones and pushing borders as well as a conspicuous lymphocytic infiltrate.[1,4,6] In the population based Carolina Breast Cancer Study (CBCS), basal like breast cancers (defined by triple negative status plus EGFR or cytokeratin 5 positivity) were virtually all of ductal or mixed histology (90%), and of high grade (84%), which is similar to our results.[7]

In our analysis, the prognostic significance of putative well-known prognostic factors was assessed. We considered well-established prognostic factors such as menopausal status, age, nodal status, size of the tumour, grade, the presence of LVI, uPA, PAI-1, and type of adjuvant ChT. In the multivariate analysis only age and nodal status were found to be independent prognostic factors for DFS, whereas for OS only nodal status.

In patients older than 65 years the risk of relapse was 1.79-fold higher compared with younger patients (95%CI= 1.14-2.82, p=0.012). The explanation for this finding is probably in the difference in the treatment modality which is one of the most important prognostic factor in oncological patients.[8] Due to the fact, that the elderly patients were treated with adjuvant ChT in a significantly smaller proportion compared to younger patients (46.8 vs. 91.1%, p< 0.001) such result was not surprising.

Since the nodal status is well established as one of the strongest prognostic factor in breast cancer, it was expected to show its prognostic value also in our study. The patients with positive lymph nodes had a 2.71-fold higher risk of relapse (95%CI= 1.64-4.46, p=0.002) and 2.96 higher risk of death (95%CI= 1.51-5.82, p<0.001) comparing to patients with negative axillary lymph nodes. These results are in line with some other studies.[1,7,9,] However, some other studies did not confirm the prognostic significance of the nodal status in TNBC[10,11], therefore, the earlier detection[12], which can improve OS in breast cancer patients, needs to be demonstrated.

Next to nodal status and age, tumour size and LVI were found as prognostic markers in the univariate analysis but lost the independency in multivariate analysis. In multiple recently published

studies these tumour characteristics were demonstrated as important prognostic factors.[9,13,14]

The results from published literature showed that patients with TNBC have an increased likelihood of distant recurrence and of death compared to women with other types of breast cancer. The pattern of recurrence is also qualitatively different. In our analysis, we found a pattern of high recurrence rates in the first 3 years following the diagnosis and a clear decline in recurrence rate over the next 3 years (Figure 1). The study of Dent *et al.*, which included large cohort of 1601 breast cancer patients demonstrated increased likelihood of distant recurrence (HR 2.6; 95%CI 2.0-3.5; p<0.0001) and death (HR 3.2; 95%CI 2.3-4.5; p<0.0001) within 5 years of diagnosis in the subgroup of 180 TNBC patients. On the contrary, among other, non-TNBC group, the recurrence risk was mostly constant over the period of the follow up.[13] The study evaluating the response to neoadjuvant ChT among more than 1000 patients treated at the University of Texas M.D. Anderson Cancer Center corroborated the above prognostic findings. Results demonstrated decreased 3-years progression free and overall survival rates for triple-negative compared with non- triple-negative breast cancer. Consistently with previous reports, recurrences and death rates were higher only in the first 3 years following the diagnosis.[15] The observed pattern speaks of the early aggressive nature of TNBC. Thus despite having a high risk of early recurrence, it seems that women with TNBC who are disease free after 5 years are unlikely to die of breast cancer.

Few women (7.1%) in our study cohort experienced a local before distal recurrence. This result is in line with some other studies.[9,13,14] The high rate of distal recurrence and the relative rarity of local recurrences suggest that the mode of spread of these cancers is haematogenous and that these patients have a tendency to develop visceral metastases early in the course of their disease.

In addition to patterns observed in the timing of recurrence, the preferential site of relapse has also been identified among TNBC.[1,4] Predominant localisation of the first relapse in our study were visceral organs (67.1%). Liedke *et al.* reported that TNBC patients have likewise higher rates of recurrence in visceral organs with lower rates of bone disease (74 vs. 13%, p=0.027), compared with hormone sensitive tumours.[14] In the largest report to date, data on 12 858 patients, 2143 of them were triple negative, indicate on increased risk for lung and brain metastases as first site of recurrence and a lower risk for bone recurrence in patients with

TABLE 3. Treatment differences according to age groups. Comparison of proportion of patients treated with adjuvant chemotherapy (ChT) according to age

Age group	ChT yes (%)	ChT no (%)
≥ 65 years (N=77)	41 (53.2)	36 (46.8)
< 65 years (N=192)	175 (91.1)	17 (8.9)
p<0.001*		

* Pearson Chi-Square

TNBC.[15] Recent studies also indicate the increased incidence and uniquely aggressive nature of brain metastases in TNBC patients compared with other subtypes. Beside that diagnosis of central nervous spread is mostly followed by the shorter median survival of 3-5 versus 7-12 months in patients with TNBC compared with non-TNBC.[1,4]

It is not yet certain whether the poor prognosis of TNBC is due to the aggressive behaviour or because of the lack of the targeted therapy. The results from neoadjuvant and metastatic studies show that TNBC is relatively chemosensitive disease, with a good initial response to anthracycline and anthracycline/taxane ChT, but with a rapid relapse rate.[1,15,17,18] In our cohort 80% of patients received adjuvant ChT. The majority of them were treated with anthracycline based ChT (60%), a quarter of patients received anthracyclines beside taxanes as well and only minority combination of cyclophosphamide, methotrexate and 5-fluoracil (CMF) (Table 1). We did not find a significant difference in outcome according to the treatment schedule.

To date novel therapeutic options are needed to target this aggressive type of breast cancer. Because of the lack of expression of hormonal receptors and HER2, ChT still remains the only possible systemic therapeutic option in the adjuvant and metastatic setting. There is currently no specific systemic regimen recommended for the treatment of TNBC and there is little data on which to base the treatment selection. Numerous efforts are currently being undertaken to improve prognosis for patients with TNBC. They comprise both optimization of choice and scheduling of common cytotoxic agents as well as the introduction of novel targeted agents. In terms of ChT DNA-damaging platinum chemotherapeutic agents are quickly emerging as the ChT »backbone« of choice in TNBC, especially when combined with novel agents such are poly ADP-ribose polymerase 1 (PARP1) inhibitors. Tumours with BRCA1 dysfunction, the majority of which are triple negative, namely harbour deficient

double-stranded DNA break repair, which leads to increased sensitivity to these agents. The association between BRCA1 dysfunction and TNBC has led to several studies in metastatic and adjuvant/neoadjuvant setting evaluating platinum agents in the setting of TNBC.[1]

As we are gaining a deeper understanding of the biology processes driving triple-negative breast cancer, the arena of targeted therapeutic agents is evolving. Potential targets for the treatment include: surface receptors such as epidermal growth factor receptor (EGFR), or c-Kit; protein kinase components of the mitogen activated protein (MAP)-kinase pathway; protein kinase components of the protein kinase B (Akt) pathway; induction of DNA damage by specific chemotherapy agents that cause interstrand and double-stranded breaks; and inhibition of already defective DNA repair by PARP1 inhibition.[6] New knowledge on TNBC biology has, thus, revealed several promising targeted strategies, next to PARP1 inhibitors also EGFR-targeted agents (cetuximab), antiangiogenic agents (bevacizumab), inhibitors of Src-family kinases (dasatinib), histone deacetylase inhibitors and others, which are currently being tested in ongoing studies.[1] One of the most exciting finding in the field of TNBC are definitely PARP-1 inhibitors. Results from two phase II clinical trial with two of them were presented in year 2009. A single arm trial of olaparib as single agent showed promising results in BRCA-deficient population.[19] In randomised phase II study BSI-201 in combination with ChT with carboplatin and gemcitabine significantly improved overall and progression-free survival in women with metastatic TNBC, compared with ChT alone.[20]

Conclusions

In conclusion, reviewing our data we were able to confirm that the TNBC is aggressive disease with a distinct pattern of recurrence. This pattern is characterized by a rapidly raising rate of recurrence within the first 3 years after the diagnosis and by a decline in a recurrence risk after 5 years from the diagnosis. Given that fact and the high risk of visceral metastases, these breast cancer patients may require closer surveillance in the initial years of the follow-up. However, the hypothesis that earlier detection and aggressive therapy of metastatic recurrence could improve survival needs to be demonstrated. Current results illustrate the need to develop novel therapeutic alternatives for this subgroup of patients.

References

1. Gluz O, Liedtke C, Gottschalk N, Pustzai L, Nitz U, Harbeck N. Triple-negative breast cancer-current status and future directions. *Ann Oncol* 2009; **20:** 1913-27.

2. Podkrajšek M, Žgajnar J, Hočevar M. What is the most common mammographic appearance of T1a and T1b inasive breast cancer? *Radiol Oncol* 2008; **42:** 173-80.

3. Dawson SJ, Provenzano E, Caldas C. Triple negative breast cancers: Clinical and prognostic implications. *Eur J Cancer* 2009; **45:** 27-40.

4. Anders KC, Carey LA. Biology, metastatic patterns, and treatment of patients with triple-negative breast cancer. *Clin Breast Cancer* 2009; **9(Suppl 2):** S73-81.

5. Elston CW, Ellis IO. Pathological prognostic factors in breast cancer. The value of histological grade in breast cancer: experience from a large study with long-term follow-up. *Histopathology* 1991; **19:** 403-10

6. Cleator S, Heller W, Coombes RC. Triple-negative breast cancer: therapeutic options. *Lancet Oncol* 2007; **8:** 235-44.

7. Carey LA, Perou CM, Livasy CA, Dressler LG, Cowan D, Conway KS, et al. Race, breast cancer subtypes, and survival in the Carolina Breast Cancer Study. *JAMA* 2006; **295:** 2492-502.

8. Debevec L, Jeric T, Kovac V, Bitenc M, Sok M. Is there any progress in routine management of lung cancer patients? A comparative analysis of an institution in 1996 and 2006. *Radiol Oncol* 2009; **43:** 47-53.

9. Tian XS, Cong MH, Zhou WH, Zhu J, Chen YZ, Liu Q. Clinicopathologic and prognostic characteristics of triple-negative breast cancer. *Onkologie 2008*; **31:** 610-4.

10. Shibuta K, Ueo H, Furusawa H, Komaki K, Rai Y, Sagar Y, et al. The relevance of intrinsic subtype to clinicopathological features and prognosis in 4266 Japanese women with breast cancer. *Breast Cancer* 2010; Jun 23. [Epub ahead of print]. DOI: 10.1007/s12282-010-0209-6.

11. Nishimura R, Arima N. Is triple negative a prognostic factor in breast cancer? *Breast Cancer* 2008; **15:** 303-8.

12. Dent R, Trudeau M, Pritchard KI, Hanna WM, Kahn HK, Sawka CA, et al. Triple-negative breast cancer: clinical features and patterns of recurrence. *Clin Cancer Res* 2007; **13:** 4429-34.

13. Plesnicar A, Golicnik M, Fazarinc IK, Kralj B, Kovac V, Plesnicar BK. Attitudes of midwifery students towards teaching breast-self examination. *Radiol Oncol* 2010; **44:** 52-6.

14. Viale G, Rotmensz N, Maisonneuve P, Bottiglieri L, Montagna E, Luini A, et al. Invasive ductal carcinoma of the breast with "triple-negative" phenotype: prognostic implications of EGFR immunoreactivity. *Breast Cancer Res Treat* 2009; **116:** 317-28.

15. Liedke C, Mazouni C, Hess KR, Andre F, Tordai A, Mejia JA, et al. Response to neoadjuvant therapy and long-term survival in patients with triple-negative breast cancer. *J Clin Oncol* 2008; **26:**1275-81.

16. Lin NU, Vanderplas A, Hughes ME, Theriault R L, Edge SB, Wong Y, et al. Clinopathological features and sites of recurrence according to breast cancer subtype in the National Comprehensive Cancer Network (NCCN). [Abstract]. *J Clin Oncol* 2009; **27(15 Suppl):** Abstract 543.

17. Keam B, Im SA, Kim HJ, Oh DY, Kim JH, Lee SH, et al. Prognostic impact of clinicopathological parameters in stage II/III breast cancer treated with neoadjuvant docetaxel and doxorubicin chemotherapy: paradoxical features of the triple negative breast cancer. *BMC Cancer* 2007; **7:** 203.

18. Carey LA, Dees EC, Sawyer L, Gatti L, Moore DT, Collichio, et al. The triple negative paradox: primary tumor chemosensitivity of breast cancer subtypes. *Clin Cancer Res* 2007; **13:** 2329-34.

19. Tutt A, Robson M, Garber JE, Domchek S. Phase II trial of the oral PARP inhibitor olaparib in BRCA-deficient advanced breast cancer. [Abstract.] *J Clin Oncol* 2009; **27(Suppl 18):** 803s.

20. O'Shaughnessy J, Osborne C, Pippen J, Yoffe M, Patt D, Monaghan G, et al. Efficacy of BSI-201, a poly (ADP-ribose) polymerase-1 (PARP1) inhibitor, in combination with gemcitabine/carboplatin (G/C) in patients with metastatic triple-negative breast cancer (TNBC): Results of a randomized phase II trial. [Abstract]. *J Clin Oncol 2009*; **27(Suppl 18):** 793s.

Metastatic tumours to the thyroid gland: report of 3 cases and brief review of the literature

Enver Vardar[1], Nazif Erkan[2], Umit Bayol[1], Cengiz Yılmaz[3], Murat Dogan[2]

[1] SB Izmir Tepecik Teaching Research Hospital, Pathology Department, Turkey
[2] SB Izmir Bozyaka Teaching Research Hospital, Surgery Department, Turkey
[3] SB Izmir Bozyaka Teaching Research Hospital, Radiology Department, Turkey

Correspondence to: Nazif Erkan, M.D., Assoc. Prof. of Surgery, Flamingo 9 D: 39 Mavişehir Karşıyaka, İzmir, Turkey. Phone: +90 505 530 7807; Fax: +90 232 227 7201; E-mail: naziferkan@gmail.com

Background. Metastases to the thyroid are encountered rarely in clinical practice, but the number of cases seems to have increased in recent years. The reason of this increase may be a more frequent use of fine-needle aspiration biopsy (FNAB) and the use of more sophisticated, complicated imaging techniques in patients with thyroid masses. Also, in addition to these reasons, the use of more organo-specific immunohistochemical antibodies in the examination of surgical specimens may affect the differential diagnosis of malignant tumours.

Case reports. Three metastatic tumours to thyroid were found in the retrospective review of malignant thyroid tumours diagnosed between January 1993 and December 2007. The primary tumours were clear cell carcinoma of the kidney, squamous cell carcinoma of the lung and breast carcinoma-ductal type.

Conclusions. A detailed clinical history, careful histological examination and essential immunohistochemistry helped in attaining the correct diagnosis.

Key words: metastatic tumours; thyroid malignancy; secondary malignancies

Introduction

Despite being 2nd only to the adrenal gland in the relative vascularisation, the thyroid gland is rarely the site of the significant metastatic disease.[1] Metastatic tumours to the thyroid are seen rarely in clinical practice, but the incidence varies from 1.25% to 24.2% in autopsy series.[2-8] In autopsy series, the metastasis is usually associated with the vascular tumour embolus from tumour located in distant organ malignancy or with the direct invasion of the thyroid by a malignant focus located in the adjacent organs.[5-8] Most commonly, the primary tumour is located in the lung, gastrointestinal system, breast and kidney. Secondary tumours of the thyroid are seen almost always with metastases of other organs and systems. The surgical resection was rarely performed in the metastasis to the thyroid gland due to the presence of the phenomenon of secondary tumours of the thyroid which is rarely discernible clinically. And because of this,

the metastasis to the thyroid gland is rarely seen on the routine pathology practice. The metastasis to the thyroid gland is usually considered as a terminal event, and the effectiveness of the conventional treatment has been questioned.[2-4,7] Sporadic reports and small case series were published in the literature. We report three cases of metastatic malignancy to the thyroid with the review of the literature.

Case reports

Case 1

A 54-year-old Caucasian male presented to the outpatient clinic with the enlargement on the right thyroid lobe noted approximately 2 months earlier. In his medical history he was operated due to clear cell carcinoma of the right kidney three years ago. The pathological examination of the kidney was revealed as pT3N1M0, Grade 2. Then the adjuvant

FIGURE 1A. Large, two solid tumour islands separated with fibrous septum and normal thyroid acini (upper left) were seen (HE-X40).

FIGURE 1B. Diffuse, strong CD10 positivity were seen in neoplastic areas especially located in right part of the image (X100).

the thyroid that were thought to be an adenoma or a nodule of colloidal goitre. A fine needle aspiration biopsy of the thyroid revealed some mildly pleomorphic and hyperchromatic cells and due to this suspicious ctyological finding consistent with malignancy, bilateral near total thyroidectomy was performed.

The pathological specimen measured 5.5 x 5 x 3 cm and showed two nodules, each of them located at different lobe and measured up to 2.0 cm in the greatest dimension. A microscopic examination showed the diffuse proliferation of acinary structures and large sheets of neoplastic cells in the adjacent acini with the extension into the thyroid follicular tissue. The neoplastic cells had a moderate amount of clear, vacuolar or mildly eosinophilic granular cytoplasm and pleomorphic, hyperchromatic nuclei with large nucleoli. Many of the cells showed multinucleation, nuclear lobulation and high mitotic activity, as shown on immunohistochemical staining of tumour tissue sections (Figure 1A). CD10 (Figure 1B), vimentin and pancytokeratin positivity, however, in the same tumour areas cells were negative with TTF-1 (Figure 1C), thyroglobulin and calcitonin.

The patient was uneventful after the operation, and the adjuvant chemotherapy treatment for the metastatic disease was planned, however, he again refused chemotherapy. Eighteen months after the thyroid surgery, he was admitted to our emergency service with right hemiplegia. Cranial CT revealed a metastatic tumour and he was operated for brain metastases. During operation, the metastasis was removed successfully but he died due to pulmonary embolia 5 days after the operation.

Case 2

A 63-year-old Caucasian male presented with a growing thyroid mass over the past 2 months. The clinical examination showed the enlarged right lobe of the thyroid. Ultrasonography and computed tomography (CT) scan of the thyroid revealed a growing single nodule in the right lobe and the diameter of the nodule measured 1.4 cm. The patient was operated due to the presence of lung malignancy eleven months before and diagnosed as primary squamous cell carcinoma of the right lung. After right lobectomy, pathology was reported as pT2N2M0, Stage 3A. The central nervous system, bilateral neck, liver and spleen were normal. Adjuvant chemotherapy that consisted of cisplatin and etoposide regimen was given postoperatively.

chemotherapy and the interferon treatment were planned but he refused any treatment and he has been followed after the operation by routine examinations such as liver functions (SGOT, SGPT, alkaline phosphatase, GGT, bilirubin levels), urea, creatinine levels, abdominal ultrasonography, bone scintigraphy, chest X-ray.

During that follow up period, the patient had no symptoms and routine tests were within normal limits. The physical examination after three years revealed solitary nodule on the right lobe of

TABLE 1. General characteristics of the patients

	Age	Gender	Primary tumour surgery	Primary tumour diagnosis	Metastasis in thyroid
Case 1	54	Male	Nephrectomy	Kidney renal cell carcinoma	Bilateral
Case 2	63	Male	Lung lobectomy	Lung squamous cell carcinoma	Unilateral right
Case 3	43	Female	Mastectomy+ axillary dissection	Breast ductal carcinoma	Unilateral left

The fine needle aspiration biopsy of the thyroid right lobe of the patient demonstrated distinct malignant cytologic findings and after that total thyroidectomy was performed and sent for a histopathological examination. The microscopic examination showed thyroid tissue partially replaced by a neoplastic infiltrate composed of pleomorphic cells in bilateral lobe in addition to nodule located in the right lobe of the thyroid. Some of the cells have intercellular desmosomes and keratinisation that the hallmark of squamous cell carcinoma (Figure 2). Desmoplastic stroma was seen mainly in between squamous cell carcinoma areas. TTF-1, thyroglobulin, calcitonin, CK20 and CK7 were negative in metastatic tumour areas.

The patient died after 6 months due to disseminated metastases.

Case 3

A 43-year-old female was admitted with complaints of a mass in the thyroid for the past 2 months. The clinical examination showed the enlarged bilateral thyroid gland. An ultrasonography of the thyroid revealed diffuse enlargement and multinodular pattern. Left modified radical mastectomy and left axillary dissection were performed due to the presence of the malignant tumour in her left breast. Pathology was reported as pT2N2M0 and stage 3A invasive ductal carcinoma.

Radiotherapy and chemotherapy were applied and regular follow-ups were done for three years. Bilateral total thyroidectomy was performed and no problem was seen in the surgery of thyroid. In addition to the nodular appearance of cut surface, multiple, tiny whitish-solid areas were seen. In microscopic evaluation, findings consistent with colloidal goitre were seen. Also, between nodular structures of thyroid acini, small solid tumour islands were present (Figure 3A). Pleomorphic, hyperchromatic nuclei with mitotic figures were present in these tumour sheets. There were no
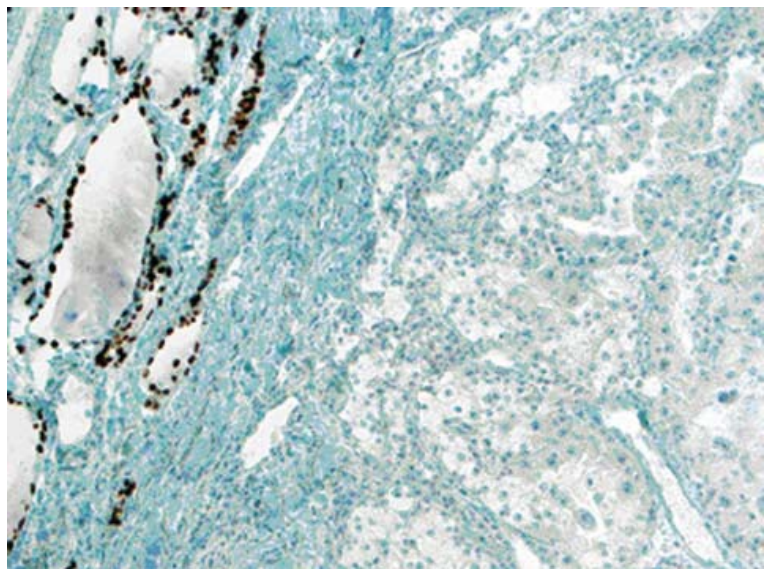
FIGURE 1C. TTF-1 positivity was seen in residual thyroid follicles located in left part of the image (X100).
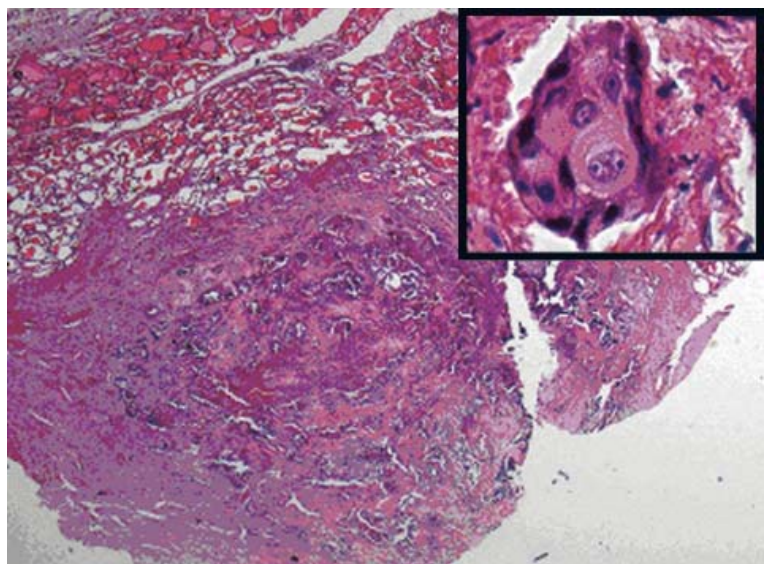
FIGURE 2. Large, solid tumour island contain necrosis in central portion were seen in above of the image. Residual normal thyroid follicles are present in left upper part of the image (HE-X20). Squamous differentiation consistent with acidophilic cytoplasm, vesicular nuclei and intercellular bridges were seen in tumour cells (inset) (HE-X400).
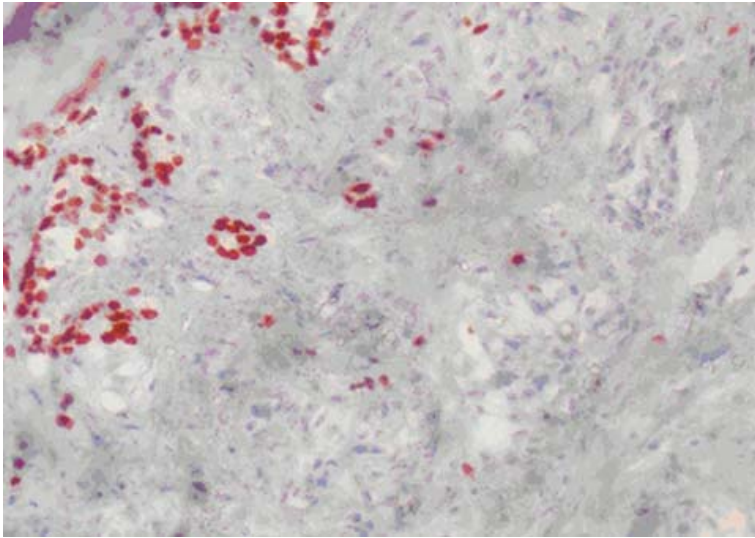
FIGURE 3A. Small, ductuli like tumour cells, residual thyroid follicles and pleomorphic tumour cells in high magnification and necrosis were seen (inset) (HE-X400).
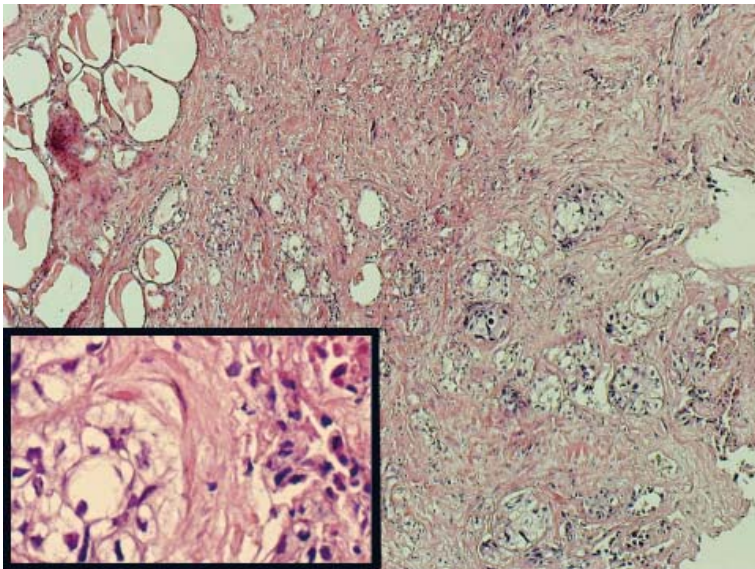
FIGURE 3B. TTF-1 nuclear immunreactivity were seen in residual thyroid follicles located in upper left corner of the image whereas tumour cells were negative in case 3 (X100).

specific findings except abortive glandular appearance. Immunohistochemically, tumour cells were stained with CK7 and focally with ER and metastatic tumour cells were negative with, progesterone, cerbB-2, TTF-1 (Figure 3B), thyroglobulin, CEA and calcitonin.

After the operation for the metastatic disease, the adjuvant chemotherapy was planned but she refused that treatment. The patient died after 22 months due to the disseminated metastases in liver and bone.

Since there are no specific tumour markers for squamous cell cancer of the lung, clear cell cancer of the kidney and invasive ductal cancer of the breast, we did not use any tumour marker for the detection of metastases or local recurrence of the disease during the follow-up of all three patients.

Discussion

The metastatic tumour to the thyroid gland is a rare malignant tumour of highly aggressive, commonly occurring in primary malignant tumours of kidney, gastrointestinal system, lung and breast.[1-4] As the above mentioned primary malignant tumours occur mostly in elderly population[9], also the metastatic malignancy to the thyroid gland is observed in the elderly individuals. They are in their sixth and seventh decades of life and the mean age of our patients were also approximately 60 years similar to that described in the literature.[10,11]

An objective estimate of the incidence of the clinical metastasis in the thyroid comes from recent series related with the fine-needle aspiration biopsy (FNAB) performed for tumours of thyroid, which report incidences of up to 7.5%.[12,13] FNAB revealed malignant cytologic features in two of the three patients, but interpreted as only malignancy without any additional comment related with primary or metastatic. The overall experience from series of the patients with metastases to the thyroid gland is variable, but a long-term survival after the surgical intervention to the thyroid is not reported frequently in the literature.[14-16]

The clinical history and the pathological diagnosis of the primary site malignancy largely influence the route of histopathologic diagnosis. In our first case, a definitive diagnosis requires absolutely the finding of positivity for CD10 and/or renal cell carcinoma antigen and negativity for thyroglobulin and TTF-1 in areas of clear cell carcinoma in the thyroid in order to differentiate the metastatic clear cell carcinoma of kidney from the primary clear cell malignancy from thyroid.

As in our second case, if patient has a history of primary squamous cell carcinoma of the lung, the differential diagnosis of squamoid malignancy located in the thyroid should be easy. The infiltrative pattern of the tumour in addition to disseminated tumour emboli in lymphatic vessels also should be helpful findings for the metastasis. Negativity of TTF-1 and thyroglobulin of tumour cells might be helpful in metastatic squamous cell carcinoma in the differentiation from the primary squamous

cell carcinoma of the thyroid that reported exceptionally.[17,18]

There is no very characteristic feature of the metastatic breast carcinoma especially lobular malignancy. To the best of our knowledge, a very few reports described immunohistochemical staining properties. In ductal type carcinoma, the presence of carcinoma containing comedonecrosis area should raise the possibility of the metastatic origin especially from the breast. Also, in addition to positivity of estrogen, progesteron, cerbB-2, gross cystic disease fluid protein-15 (GCDFP-15) and negativity of thyroglobulin, TTF-1, CEA and calcitonin will make possible the differential diagnosis of tumours originated from the breast. In our case, CK7 positivity and estrogen positivity were presented and markers like thyroglobulin, TTF-1, CEA and calcitonin were negative.

The management and the extent of surgery in metastatic involvement of the thyroid gland have not been firmly determined by a uniform international consensus. The management depends on the primary site of the original tumour, the presence of other metastases and symptoms caused by the thyroid mass. Generally, patients with the thyroid metastasis who have already demonstrated metastases to organs other than the thyroid gland had a poor prognosis.

On the other hand, in cases with the solitary thyroid metastasis, there have been several case reports showing that a long term survival is possible after thyroidectomy. The metastasis operation may improve a prognosis in certain cases also in other patients with the advance oncological disease.[19] Therefore, a surgical resection is regarded as the best treatment for a metastatic tumour, especially, if isolated, the solitary thyroid metastasis was found. There is also still a doubt about the extent operation in thyroid surgery because of the complications after total thyroidectomy.[20] If the metastasis is known preoperatively, lobectomy and isthmectomy are enough but when the diagnosis is doubtful or multifoci of metastasis are found, total tyhroidectomy is the choice of the surgical treatment.

There is also the possibility of metastases to cervical lymph nodes, but there is no data that determinate the importance of the lymph node dissection. However, when the diagnosis is established postoperatively only, based on the histopathological examination of the surgical specimen, a secondary radical procedure after previously performed subtotal thyroidectomy seems unwarranted. As the adjuvant treatment, chemotherapy and radiotherapy could be useful according to the type of primary cancer that metastases to the thyroid. Also the interferon treatment may be useful for metastatic clear cell cancer of kidney.[10,21,22] In cases with an anaesthetic risk or co-morbid condition that preclude surgery, the radiotherapy should be considered.

In our three cases, FNAB only shows suspicious of malignant cytology and the type of surgery is total thyroidectomy in two cases and bilateral near total thyroidectomy in one patient who accepted useful surgery for the malignant disease of the thyroid gland. Postoperatively, we could not use adjuvant chemotherapy since the patients refused it.

In conclusion, the occurrence of metastatic malignancy to the thyroid is very unusual. It should be considered in differential diagnosis of an atypical histological appearance of the unexpected course of the tumour of the thyroid. Very careful histopathological examination and immunohistochemical panel antibody study of the lesion are necessary to confirm the diagnosis. It is important to exclude a systemic dissemination of any primary tumour located elsewhere and the prognosis in a patient with metastatic malignancy located in the thyroid is poor. The appearance of the unusual histological type of tumour in thyroid should be considered seriously and warrants a detailed immunohistochemical panel. Metastases resection is the choice of the treatment in a case of the isolated solitary metastasis.

References

1. Willis RA. Metastatic tumors in the thyroid gland. *Am J Pathol* 1931; **7:** 187-208.

2. Abrams HL, Spiro R, Goldstein N. Metastases in carcinoma: analysis of 1,000 autopsy cases. *Cancer* 1950; **3:** 74-85.

3. Shimaoka K, Sokal J, Pickrea J. Metastatic neoplasms in the thyroid gland. *Cancer* 1962; **15:** 557-65.

4. Silverberg SG, Vidone RA. Metastatic tumors in the thyroid. *Pacif Med Surg* 1966; **74:** 175-80.

5. Boggess MA, Hester TO, Archer SM. Renal clear cell carcinoma appearing as a left neck mass. *Ear Nose Throat J* 1996; **75:** 620-2.

6. Berge T, Lundberg S. Cancer in Malmo 1958–1969. An autopsy study. *Acta Pathol Microbiol Scand* 1977; **Suppl 260:** 1-235.

7. Chen H, Nicol TL, Udelsman R. Clinically significant, isolated metastatic disease to the thyroid gland. *World J Surg* 1999; **23:** 177-81.

8. Chung SY, Kim EK, Kim JH, Oh KK, Kim DJ, Lee YH, et al. Sonographic findings of metastatic disease to the thyroid. *Yonsei Med J* 2001; **42:** 411-7.

9. Debevec L, Jeric T, Kovac V, Bitenc M, Sok M. Is there any progress in routine management of lung cancer patients? A comparative analysis of an institution in 1996 and 2006. *Radiol Oncol* 2009; **43:** 47-53.

10. Heffess CS, Wenig BM, Thompson LD. Metastatic renal cell carcinoma to the thyroid gland: a clinicopathologic study of 36 cases. *Cancer* 2002; **95:** 1869-78.

11. Cichoń S, Anielski R, Konturek A, Barczyński M, Cichoń W. Metastases to the thyroid gland: seventeen cases operated on in a single clinical center. *Langenbecks Arch Surg* 2006; **391:** 581-7.

12. Michelow PM, Leiman G. Metastases to the thyroid gland: diagnosis by aspiration cytology. *Diagn Cytopathol* 1995; **13:** 209-13.

13. Watts NB. Carcinoma metastatic to the thyroid: prevalence and diagnosis by fine-needle aspiration cytology. *Am J Med Sci* 1987; **293:** 13-7.

14. McCabe DP, Farrar WB, Petkov TM, Finkelmeier W, O'Dwyer P, James A. Clinical and pathologic correlations in disease metastatic to the thyroid gland. *Am J Surg* 1985; **150:** 519-23.

15. Nakhjavani MK, Gharib H, Goellner JR, van Heerden JA. Metastases to the thyroid gland: a report of 43 cases. *Cancer* 1997; **19:** 574-8.

16. Freund HR. Surgical treatment of metastases to the thyroid gland from other primary malignancies. *Ann Surg* 1965; **162:** 285-90.

17. Long JL, Strocker AM, Wang MB, Blackwell KE. EGFR expression in primary squamous cell carcinoma of the thyroid. *Laryngoscope* 2009; **119:** 89-90.

18. Eom TI, Koo BY, Kim BS. Coexistence of primary squamous cell carcinoma of thyroid with classic papillary thyroid carcinoma. *Pathol Int* 2008; **58:** 797-800.

19. Ocvirk J. Advances in the treatment of metastatic colorectal carcinoma. *Radiol Oncol* 2009; **43:** 1-8.

20. Besic N, Zagar S, Pilko G, Peric B, Hocevar M. Influence of magnesium sulphate infusion before total thyroidectomy on transient hypocalcemia – a randomised study. *Radiol Oncol* 2008; **42:** 143-50.

21. Wood K, Vini L, Harmer C. Metastases to the thyroid gland: the Royal Marsden experience. *EJSO* 2004; **30:** 583-88**.**

22. Lesalnieks I, Winter H, Bareck E, Sotiropoulos GC, Goretzki PE, Klinkhammer-Schalke M, et al. Thyroid metastases of renal cell carcinoma: clinical course in 45 patients undergoing surgery. Assesment of factors affecting patients survival. *Thyroid* 2008; **18:** 615-24.

case report

Mesenteric fibromatosis with intestinal involvement mimicking a gastrointestinal stromal tumour

Marek Wronski[1], Bogna Ziarkiewicz-Wroblewska[2], Maciej Slodkowski[1], Wlodzimierz Cebulski[1], Barbara Gornicka[2], Ireneusz W. Krasnodebski[1]

[1] Department of General, Gastroenterological and Oncological Surgery, Medical University of Warsaw, Warsaw, Poland

[2] Department of Pathology, Medical University of Warsaw, Warsaw, Poland

Correspondence to: Dr. Marek Wronski, Katedra i Klinika Chirurgii Ogolnej, Gastroenterologicznej i Onkologicznej WUM, ul. Banacha 1A, 02-097 Warsaw, Poland. Phone: +48-22-599 2482, Fax: +48-22-599 2057; E mail: mwronski@vp.pl

Disclosure: No potential conflicts of interest were disclosed.

Introduction. Mesenteric fibromatosis or intra-abdominal desmoid tumour is a rare proliferative disease affecting the mesentery. It is a locally aggressive tumour that lacks metastatic potential, but the local recurrence is common. Mesenteric fibromatosis with the intestinal involvement can be easily confused with other primary gastrointestinal tumours, especially with that of the mesenchymal origin.
Case report. We report a case of a 44-year-old female who presented with an abdominal mass that radiologically and pathologically mimicked a gastrointestinal stromal tumour.
Conclusions. The diagnosis of mesenteric fibromatosis should always be considered in the case of mesenchymal tumours apparently originating from the bowel wall that diffusely infiltrate the mesentery.

Key words: mesenteric fibromatosis; desmoid tumour; gastrointestinal stromal tumour; GIST; differential diagnosis;

Introduction

Mesenteric fibromatosis (MF) or intra-abdominal desmoid tumour is a rare proliferative disease affecting the mesentery. MF is a locally aggressive tumour that lacks metastatic potential, but the local recurrence is common. It resembles gastrointestinal stromal tumours (GIST) that are mesenchymal neoplasms of the digestive tract and show a varied malignant potential. Although GISTs and mesenteric fibromatosis are distinct entities, they are often confused clinically, radiologically and not uncommonly pathologically as well. Misdiagnosis might result in inappropriate therapeutic decisions and worse prognosis.

We report a case of a 44-year-old female who presented with an abdominal mass that initially suggested a gastrointestinal stromal tumour.

Case report

A 44-year-old female was admitted to our department because of the epigastric pain for the preceding two weeks. Her medical history was significant for arterial hypertension, Hashimoto thyroiditis and hypercholesterolemia. Her surgical history revealed a cesarean section. There were no desmoid tumours in her family.

The physical examination revealed a mass on palpation in the mid-abdomen that was easily movable. The physical examination was otherwise normal. Laboratory findings were unremarkable. The level of CEA was within normal limits. A transabdominal ultrasound (US) showed an ovoid well-delineated homogenously hypoechoic mass that was 10.1 x 6.0 x 7.2 cm in size. There was a hyperechoic area in the central part of the tumour with posterior acoustic shadowing that corresponded to intraluminal air. The tumour was circumferentially attached to the wall of the small bowel (Figure 1). An abdominal computed tomog-
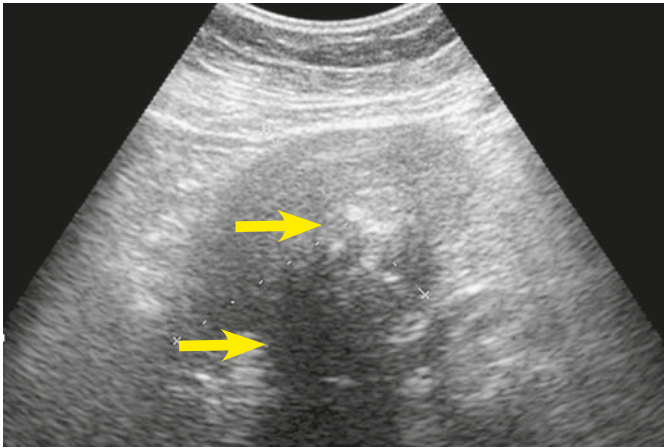
FIGURE 1. The sonographic appearance of an intra-abdominal desmoid with involvement of the small bowel: a well-defined grossly homogenous hypoechoic mass circumferentially encroaching the intestinal wall; the hyperechoic central part of the tumour corresponds to intraluminal air that results in posterior acoustic shadowing (arrows).

FIGURE 2. CT scan shows the desmoid tumour of the mesentery infiltrating the small bowel: a well-defined hypodense and homogenous mass diffusely attached to the bowel wall.

raphy (CT) revealed a 8.2 x 7.2 x 7.4 cm mass infiltrating the small bowel. The tumour attenuation was of 33 Hounsfield units and it enhanced poorly and homogenously with an intravenous contrast (Figure 2). The above preoperative imaging studies suggested a GIST involving the small bowel.

The patient underwent an elective laparotomy. Intraoperatively, there was an approximately 10 cm well-circumscribed mass in the mesentery that in-

filtrated the wall of the small bowel and narrowed its lumen (Figure 3). On inspection, there were also 2-3 small tubercules attached to the serosa of the adjacent bowel that were included within the resection margins. Several similar lesions were found along the distal part of the small bowel and one of them was excised for the pathological evaluation. This gross appearance suggested a gastrointestinal stromal tumour with the peritoneal dissemination. The resection of a 25 cm segment of the small bowel was performed. The postoperative course was uneventful and the patient was discharged in a good health condition. A follow-up US revealed no desmoid recurrence a year after the operation.

The primary pathological diagnosis in this particular case was a CD117-negative gastrointestinal stromal tumour. The small serosal tubercules were found to be mesothelial cysts. The principal diagnosis was changed, however, after a consultation at a referral oncological centre. The microscopic examination of the resected specimen identified a fibromatosis in the mesentery. Histologically, the desmoid tumour was composed of spindle cells with elongated coma-shaped nuclei and the immunohistochemistry was negative for both CD117 and for CD34. Beta-catenin overexpression was present on immunohistochemistry (Figure 4). No mitoses were found in 50 high power fields.

Discussion

Mesenteric fibromatosis is a type of fibroblastic proliferation affecting the mesentery that develops usually as a consequence of surgical trauma, but it may occur spontaneously. Patients with familial adenomatous polyposis (FAP, Gardner's syndrome) are especially predisposed to the development of mesenteric fibromatosis.[1] Desmoids develop in approximately 10% of FAP patients and most are intra-abdominal. Similarly, fibromatoses associated with FAP follow a more aggressive course and the recurrence after the resection is common.[2]

The pathogenesis of fibromatoses has been unclear for many years. Currently, these tumours are regarded as a clonal proliferation of myofibroblasts that show APC (adenomatous polyposis coli) gene mutations. These mutations lead to the over expression of beta-catenin.[1,3,4]

The clinical behaviour and the natural course of mesenteric fibromatoses are unpredictable. Some desmoid tumours remain stable for years and several cases of the spontaneous tumour regression without any treatment have been reported.[5]

Nevertheless, a progressive and invading tumour can result in a diffuse infiltration of the mesentery and bowel leading to intestinal ischemia or to the obstruction. The treatment modality in mesenteric fibromatoses is still controversial. The results of the treatment might be biased due to the unpredictable course of this disease with some tumours regressing or remaining stable without any treatment. The management of desmoids should be individualized and multimodal. The surgical resection should be performed only in localized tumours that do not invade the root of the mesentery. Intra-abdominal desmoids can be resected in 53-67% of cases.[6] The aggressive surgical treatment of mesenteric desmoids may result in short bowel syndrome or multiple enterocutaneous fistulas requiring a long-term parenteral nutrition. Fibromatoses are locally aggressive tumours that tend to recur when incompletely resected. A high rate of recurrence after the surgical resection results from the incomplete resection, multicentric disease or surgical trauma as a new precipitating factor. Recent studies report comparable recurrence rates after R0 and R1 resection in extra-abdominal desmoids.[7,8] Nevertheless, there are no data to support a similar influence of microscopically positive margins on recurrence in intra-abdominal desmoids.

Advanced and unresectable tumours or when the resection will result in short bowel syndrome are best treated within a clinical trial of cytotoxic chemotherapy or other experimental therapies. Radiotherapy is rarely used in intra-abdominal desmoids because of a high risk of radiation enteritis. There are no established chemotherapy regimens used in fibromatoses. Most chemotherapeutic protocols use doxorubicin.[9] Recently, a successful therapy of a desmoid tumour resistant to traditional chemotherapeutic regimens was reported with imatinib, a tyrosine kinase inhibitor that is successfully used in advanced gastrointestinal stromal tumours.[10,11]

In a series reported by Bertagnolli *et al.*[9], 96% of patients with mesenteric desmoids had either a radiographically stable disease or no recurrence for a median of 50 months using a multimodal treatment combining watchful waiting, surgery and chemotherapy.

The growth of desmoid tumours is usually limited to the mesentery, but the infiltration of the adjacent bowel is not uncommon. MF may infiltrate the muscularis propria or even the submucosa.[12] The diagnosis of mesenteric fibromatosis is usually straightforward in the cases without a concomitant intestinal involvement. On the other hand,

Ⓐ

Ⓑ
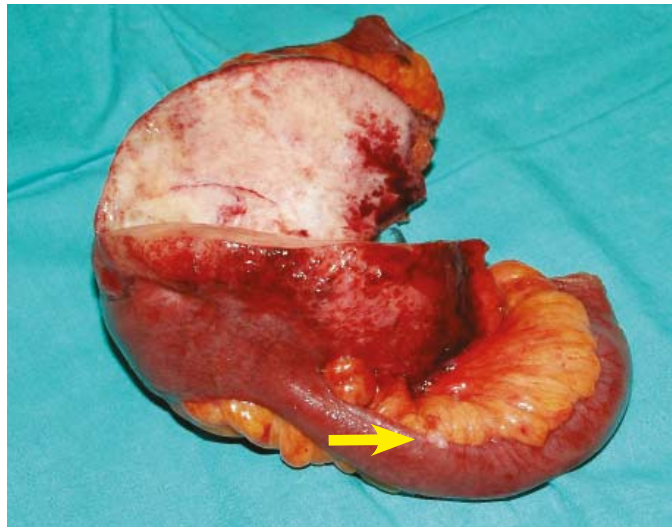
FIGURE 3. Macroscopic view of the resected specimen: A - a mesenteric mass encroaching the bowell wall, B – cut surface of the desmoid tumour showing grayish and glistening, homogenous desmoid tumour. A tubercule attached to the bowel serosa and mimicking peritoneal tumour deposits proved to be a mesothelial cyst (arrow).
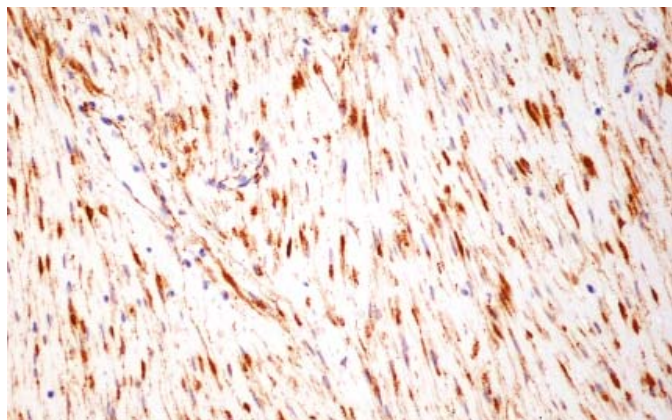
FIGURE 4. Microscopic view of mesenteric fibromatosis: immunostaining for beta-catenin.

TABLE 1. The clinicopathological features useful in differentiating mesenteric fibromatosis from gastrointestinal stromal tumours (GIST)

	Mesenteric fibromatosis	GIST
Demographics	25-35 year, F>M	50-60 year, F=M
Clinical manifestations	Asymptomatic, unless large, infiltrating bowel or compressing the ureters and vasculature; Common: abdominal pain Rare: GI bleeding, perforation	Common: abdominal pain, GI bleeding Rare: GI perforation, obstruction
Location	Small bowel mesentery	Anywhere along the GI tract; most common in the stomach and small bowel
US	Smooth well-defined margins, homogenous or heterogenous tumour of variable echogenicity	Extraluminal hypoechoic mass, small tumours are homogenous, large tumours are heterogenous with multiple anechoic patchy spaces or large central area of low echogenicity
CT	Well-defined homogenous mass, isodense or hyperdense relative to muscle, 1/3 show infiltrative margins, cystic degeneration is rare	Well-defined heterogenous mass with peripheral solid rim enhancing with contrast, central fluid attenuation (necrosis, haemorrhage, cystic degeneration); small tumours show homogenous enhancement
MRI	Tumour of low signal intensity relative to muscle on T1-weighted images and variable signal intensity on T2-weighted images	Tumour of low signal intensity relative to muscle on T1-weighted images and high signal intensity on T2-weighted images
Gross appearance	Hard and firm mass, cut with gritty sensation, white-greyish and glistening on cut section	Soft and fleshy tumours that often show areas of necrosis, haemorrhage and cystic degeneration on cut surface
Microscopic view	Homogenously distributed spindle cells without atypia, abundant collagen, thick-walled arteries and dilated thin-walled veins, mild cellularity, infiltrative pattern of growth	Spindle or epithelioid cells forming fascicles and palisades often with atypia and atypical mitoses, moderate to high cellularity, necrosis often present, expanding pattern of growth
Immunostaining profile	β-catenin (+) CD117 (+) in up to 75% CD34 (-) vimentin (+) smooth muscle actin (+) in 75% desmin (+) in 50%	β-catenin (-) CD117 (+) in 90% CD34 (+) in 42% vimentin (+) smooth muscle actin (+) in 63% desmin (+) in 8%

GI, gastrointestinal

desmoid tumours encroaching the bowel wall present a diagnostic challenge and might be easily confused with primary intestinal tumours, especially gastrointestinal stromal tumours. Difficulties in differentiating these two tumours of distinct pathogenesis, natural course and prognosis are still not uncommon.[12-14]

Desmoid tumours are firm masses. On cross section these tumours are grayish and grossly homogenous. In comparison, GISTs are usually soft and fleshy. On cut surface, these tumours commonly have areas of necrosis and haemorrhage. In contrast to MF, the gross appearance of GISTs is highly dependant on their size, with large tumours being morphologically more heterogeneous. It follows that a large tumour that is firm and homogenous on cross section without obvious haemorrhagic and necrotic areas is highly suggestive of intra-abdominal fibromatosis. Sometimes, differentiating these two distinct tumours is difficult because of a possible clinical, macroscopic and even histological overlap. Nevertheless, the diagnosis of mesenteric fibromatosis is based on the microscopic examination and immunostaining. It is noteworthy that a CD117 antigen, expressed commonly in GISTs, can be positive in up to 75% cases of mesenteric fibromatosis.[11-13] Moreover, both MF and GISTs express vimentin and stain variably for smooth muscle actin and desmin. In contrast to GISTs, MF does not express CD34 and S100 protein. Recently, the expression of beta-catenin was revealed in fibromatoses that might prove helpful in the differential diagnosis in doubtful cases.[1,15,16]

Radiographically, mesenteric fibromatosis may present as a mass-like or infiltrative lesion.[17] Infiltrative desmoid tumours image as an ill-defined whorled thickening of the mesentery and are usually easily recognized. Mass-like desmoids are more challenging. These desmoids appear as well-defined tumours and are often confused with other primary neoplasms, especially gastrointestinal stromal tumours. Nevertheless, the distinction between these two tumours is important because of vital prognostic and therapeutic implications. In

Table 1 the principal features of the mass-like mesenteric fibromatosis and gastrointestinal stromal tumours that might prove helpful in differentiating these two entities are summarized.[12,13,17-21] On the other hand, it should be remembered that a recurrent mass after oncological operations may prove to be an intra-abdominal desmoid, and not necessarily a metastasis. Lee *et al.*[22] reported a case of intraabdominal fibromatosis that occurred after the resection of a gastric stromal tumour. A similar case of intra-abdominal fibromatosis suspicious of local recurrence was reported after gastrectomy for gastric cancer.[23] Failure to differentiate mesenteric fibromatosis from other tumours may lead to an inappropriate treatment and a worse prognosis.

In conclusion, the diagnosis of mesenteric fibromatosis should always be considered in mesenchymal tumours originating from the bowel wall that diffusely infiltrate the mesentery.

References

1. Zhou YL, Boardman LA, Miller RC. Genetic testing for young-onset colorectal cancer: case report and evidence-based clinical guidelines. *Radiol Oncol* 2010; **44:** 57-61.

2. Gurbuz AK, Giardiello FM, Petersen GM, Krush AJ, Offerhaus GJ, Booker SV, et al. Desmoid tumours in familial adenomatous polyposis. *Gut* 1994; **35:** 377-81.

3. Bridge JA, Sreekantaiah C, Mouron B, Neff JR, Sandberg AA, Wolman SR. Clonal chromosomal abnormalities in desmoid tumors. Implications for histopathogenesis. *Cancer* 1992; **69:** 430-6.

4. Alman BA, Li C, Pajerski ME, Diaz-Cano S, Wolfe HJ. Increased beta-catenin protein and somatic APC mutations in sporadic aggressive fibromatoses (desmoid tumors). *Am J Pathol* 1997; **151:** 329-34.

5. Biasco G, Pantaleo MA, Nobili E, Monti C. Spontaneous regression of a desmoid intraabdominal tumor in a patient affected by familial adenomatous polyposis. *Am J Gastroenterol* 2004; **99:** 1621-2.

6. Smith AJ, Lewis JJ, Merchant NB, Leung DH, Woodruff JM, Brennan MF. Surgical management of intra-abdominal desmoid tumours. *Br J Surg* 2000; **87:** 608-13.

7. Lev D, Kotilingam D, Wei C, et al. Optimizing treatment of desmoid tumors. *J Clin Oncol* 2007; **25:** 1785-91.

8. Gronchi A, Casali PG, Mariani L, Lo Vullo S, Colecchia M, Lozza L, et al. Quality of surgery and outcome in extra-abdominal aggressive fibromatosis: a series of patients surgically treated at a single institution. *J Clin Oncol* 2003; **21:** 1390-7.

9. Bertagnolli MM, Morgan JA, Fletcher CD, Raut CP, Dileo P, Gill RR, et al. Multimodality treatment of mesenteric desmoid tumours. *Eur J Cancer* 2008; **44:** 2404-10.

10. Wcislo G, Szarlej-Wcislo K, Szczylik C. Control of aggressive fibromatosis by treatment with imatinib mesylate. A case report and review of the literature. *J Cancer Res Clin Oncol* 2007; **133:** 533-8.

11. Zokalj I, Culinovic-Caic R, Magas Z, Pavcec Z, Saghir H, Igrec J, et al. Gastric gastrointestinal stromal tumour. *Radiol Oncol* 2008; **42**: 187-95.

12. Yantiss RK, Spiro IJ, Compton CC, Rosenberg AE. Gastrointestinal stromal tumor versus intra-abdominal fibromatosis of the bowel wall: a clinically important differential diagnosis. *Am J Surg Pathol* 2000; **24:** 947-57.

13. Rodriguez JA, Guarda LA, Rosai J. Mesenteric fibromatosis with involvement of the gastrointestinal tract. A GIST simulator: a study of 25 cases. *Am J Clin Pathol* 2004; **121:** 93-8.

14. Colombo P, Rahal D, Grizzi F, Quagliuolo V, Roncalli M. Localized intra-abdominal fibromatosis of the small bowel mimicking a gastrointestinal stromal tumor: a case report. *World J Gastroenterol* 2005; **11:** 5226-8.

15. Bhattacharya B, Dilworth HP, Iacobuzio-Donahue C, Ricci F, Weber K, Furlong MA, et al. Nuclear beta-catenin expression distinguishes deep fibromatosis from other benign and malignant fibroblastic and myofibroblastic lesions. *Am J Surg Pathol* 2005; **29:** 653-9.

16. Montgomery E, Torbenson MS, Kaushal M, Fisher C, Abraham SC. Beta-catenin immunohistochemistry separates mesenteric fibromatosis from gastrointestinal stromal tumor and sclerosing mesenteritis. *Am J Surg Pathol* 2002; **26:** 1296-301.

17. Azizi L, Balu M, Belkacem A, Lewin M, Tubiana JM, Arrive L. MRI features of mesenteric desmoid tumors in familial adenomatous polyposis. *AJR Am J Roentgenol* 2005; **184:**1128-35.

18. Wronski M, Cebulski W, Slodkowski M, Krasnodebski IW. Gastrointestinal stromal tumors: ultrasonographic spectrum of the disease. *J Ultrasound Med* 2009; **28:** 941-8.

19. Ko SF, Lin JW, Ng SH, Huang CC, Wan YL, Huang HY et al. Spontaneous isolated mesenteric fibromatosis: sonographic and computed tomographic findings with pathologic correlation. *Ultrasound Med Biol* 2006; **32:** 1141-9.

20. Levy AD, Rimola J, Mehrotra AK, Sobin LH. From the archives of the AFIP: benign fibrous tumors and tumorlike lesions of the mesentery: radiologic-pathologic correlation. *Radiographics* 2006; **26:** 245-64.

21. Lau S, Tam KF, Kam CK, Lui CY, Siu CW, Lam HS et al. Imaging of gastrointestinal stromal tumour (GIST). *Clin Radiol* 2004; **59:** 487-98.

22. Lee CK, Hadley A, Desilva K, Smith G, Goldstein D. When is a GIST not a GIST? A case report of synchronous metastatic gastrointestinal stromal tumor and fibromatosis. *World J Surg Oncol* 2009; **7:** 8.

23. Komatsu S, Ichikawa D, Kurioka H, Koide K, Ueshima Y, Shioaki Y, et al. Intra-abdominal desmoid tumor mimicking lymph node recurrence after gastrectomy for gastric cancer. *J Gastroenterol Hepatol* 2006; **21:** 1224-6.

Dosimetric evaluation of a 320 detector row CT scanner unit

Mario de Denaro and Paola Bregant

S.C. di Fisica Sanitaria, A.O.U. "Ospedali Riuniti" di Trieste, Trieste, Italy

Correspondence to: Dr. Mario de Denaro, Struttura Complessa di Fisica Sanitaria, Azienda Ospedaliero Universitaria "Ospedali Riuniti" di Trieste, Ospedale Maggiore, Centro Tumori, Via Pietà 19, 34100 Trieste, Italy. Phone: +39 040 399 2341; Fax: +39 040 399 2367; E-mail: mario.dedenaro@aots.sanita.fvg.it

Background. The technologic improvements in Multislice scanners include the increment in the X-ray beam width. Some new CT scanners are equipped with a 320 detector row which allows a longitudinal coverage of 160 mm and a total of 640 slices for a single rotation. When such parameters are used the length of the traditional pencil chamber (10 cm) is no more appropriate to measure the standard weighted computed tomography dose index $(CTDI_w)$ value.

Materials and methods. Dosimetric measurements were performed on a 640 slices Toshiba Aquilion One CT scanner using common instrumentation available in Medical Physics Departments.

Results. For the measurements in air, two different ionization chambers were completely exposed to the beam. Dosimeters showed an acceptable agreement in the measurements. To evaluate the actual shape of the dose profile strips of Gafchromic XRQA film were used. Films were previously calibrated on site. From the graphic response of the scanned film it is possible to evaluate the full width at half maximum (FWHM) of the dose profile which represent the actual beam width.

Conclusions. Computed Tomography Dose Index (CTDI) and Dose Length Product (DLP) need to be changed when the beam width of the CT scanner is over 100 mm. To perform dose evaluation with the conventional instrumentation, two parameters should be considered: the average absorbed dose and the actual beam width. To measure the average absorbed dose, the conventional ionization chamber can be used. For the measurement of the width of the dose profile, Gafchromic XRQA film seemed to be suitable.

Key words: multislice CT; pencil chamber; computed tomography dose index; dose profile; Gafchromic film

Introduction

The advent of multislice scanners technology[1] leads to a continuous increment of the X-ray beam width along the cranio-caudal direction. The new CT scanner from Toshiba, *Aquilion One*, is equipped with the 320 detector rows each one 0.5 mm wide. This new technology allows a longitudinal coverage of 160 mm at rotation time of 0.35 seconds. The important change in dosimetric evaluation is needed to adapt the CT dosimetry metrics to the new standard.[2-5] With a 160 mm beam width as an operating condition, the length of the traditional pencil chamber (10 cm) is no more appropriate to evaluate the standard computed tomography dose index (CTDI).[6] Despite this problem the CTDI and the dose length product (DLP) values are still dis-

played on the scanner console. The problem for medical physicists, who must carry out quality assurance and dose optimization on the new CT equipment, is that suitable instrumentation is usually not available. In the present work we suggest some dosimetric measurements that can be carried out on a 320 row CT scanner unit, by means of conventional dosimetric instrumentation.

Material and methods

Some measurements on a *640 slices Toshiba Aquilion One* CT scanner were carried out by means of common instrumentation typically employed at Medical Physics Departments. CT scanners providing 160 mm beam width allows to completely

expose the 6cc ionization chamber of a Radcal Dosimeter, model 9015, commonly employed in the conventional radiodiagnostic measurement. To evaluate the average absorbed dose due to the primary beam, we compared the measurement carried out in air at the isocenter of the gantry, during a single rotation, exposing together the Radcal Dosimeter and the standard 10 cm long CT pencil chamber (WDCT 10, Wellhofer, Germany), connected to PMX-III electrometer. The average absorbed dose alone does not give information regarding the profile of the dose along the cranio-caudal direction (Z axis); it is a parameter to be considered to evaluate the shape and the actual width of the beam. To measure the dose profile free in air Gafchromic XRQA film was exposed to the primary beam during a single axial rotation. The film was previously calibrated exposing small pieces of Gafchromic (2 x 2 cm) to increasing doses; the Gafchromic films were put close to a reference ionization chamber. A calibration curve specific for the CT scanner beam quality was then obtained and it was used to convert the pixel values of the film into dose values (Figure 1).[7]

The exposed film was then scanned by a regular scanner (Epson 1680 pro) using red-green-blue (RGB) modality at 48 bits of depth and spatial resolution of 72 dots per inch. Only the red component of the image was considered. The dose profile was obtained correcting the pixel values by the calibration curve (Figure 2).

From the graph the full width at half maximum (FWHM) of the dose profile can be evaluated. FWHM is a parameter which is related to the Z-axis geometric efficiency. $CTDI_{air,300}$ (CTDI value using an integration interval of 300 mm) and $CTDI_{air,100}$ (CTDI value using an integration interval of 100 mm) were evaluated and compared (Figure 3).[2]

Finally, we put a strip of Gafchromic film in the holes of a standard CT dosimetric PMMA phantom (Figure 4) to evaluate the average absorbed dose inside the phantom (Figure 5).

Results

The measurement performed by the Radcal dosimeter showed an acceptable agreement with the values obtained by the Wellhofer pencil chamber (Table 1). The comparison was meaningful because the 6 cc chamber of the Radcal dosimeter is completely exposed by the beam width.

To maintain the meaning of the CTDI, the integration interval for 160 mm beam width must be
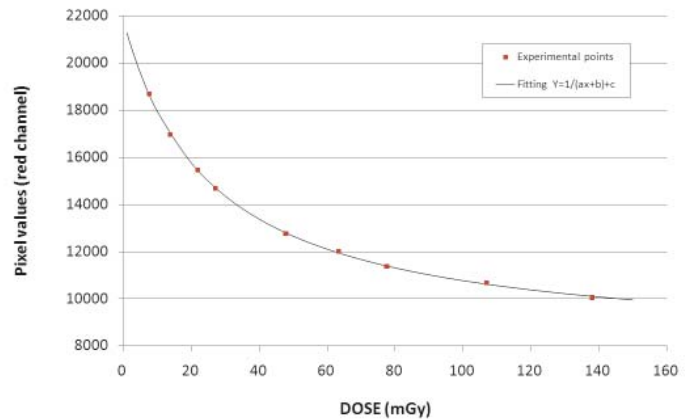
FIGURE 1. Fitting curve for the calibration of Gafchromic XRQA film.
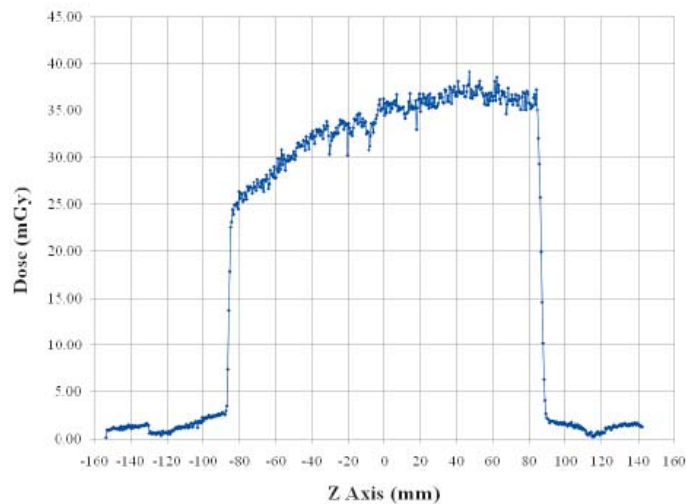
FIGURE 2. Dose profile measured by Gafchromic XRQA film.
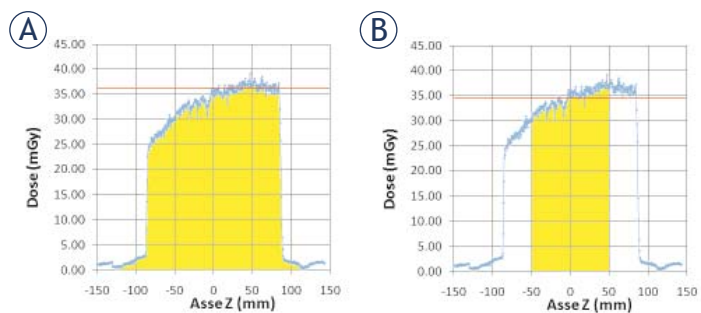
FIGURE 3. (A) Computed tomography dose index (CTDI)air,300. (B) CTDIair, 100.

extended to a value of at least 300 mm.[2] For the measurement of the weighted computed tomography dose index ($CTDI_w$) a PMMA phantom is required, but at the moment it is very difficult to find and manage a PMMA phantom with a length

TABLE 1. Absorbed dose evaluated with two different dosimeters

Dosimeter	Dose FOV Head (mGy/mAs)	Dose FOV Body (mGy/mAs)
Wellhöfer pencil chamber (WDCT 10), with PMX-III	0.257	0.225
Radcal model 9015with 6cc chamber 10X5-6	0.272	0.243

FOV, field-of-view; WDCT 10, Wellhöfer CT pencil chamber 10 cm long
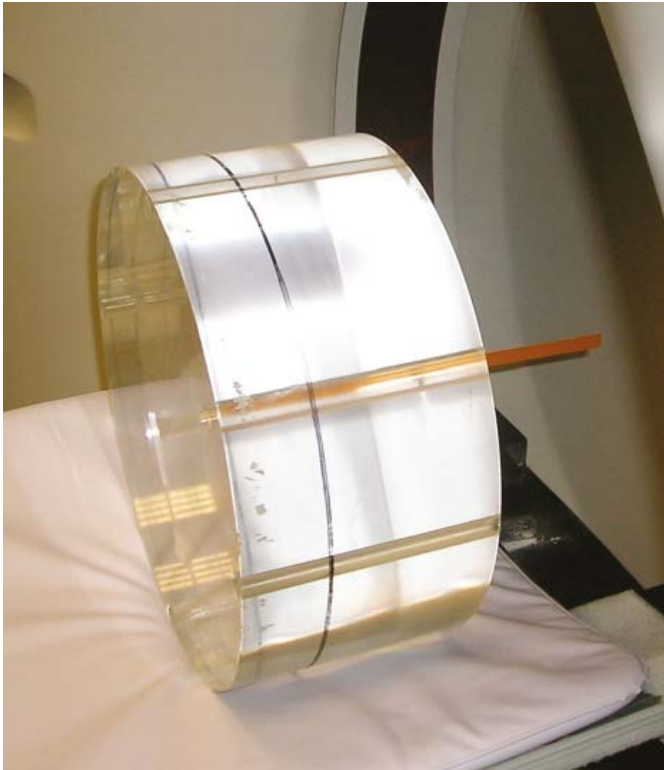
FIGURE 4. Strip of Gafchromic film inserted inside the hole of a poliymethyl methacrylate (PMMA) phantom.
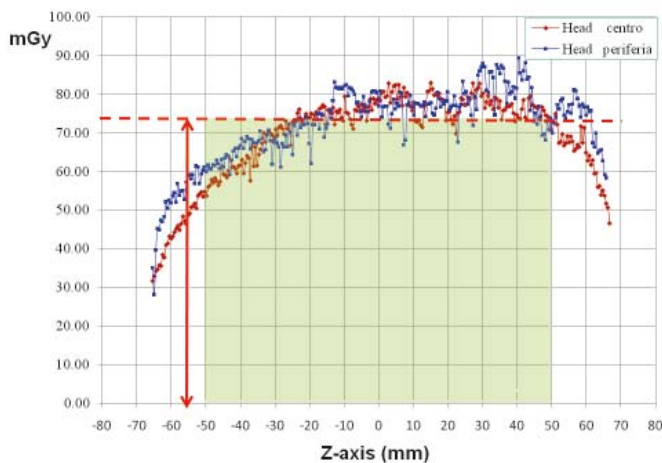
FIGURE 5. Average dose evaluation by Gafchromic film into the poliymethyl methacrylate (PMMA) phantom.

of 300 mm. Moreover, also for the measurement of CTDI in air the length of the conventional pencil chamber (100 mm) is inappropriate. A way to perform dosimetric measurements using conventional instrumentation is to use the ionization chamber for the measurement of the average absorbed dose and Gafchromic film for the evaluation of the actual shape of the dose profile along z-axis. In Figure 1 the shape of the dose profile is plotted; an asymmetry appears evident in the profile due to the anode heel effect. Analysing the profile FWHM was calculated to be 171.8 mm pointing out an overbeaming of 11.8 mm. Z-axis geometric efficiency was also evaluated; it is defined by the International Electrotechnical Commission (IEC)[8] as the ratio between the integral over the range subtended by detectors and total integral of the dose profile. The measured value of 95.4% showed for this parameter a low contribution of the penumbra effect.

In Figure 3 two different intervals of integration to evaluate the $CTDI_{air}$ are presented; the value of $CTDI_{air,300}$ was 36.7 mGy and the value of $CTDI_{air,100}$ was 34.5 mGy. The result was as expected because the longer interval takes into account also the contribution due to the tails of the dose profile.

To obtain an estimation of the absorbed dose inside the PMMA phantom, a strip of Gafchromic film was inserted in the phantom holes. The resulting value of 74.7 mGy was compared with the value of 81.4 mGy displayed at the CT console as $CTDI_{vol}$. The comparison showed a significant underestimation of the measured value probably due to the length of the PMMA phantom (15 cm) which is not long enough to simulate completely the effect of the scattered radiation.

Discussion

Multislice CT scanners lead to a progressive increment in the X-ray beam width along z-axis. CTDI appears to be no more suitable to represent the main dosimetric quantity in CT dosimetry. Recent publications try to find new dose parameters more representative of the technological state of art.[9]

The conventional quality assurance and the dose assessment would require an upgrade in the conventional instrumentation, but new suitable dosimeters and phantoms are not yet available for most Medical Physics Department. Nevertheless, dosimetric parameters for a CT scanner with a beam width of 16 cm can be estimated by means of commonly available dosimetric instrumentation.

The average absorbed dose related to a single axial rotation can be measured by conventional ionization chambers, while the geometric dose distribution along a profile in the cranio-caudal direction (Z-axis) can be evaluated exposing Gafchromic film to the primary beam.

References

1. Beslic S, Beslic N, Beslic S, Sofic A, Ibralic M, Karovic J. Diagnostic imaging of traumatic pseudoaneurysm of the thoracic aorta. *Radiol Oncol* 2010; **44:** 158-63.

2. Geleijns J, Salvadó Artells M, de Bruin PW, Matter R, Muramatsu Y, McNitt-Gray MF. Computed tomography dose assessment for a 160 mm wide, 320 detector row, cone beam CT scanner. *Phys Med Biol* 2009; **54:** 3141-59.

3. *The measurement, reporting, and management of radiation dose in CT.* Report of AAPM Task Group 23 of the Diagnostic Imaging Council CT committee. College Park: American Association of Physicists in Medicine; January, 2008.

4. *Comprehensive methodology for the evaluation of radiation dose in x-ray computed tomography.* Report of AAPM Task Group 111: The Future of CT Dosimetry. College Park: American Association of Physicists in Medicine; February, 2010.

5. Rimondini A, Pozzi Mucelli R, De Denaro M, Bregant P, Dalla Palma L. Evaluation of image quality and dose in renal colic: comparison of different spiral-CT. *Eur Radiol* 2001; **11:** 1140-6.

6. Brenner DJ. Is it time to retire the CTDI for CT quality assurance and dose optimization? *Medical Physics* 2005; **32:** 3225-6.

7. de Denaro M, Bregant P, Severgnini M, de Guarrini F. In vivo dosimetry for estimation of effective doses in multislice CT coronary angiography. *Medical Physics* 2007; **34:** 3705-10.

8. IEC 60601-2-44. Particular requirements for the safety of X-ray equipment for computed tomography. In: 62B - Committee on Diagnostic Imaging Equipment, editor. *Medical electrical equipment.* Part 2-44. Edition 2.1. Geneva: International Electrotechnical Commission November, 2002.

9. IEC 60601-2-44. Particular requirements for the basic safety and essential performance of X-ray equipment for computed tomography. In: 62B - Committee on Diagnostic Imaging Equipment, editor. *Medical electrical equipment.* Part 2-44. Edition 3.0. Geneva: International Electrotechnical Commission; February, 2009.

Verification of quality parameters for portal images in radiotherapy

Csilla Pesznyák[1,2], István Polgár[1], Csaba Weisz[1], Réka Király[1], Pál Zaránd[1]

[1] Uzsoki Hospital, Municipal Centre for Oncoradiology, Budapest, Hungary

[2] Budapest University of Technology and Economics, Institute of Nuclear Techniques, Budapest, Hungary

Background. The purpose of the study was to verify different values of quality parameters of portal images in radiotherapy.

Materials and methods. We investigated image qualities of different field verification systems. Four EPIDs (Siemens OptiVue500aSi®, Siemens BeamView Plus®, Elekta iView® and Varian PortalVision™) were investigated with the PTW EPID QC PHANTOM® and compared with two portal film systems (Kodak X-OMAT® cassette with Kodak X-OMAT V® film and Kodak EC-L Lightweight® cassette with Kodak Portal Localisation ReadyPack® film).

Results. A comparison of the f50 and f25 values of the modulation transfer functions (MTFs) belonging to each of the systems revealed that the amorphous silicon EPIDs provided a slightly better high contrast resolution than the Kodak Portal Localisation ReadyPack® film with the EC-L Lightweight® cassette. The Kodak X-OMAT V® film gave a poor low contrast resolution: from the existing 27 holes only 9 were detectable.

Conclusions. On the base of physical characteristics, measured in this work, the authors suggest the use of amorphous-silicon EPIDs producing the best image quality. Parameters of the EPIDs with scanning liquid ionisation chamber (SLIC) were very stable. The disadvantage of older versions of EPIDs like SLIC and VEPID is a poor DICOM implementation, and the modulation transfer function (MTF) values (f50 and f25) are less than that of aSi detectors.

Key words: electronic portal imaging device; quality control; portal film

Introduction

Electronic Portal Imaging Devices (EPIDs) are used for patient setup during radiotherapy sessions.[1-6] At the same time amorphous silicon (aSi) detectors also offer the possibility of implementing transit dosimetry – this, however, requires a very good quality control protocol.[7-10] A good quality control process comprises a series of procedures to be carried out regularly, with the aim of which the user may ascertain that the equipment provides good image quality and correct measured data. Users usually realize only a sudden drastic worsening of the image quality and fail to notice gradual worsening.

We tested the image qualities of different field verification systems. Four different EPIDs (Siemens OptiVue500aSi®, Siemens BeamView Plus®, Elekta iView® and Varian PortalVision™) and two Kodak films (the X-OMAT V® film in a X-OMAT® cassette and the Portal Localisation ReadyPack® film in a EC-L Lightweight® cassette) were examined with the PTW EPID QC PHANTOM®.[11]

Materials and methods

The PTW EPID QC PHANTOM® was placed on the homogeneous part of the tabletop taking into account the divergence of the beam so that the whole phantom was in the image.[12] The acquired images were analysed with the epidSoft® 2.0 computer program.[13] In our study we were interested not only in the quality of the images but also in the results given by the software for different file formats of the same image, such as JPEG, DCM, BMP, TIF, etc. We investigated the effect of different doses on the quality of the images. Figure 1 shows the

phantom elements that were used for the calculation of different parameters.

Linearity of Copper Steps Wedges: two copper steps were used for linearity determination. The copper steps are designed in such a way that a range of 0% to 50% absorption rate is covered for a typical accelerator at 6 MV beam energy. The linearity curve was calculated from the mean of the gray values of each of the copper steps. The results were the levels 0%, 5%, 10%, 15%, 20%, 25%, 30%, 35%, 40% and 50%. For the display an additional 45% value was calculated from the 40% and 50% values by linear interpolation.

The *Local dependence of Linearity* was determined by means of the brass steps in the corners and at the bottom right side of the phantom (Figure 1.2). Each of these six sets of brass steps consists of four steps, which cover approximately 10%, 20% and 40% absorption rate at 6 MV. Linearity curve is calculated for each block from the mean of the gray values of the steps.

Signal-to-Noise Ratio (SNR) was also determined by means of the two copper steps (Figure 1.1). The SNR was calculated for each absorption level of the copper step.

Modulation Transfer Function (MTF) and High Contrast Resolution: the regions denoted by number 5 in the middle area of the phantom in Figure 1 were used for the determination of the MTF and the high contrast resolution (in horizontal and vertical direction). The mean of the gray values of the lamellae (maximal) and the mean of the gray values of the gaps (minima) were determined for each lamella block.

The *Low Contrast Resolution* was determined with the help of region 4 with 27 holes having different diameters and depths (Figure 1). For each hole the contrast difference of the hole and a specified area around the hole were calculated and represented in a column diagram. The diameters and depths of the holes are similar to those of the Las Vegas phantom, but Las Vegas phantom gives only visual information, while the PTW EPID QC PHANTOM® also gives the numeric analysis (Figure 2).

In the case of Varian's PortalVision™, the control software of the linac used 7 MUs for one portal image.[14,15] The Siemens video based BeamView Plus® was irradiated with 8, 10 and 16 MUs. The EPID was irradiated with 1, 2, 4, 6 and 8 MUs in the case of the Siemens OptiVue500aSi® and the Elekta iView®.[16-18] For portal films, we put both the phantom and the portal film cassette on the top of the treatment table. The Kodak Portal Localisation
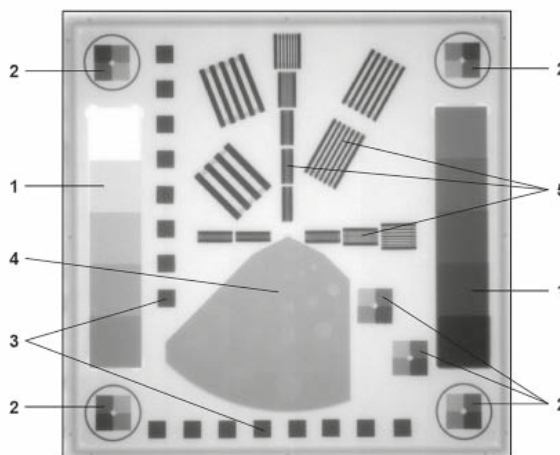
FIGURE 1. Structure of the PTW EPID QC PHANTOM®, 1. Signal linearity and signal noise ratio, 2. Isotropy of signal linearity, 3. Geometric isotropy (distortion), 4. Low-contrast resolution, 5. High-contrast resolution (MTF).

(A)
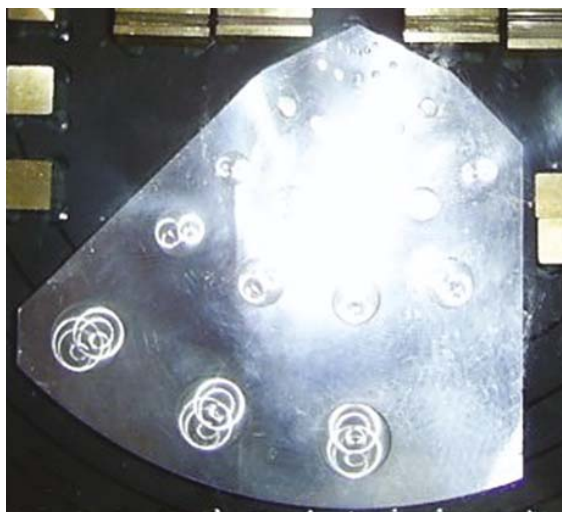
(B)

FIGURE 2. Controlling the low contrast resolution with (A) Las Vegas test tool and (B) PTW EPID QC PHANTOM®.

TABLE 1. Results of the portal image analysis with the epidSoft®2.0 program for the different equipments

Equipment	File format	MU	MFT		SNR	LCSW (%)	LDL (%)
			f50	f25			
PortalVision™	dicom 3.0	7+7	0.288	0.402	52.8	0.57	1.43
PortalVision™	dicom RI	7+7	0.239	0.342	2532.7	0.67	1.63
PortalVision™	bmp	7+7	0.251	0.355	107.3	0.60	1.50
BeamView Plus®	dcm	8	0.307	0.437	38.1	12.9	3.24
BeamView Plus® 15MV	bmp	8	0.225	0.378	40.7	11.0	2.16
BeamView Plus®	bmp	8	0.216	0.399	23.2	10.8	2.47
BeamView Plus®	bmp inverse	8	0.310	0.435	37.8	12.8	2.92
BeamView Plus®	bmp	10	0.242	0.402	54.2	11.6	2.75
BeamView Plus®	bmp	8+8	0.241	0.399	40.8	10.9	2.16
BeamView Plus® 15MV	bmp	8+8	0.23	0.388	56.6	12.3	2.46
OptiVue500aSi®	dcm	1	0.317	0.574	93.3	6.33	2.45
OptiVue500aSi®	dcm	2	0.315	0.573	105.3	6.15	2.48
OptiVue500aSi®	dcm	4	0.315	0.569	95.3	6.16	2.37
OptiVue500aSi®	dcm	6	0.315	0.563	86.4	6.10	2.32
OptiVue500aSi®	dcm	8	0.315	0.563	72.9	6.08	2.23
Elekta iView®	bmp	1	0.323	0.597	115.3	5.07	1.58
Elekta iView®	bmp	2	0.324	0.602	102.9	5.01	1.18
Elekta iView®	bmp	4	0.321	0.576	99.2	5.06	1.28
Elekta iView®	bmp	6	0.315	0.572	90.8	5.03	1.48
Elekta iView®	bmp	8	0.305	0.539	72.4	4.67	1.34
X-OMAT® film	bmp	20	0.322	0.609	248.1	4.62	1.52
X-OMAT® film	tif	20	0.333	0.548	167.8	3.61	2.59
X-OMAT® film	dicom RI	20	0.207	0.396	146.8	3.59	2.32
X-OMAT® film	dicom RI	40	0.275	0.692	105.6	2.34	2.68
EC-L® film	dicom RI	1	0.336	0.596	90.2	5.01	1.89
EC-L® film	dicom RI	2	0.316	0.569	100.7	4.71	2.36
EC-L® film	dicom RI	4	0.331	0.574	92.5	5.00	1.71
EC-L® film	dicom RI	6	0.306	0.563	88.6	6.84	3.96
EC-L® film	tif	1	0.324	0.572	113.1	4.97	1.89
EC-L® film	tif	2	0.312	0.563	119.9	4.66	2.48
EC-L® film	tif	4	0.324	0.584	110.2	4.96	1.71
EC-L® film	tif	10	0.291	0.600	88.2	10.02	3.63

**LCSW, Linearity of Copper Step Wedge

***LDL, Local Dependence of Linearity

ReadyPack® film was irradiated with 1, 2, 4, 6 and 10 MUs, while for Kodak X-OMAT V® film we used 7, 20 and 40 MUs, because it's lower sensitivity. We digitized the films with the LUMISYS Lumiscan® 50 with two different softwares. One was the PTW's Mephysto® program, where we saved the images in TIF and PTW file format, and the other was the P2 System LumiDicom® program[19,20], where we saved the images in DCM and BMP file format. The reference values shall be determined during the acceptance test of the equipment. In the measurement protocol, the usable file format shall be defined since the implementation of DICOM is not complete at these systems.
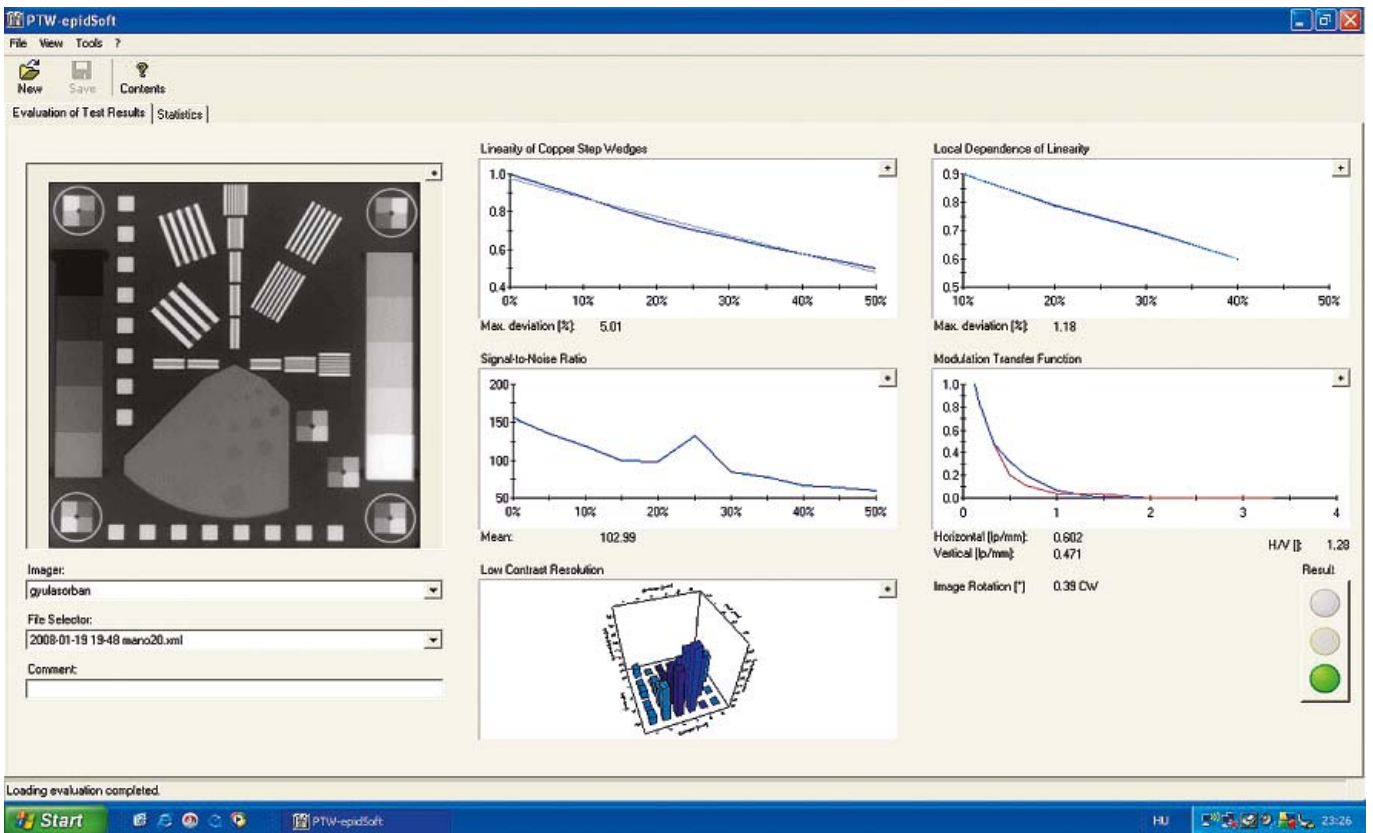
FIGURE 3. The image analysis with the epidSoft®2.0 program.

Results and discussion

The epidSoft®2.0 program makes both, the numeric and the graphic analysis of the portal images; a screenshot can be seen in Figure 3. We analysed about 70 images taken under different conditions (Table 1). Comparing the f50 and f25 values of the MTF we resolved that the amorphous silicon EPID provides the best high contrast resolution. These results were very close to the MTF of the Kodak Portal Localisation ReadyPack® film with the EC-L Lightweight® cassette. For the MTF f50 and f30 we found few published data in the international literature [21-23]; these are listed in Table 2. We also tested the constancy of the characteristics in the case of Varian's PortalVision™ images with PTW EPID QC Phantom®. The graphic interpretation of the measurements is in Figure 5. In Figure 3, the upper left diagram, the measured values of daily Linearity of Copper Step Wedge curves are compared with those of calculated from the linear regression line of daily measurements on the base of equation 1.
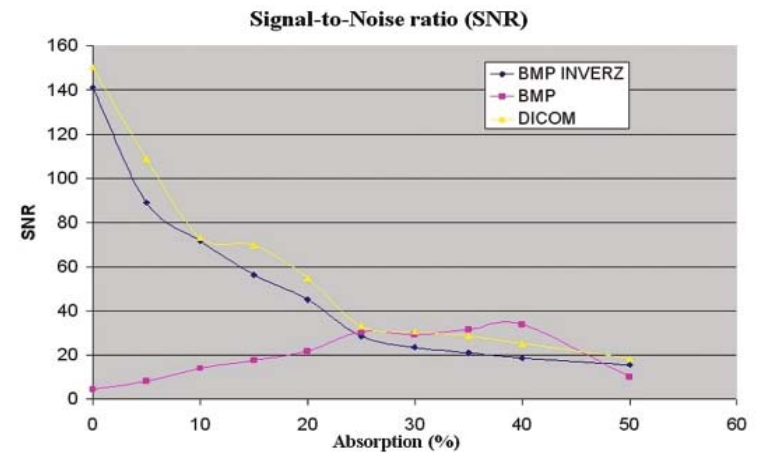
FIGURE 4. SNR as a function of absorption for Siemens BeamView Plus® in the case of different file format: DICOM, bmp and inverse bmp.

$$d_{max} = max\left[\frac{|y_i - I_i|}{I_i}\right]$$

$$i = 0....N \qquad\qquad [1.]$$

The linearity curve is given by the points (x_1, y_1), ...(x_N, y_N) and the regression line is given by the points (x_1, I_1), ...(x_N, I_N).

TABLE 2. Demonstration of the quantities to be used for the quality control of the EPIDs found in the references

EPID	Pixel matrix	Pixel size (mm)	Dose (MU)	CNR	f50 (lp/mm)	f30 (lp/mm)
			Clements at al. 2002, PIPSpro® QC-3V fantom [118]			
Varian aS500™	512 x 384	0.78	5	260	0.392	0.600
Elekta iViewGT®	1024 x 1024	0.4	100	448	0.461	0.767
Siemens FP-A	1024 x 1024	0.4	100	611	0.454	0.696
			Hermann at al. 2001. [119]			
BeamView Plus®	512 x 512				0.204	
PortalVision™	256 x 256				0.258	
			Wong, 1999. [120]			
BeamView Plus®	512 x 512				0,214 0,192 (15 MV)	
PortalVision™	256 x 256				0,258	
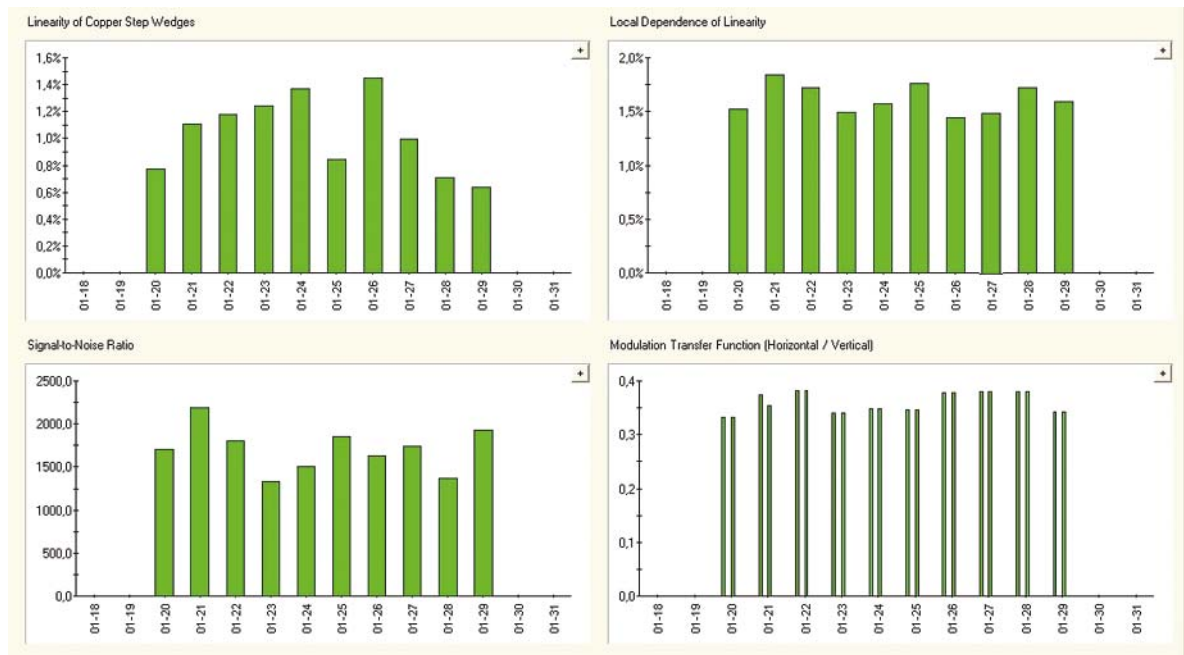
FIGURE 5. The graphic representation of the Varian PortalVision™ equipment's stability test: A. linearity of copper step wedge, B. local dependence of linearity, C. MTF f(25) vertical and horizontal component, D. signal-to-noise ratio average value.

We have determined the 10 days stability of the system. The daily maxima are plotted vs. time in a 10 days interval in the upper left diagram of Figure 5. The maximum of the daily deviation is on an average 1.03 ± 0.27% representing a sufficient stability of the measurement system. A similar analysis was made for the Local Dependence of Linearity resulting in 1.62 ± 0.19% average daily maximum deviation. For the signal-to-noise curve, the average of mean value and standard deviation, were 1656 ± 189. The average value for MTF f50 was 0.247 ± 0.011 lp/mm and for MTF f25 we received 0.360 ± 0.018 lp/mm. Measurements shown in the Figure 5 represent a good stability of the system.

The signal-to-noise curve for the Siemens BeamView Plus® and the Varian's PortalVision™ depend of the image file format. In Figure 5 we can see the Siemens BeamView Plus® SNR curves for DICOM, BMP and the inverse BMP file format. We supposed that two older generations of EPIDs had a DICOM implementation problem.[24]

If we use the Las Vegas phantom for quality control, then the image quality is acceptable when we can see 17 holes from 28 holes.[25] We applied the same criteria for the PTW EPID QC PHANTOM®. All equipments gave good results, except the Kodak X-OMAT V® film: we found only 9 holes after irradiating the film with a 10 times higher dose

Kodak X-OMAT® 20 MU

	Depth [mm]				
	0,5	1,0	2,0	3,2	4,8
1	0.23	0.16	0.17	0.86	0.16
2	0.00	0.01	0.00	0.06	0.46
4	0.00	0.14	0.17	0.14	0.68
7	0.07	0.14	0.21	0.78	1.17
10	0.71	0.76	0.66	1.21	
15	0.04	0.49	0.74		

(D [mm] labels rows)

Kodak EC-L® 2 MU

	Depth [mm]				
	0,5	1,0	2,0	3,2	4,8
1	0.01	0.12	0.24	0.33	0.38
2	0.18	0.05	0.71	0.68	1.65
4	0.21	0.55	0.84	1.39	1.77
7	0.08	0.58	1.23	1.90	2.51
10	0.36	0.72	0.97	1.84	
15	0.62	0.56	1.34		

(D [mm] labels rows)
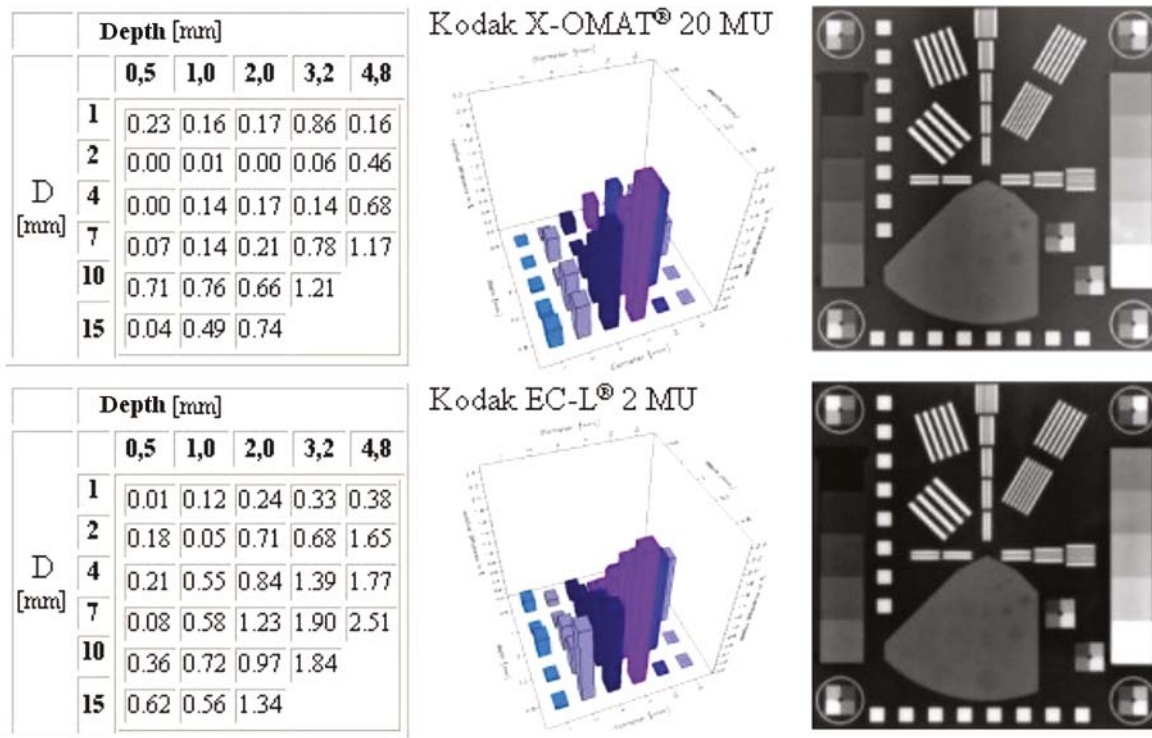
FIGURE 6. Comparison of results for low contrast resolution with PTW EPID QC PHANTOM® for Kodak X-OMAT® cassette with Kodak X-OMAT V® film and the Kodak EC-L Lightweight® cassette with Kodak Portal Localisation ReadyPack® film.

than the Kodak Portal Localisation ReadyPack® film. The numeric and graphic interpretation of the low contrast resolution for portal films is in the Figure 6.

When the Kodak Portal Localisation ReadyPack® film with EC-L Lightweight® cassette was overexposed (Table 1), we received a too large value for Linearity of Copper Step Wedge and the image was unusable for the verification of patient setup.

Unfortunately, there is not a lot of published information regarding the physical characteristics of different EPIDs making it difficult to compare these results. On the base of physical characteristics, measured in this work, the authors suggest the use of aSi EPIDs producing the best image quality. Parameters of the EPIDs with scanning liquid ionisation chamber (SLIC) were very stable. The disadvantage of older versions of EPIDs like SLIC and VEPID is a pour DICOM implementation, and the modulation transfer function (MTF) values (f50 and f25) are less than that of aSi detectors.

Acknowledgments

References

1. Boyer AL, Antomuk L, Fenster A, Van Herk M, Meertens H, Munro P, et al. A review of electronic portal imaging devices (EPIDs). *Med Phys* 1992; **19:** 1-16.

2. Langmack K A, Phil D. Portal imaging. *Brit J Radiol* 2001; **74:** 789-804.

3. Whittington R, Bloch P, Hutchinson D, Björrngard BE. Verification of prostate treatment setup using computed radiography for portal imaging. *J Appl Clin Med Physi* 2002; **3:** 88-96.

4. Johnson LS, Milliken BD, Hodley SW, Pelizzari CA, Haraf DJ, Chen GTY. Initial clinical experience with a video-based patient positioning system. *Int J Radiat Oncol Biol Phys* 1999; **45:** 205-13

5. Pesznyák Cs, Lövey K, Weisz Cs, Polgár I, Mayer Á. Elektronikus mezőellenőrzés lineáris gyorsítón. *Magyar Onkológia* 2001; **45:** 335-41.

6. Kasabašić M, Faj D, Belaj N, Faj Z, Tomaš I. Implementing of the offline setup correction protocol in pelvic radiotherapy: safety margins and number of images. *Radiol Oncol* 2007; **41:** 48-55.

7. Cremers F, Frenzel Th, Kausch C, Albers D, Schonborn T, Schmidt R. Performance of electronic portal imaging devices EPIDs used in radiotherapy: Image quality and dose measurements. *Med Phys* 2004; **31:** 985-96.

8. Petrovic B, Grzadziel A, Rutonjski K, Slosarek K: Linear array measurements of enhanced dynamic wedge and treatment planning system (TPS) calculation for 15 MV photon beam and comparison with electronic portal imaging device (EPID) measurements. *Radiol Oncol* 2010; **44:** 199-206.

9. Nijsten SMJJG, Mijnheer BJ, Dekker LAJ, Lambin P, Minken AWH. Routine individualised patient dosimetry using electronic portal imaging devices. *Radiother Oncol* 2007; **83:** 65-75.

10. Bailey DW, Kumaraswamy L, Podgorsak MB. A fully electronic intensity-modulated radiation therapy quality assurance (IMRT QA) process implemented in a network comprised of independent treatment planning, record and verify, and delivery systems. *Radiol Oncol* 2010; **44:** 124-30.

11. Geyer P, Blank H, Alheit H. Portal verification using the KODAK ACR 2000 RT storage phosphor plate system and EC® films. *Strahlenther Onkol* 2006; **182:** 172-8.

12. Pesznyák Cs, Fekete G, Mózes Á, Kiss B, Király R, Polgár I, et al. Quality control of portal imaging with PTW EPID QC phantom®. *Strahlenther Onkol* 2009; **185:** 56-60.

13. *Epid QC phantom and epidSoft software.* Users manual. Freiburg: PTW; 2006.

14. Van Herk M, Meertens H. A matrix ionisation chamber imaging device for on-line patient set up verification during radiotherapy. *Radiother Oncol* 1988; **11:** 369-78.

15. Essers M, Hoogervorst BR, van Herk M, Lanson H, Mijnheer BJ. Dosimetric characteristics of a liquid-filled electronic portal imaging device. *Int J Radiat Oncol Biol Phys* 1995; **33:** 1265-72.

16. El-Mohri Y, Jee KW, Antonuk LE, Maolinbay M, Zhao Q. Determination of the detective quantum efficiency of a prototype, megavoltage indirect detection, active matrix flat-panel imager. *Med Phys* 2001; **28:** 2538-49.

17. Munro P, Bouius DC. X-ray quantum limited portal imaging using amorphous silicon flat-panel arrays. *Med Phys* 1998; **25:** 689-702.

18. Winkler P, Hefner A, Georg D. Dose-response characteristics of amorphous silicon EPID. *Med Phys* 2005; **32:** 3095-105.

19. Pesznyák Cs, Zaránd P, Mayer Á. Digitalization and networking of analog simulators and portal images. *Strahlenther Onkol* 2007; **183:** 117-20.

20. Pesznyák Cs, Zaránd P, Baráti Zs, Párkányi T. Mevasim szimulátor hálózatban-DICOM RT. In: Pintye É, editor. *Proc. X. Hungarian medical physics conference & workshop.* Debrecen: Cívis Copy Ltd.; 2004. p. 103-8.

21. Clements R, Luchka K, Pouliot J, Sage J, Shalev S. Initial comparison of three Am-Si EPIDs using the QC-3V Phantom. *The 7th international workshop on electronic Portal Imaging – EPI2K2.* Vancouver, BC, June, 27-29; 2002.

22. Herman MG, James MB, David AJ, McGee KP, Munro P, Shalev S, at al. Clinical use of electronic portal imaging: report of AAPM Radiation Therapy Committee Task Group 58. *Med Phys* 2001; **28:** 712-37.

23. Wong J. Current status of electronic portal imaging. *AAPM 41st annual meeting.* Nashville, Tennessee; 1999.

24. NEMA (National Electrical Manufacturers Association). *Digital imaging and communications in medicine (DICOM).* Part 3: Information object definitions. Rosslyn: NEMA; 2003. p. 855.

25. McGarry CK, Grattan MWD, Cosgrove VP. Optimisation of image quality and dose for Varian aS500 electronic portal imaging devices (EPIDs). *Phys Med Biol* 2007; **52:** 6865-77.

Magnetni nanodelci kot dostavni sistemi v onkologiji

Prijič S, Serša G

Izhodišča. Različne vrste nanodelcev, pri čemer magnetni nanodelci predstavljajo le eno izmed kategorij, nudijo na stičišču fizike, kemije in biologije številne aplikativne možnosti. Nekatere magnetne nanodelce že uporabljamo v kliniki kot povečevalce kontrasta za slikanje z magnetno resonanco. Izboljšave fizikalno-kemijskih lastnosti magnetnih nanodelcev so nujne za njihovo uporabo še na drugih področjih biomedicine, predvsem kot magnetno vodeni dostavni sistemi za različne učinkovine. Magnetne nanodelce lahko kot dostavni sistem izpostavimo magnetnemu polju. Na ta način nanodelce kopičimo in zadržimo na tarčnem mestu, kar omogoča ciljano dostavo nanje vezanih učinkovin.

Zaključki. Čeprav je ideja pripenjanja kemoterapevtikov na površino magnetnih nanodelcev vzklila že pred približno 30 leti, magnetne nanodelce kot dostavne sisteme še ne uporabljamo v klinični praksi. Nedavno se je transfekcija nukleinskih kislin, pripetih na površino magnetnih nanodelcev, izkazala kot izredno učinkovita nevirusna metoda transfekcije različnih celic in vitro. Z optimizacijo magnetofekcije bi lahko ta postala nova oblika dostavnega sistema za gensko terapijo pri zdravljenju raka.

Preiskava ^{18}F-choline PET/CT pri bolnikih z rakom prostate

Hodolič M

Izhodišča. Holin ima veliko afiniteto za vezavo na maligno tkivo prostate. Lahko ga označimo s pozitronskim sevalcem ^{18}F. Označen holin uporabljamo v PET/CT slikovni tehniki. Cilj raziskave je bil prikazati naše izkušnje s fluorome-thycholinom (^{18}F-holin) in PET/CT slikovno tehniko pri bolnikih z rakom prostate.

Metode. V raziskavo smo vključili bolnike s patohistološko ali citološko potrjenim rakom prostate, ki smo jih od maja do septembra 2010 pregledali s preiskavo ^{18}F-holin PET/CT. Dva opazovalca sta ocenjevala zgodnje in kasne scintigrame s ^{18}F-holinom ter jih primerjala s CT slikami in semikvantitativno izračunano intenziteto kopičenja izotopa (standard uptake value – SUV).

Rezultati. Preiskavo PET/CT smo naredili pri 50 bolnikih s patohistološko ali citološko potrjenim rakom prostate. Pri 18 bolnikih je bila že narejena radikalna prostatektomija, 32 pa ni bilo operiranih. Pri vseh bolnikih, ki niso bili operirani, smo v področju prostate ugotavljali patološko kopičenje radioindikatorja. Iz te skupine je 14 (44%) bolnikov imelo scintigrafske znake razsoja v lokalne ali oddaljene bezgavke ter/ali v skelet. Od 18 bolnikov, pri katerih je bila narejena radikalna prostatektomija, je 6 (33%) imelo scintigrafske znake lokalne ponovitve bolezni, pri dveh bolnikih (10%) pa smo ugotavljali scintigrafske znake oddaljenih zasevkov.

Zaključki. PET/CT s ^{18}F-holinom je visoko občutljiva, neinvazivna slikovna preiskava za predoperativno ugotavljanje razširjenosti bolezni ter ugotavljanje lokalne ponovitve bolezni po prostatektomiji pri bolnikih z rakom prostate.

Medenični hemangiopericitom: pomen difuzijske magnetne resonance pri določitvi mesta biopsije in pri oceni odgovora na zdravljenje po radioterapiji

Perdikakis E, de Bree E, Giannikaki E, Chryssou EG, Valatsou C, Karantanas A

Izhodišča. Kljub napredku slikovne diagnostike predstavlja natančnejša opredelitev tumorjev mehkih tkiv še vedno izziv. Prav tako s slikovnimi metodami ne moremo vedno natančno oceniti tkivne spremembe po zdravljenju in odgovor tumorja na zdravljenje.

Prikaz primera. Predstavljamo primer bolnice z medeničnim hemangiopericitomom, pri katerem smo uporabili različne slikovne metode za opredelitev bolezni in za sledenje bolnice.

Zaključki. Difuzijska magnetna resonanca nam lahko znatno pomaga pri določitvi mesta biopsije in pri oceni odgovora na zdravljenje po radioterapiji.

Centralni venski kateter vstavljen v levo zgornjo interkostalno veno

Štern Padovan R, Hrabak Paar M, Aurer I

Izhodišča. Za kontrolo lege centralnega venskega katetra (CVK), ki ga vstavljamo skozi notranjo jugularno veno ali podključnično veno, rutinsko uporabljamo rentgenogram prsnih organov. Za nadaljnjo ocena prehodnosti CVK uporabljamo venografijo s kontrastnim sredstvom. Pri bolnikih z zaporo/zožitvijo zgornje votle vene je konica katetra pogosto v razširjenih venskih kolateralah mediastinuma. V takih primerih je potrebno dobro poznavanje anatomije žilja prsnega koša za določitev natančnejšega položaja CVK.

Prikaz primera. Prikazujemo primer 32-letne bolnice s ponovitvami mediastinalega limfoma z že znano zaporo zgornje votle vene ter posledično razvito kolateralno azygos-hemiazygos vensko cirkulacijo. Bolnici smo vstavili CVK skozi levo podključnično veno. S CT preiskavo prsnega koša smo ugotovili, da njegova konica leži v razširjeni levi zgornji medrebrni veni in akcesorni veni hemiazygos. Ocenili smo, da je razširjena akcesorna vena hemiazygos primerna za infuzijo. Zato CVK nismo premeščali in bolnica po infuzijah ni imela nobenih težav. Ob primeru predstavljamo anatomsko-radiološko obravnavo azygos-hemiazygos venskega sistema, s poudarkom na levi zgornji medrebrni veni.

Zaključki. CT preiskava brez kontrastnega sredstva je lahko pomemben pripomoček pri oceni položaja CVK, posebej pri bolnikih, ki zaradi različnih vzrokov naj ne bi prejeli kontrastnega sredstva.

Elektrogenska terapija s plazmidom za IL-12 pri mastocitomih psov

Pavlin D, Čemažar M, Cör A, Serša G, Pogačnik A, Tozon N

Izhodišča. Mastocitomi so eden najpogostejših malignih kožnih tumorjev pri psih. Zanje je značilno zelo raznoliko biološko obnašanje, zaradi česar je lahko določanje kliničnega stadija bolezni in odločanje o ustrezni vrsti zdravljenja zelo težko. Kožne mastocitome pri psih zdravimo na različne načine, vendar je metoda izbora še vedno kirurška terapija. V naši raziskavi smo za zdravljenje mastocitomov uporabili nov terapevtski pristop, intratumoralno elektrogensko terapijo (EGT).

Materiali in metode. V raziskavo smo vključili osem psov s skupno enajstimi kožnimi noduli, ki smo jih zdravili z intratumoralno EGT s plazmidom, ki nosi zapis za humani IL-12. Lokalne učinke EGT smo določali z merjenjem velikosti tumorjev v različnih časovnih obdobjih po terapiji in s histološkim pregledom vzorcev zdravljenih tumorjev. Sistemski odgovor na EGT smo ugotavljali z določanjem IL-12 in IFN- γ v serumu živali. Morebitne stranske učinke zdravljenja smo nadzorovali z določanjem osnovne krvne slike in izbranih biokemičnih vrednosti v serumu zdravljenih živali.

Rezultati. Na zdravljenih psih je intratumoralna EGT z *IL-12* izzvala dober lokalni protitumorski učinek s statistično značilnim zmanjšanjem velikosti zdravljenih tumorjev v razponu od 15 do 83% začetnega volumna nodulov. Poleg tega smo ugotovili spremembe v histološki zgradbi zdravljenih tumorjev, ki so se kazale kot zmanjšanje števila mastocitov in vnetna infiltracija nodulov. Pri zdravljenih psih smo tudi dosegli sistemsko izločanje IL-12 in IFN-γ brez stranskih učinkov.

Zaključki. Rezultati naše raziskave nakazujejo, da bi bila EGT s plazmidom, ki nosi zapis za humani IL-12, lahko uspešna metoda zdravljenja mastocitomov pri psih, ki izzove lokalni protitumorski učinek.

Slikovnocitometrične jedrne značilke pri neoperabilnem raku glave in vratu: pilotna raziskava

Strojan-Fležar M, Lavrenčak J, Žganec M, Strojan P

Izhodišča. S slikovnim citometrom lahko izmerimo številne lastnosti jedra, ki jih lahko obravnavamo kot nadomestne označevalce za molekularnogenetske spremembe v jedrih. Cilj raziskave je bil analizirati slikovnocitometrične jedrne značilke v parnih vzorcih primarnega tumorja in zasevkov na vratu pri bolnikih z neoperabilnim karcinomom glave in vratu.

Materiali in metode. Naredili smo slikovnocitometrično analizo jeder iz celičnih suspenzij, ki smo jih pripravili iz tkiva primarnih tumorjev in vzorcev aspiracijskih biopsij s tanko iglo zasevkov na vratu. Raziskavo smo naredili pri 21 bolnikih, ki smo jih sočasno zdravili z radiokemoterapijo. Značilnosti jeder smo primerjali s kliničnimi značilnostmi in odgovorom na zdravljenje.

Rezultati. Pojav oddaljenih zasevkov in novih primarnih tumorjev je soupadal (p<0.05) s številnimi značilnostmi kromatina v celicah primarnih tumorjev, medtem ko sta mesto primarnega tumorja in odgovor bolezni na vratu na zdravljenje korelirala z značilnostmi kromatina v celicah področnih zasevkov. Številne jedrne značilnosti primarnih tumorjev in področnih zasevkov so bile povezane s stadijem TNM.

Zaključki. Ugotovili smo značilen korelacijski vzorec med uveljavljenimi napovednimi kazalci in jedrnimi značilnostmi iz vzorcev primarnega tumorja in zasevkov na vratu. Slikovnocitometrične jedrne značilke so obetaven označevalec za prepoznavo biološko različnih skupin tumorjev.

Trojno negativni rak dojke – napovedni dejavniki in preživetje

Ovčariček T, Grazio Frković S, Matos E, Možina B, Borštnar S

Izhodišča. Za trojno negativni rak dojke je značilna odsotnost izražanja hormonskih receptorjev (estrogenskih in progesteronskih) ter HER-2 receptorjev. Namen retrospektivne raziskave je bil opredeliti napovedne dejavnike za kratko- oz. dolgoročno preživetje pri bolnicah s trojno negativnim rakom dojke (TNBC), ki so bile zdravljene v rutinski klinični praksi.

Bolnice in metode. Pregledali smo dokumentacijo 269 bolnic s TNBC, ki so bile zdravljene na Onkološkem Inštitutu Ljubljana med marcem 2000 in decembrom 2006. Beležili smo podatke o značilnosti bolnic, tumorjev ter o načinih zdravljenja.

Rezultati. Srednja starost bolnic je bila 55,3 leta (23-88,5), srednje opazovalno obdobje pa 5,9 let (0,3-9,6). V tem času je 6 (7.1%) bolnic doživelo lokalno ponovitev, pri 79 (92%) so bili ugotovljeni oddaljeni zasevki, 66 (24%) bolnic je umrlo. Najpogostejše mesto prvega razsoja so bili visceralni organi (70,4%). Petletno preživetje brez bolezni (DFS) za celotno skupino je bilo 68,2 %, petletno celokupno preživetje (OS) pa 74,5%. Ugotovili smo potek bolezni z vrhom ponovitev v prvih treh letih po postavitvi diagnoze ter jasnim upadom pogostosti ponovitve v nadaljnih letih. V Coxovi univariatni analizi so se kot statistično pomembni napovedni dejavniki tako za DFS kot OS pokazali starost, prizadetost bezgavk, velikost tumorja ter invazija v krvne in limfne žile. V multivariatni analizi sta se kot neodvisna napovedna dejavnika za DFS izkazala starost (HR=1,79; 95%CI=1,14-2,82; p=0.012) in prizadetost bezgavk (HR=2,71; 95%CI=1,64-4,46; p<0.001), medtem ko je neodvisno napovedno vrednost za OS ohranila le prizadetost bezgavk (HR=2,96; 95%CI=1,51-5,82; p=0.002).

Zaključki. Izsledki naše analize bolnic s TNBC kažejo neodvisno napovedno vrednost prizadetosti bezgavk in starosti (>65 let) za DFS, medtem ko je prizadetost bezgavk edini neodvisni napovedni dejavnik za OS. Ugotavljamo za TNBC tipičen potek bolezni s pogostejšimi ponovitvami v prvih 3 letih po postavitvi diagnoze, zmanjšano pogostost ponovitev v nadaljnjih 3 letih ter večjo pogostost ponovitve bolezni v oddaljenih organih v primerjavi z lokalno ponovitvijo. Najpogostejše mesto prve ponovitve so visceralni organi.

Tumorski zasevki v ščitnici, poročilo o treh primerih in pregled literature

Vardar E, Erkan N, Bayol U, Yılmaz C, Dogan M

Izhodišča. Metastaze v ščitnico so v klinični praksi razmeroma redke, vendar se zdi, da se njihovo število v zadnjih letih povečuje. Razlog za to povečanje je diagnostika z uporabo tankoigelne biopsije in zahtevnih sodobnih slikovnih metod pri bolnikih s tumorsko maso v ščitnici. Poleg tega se v patohistološki diagnostiki malignih tumorjev uporablja vse več imunohistokemičnih označevalcev, kar izboljšujejo diagnostiko tumorske mase ščitnice.

Prikaz primerov. Z retrospektivno analizo malignih tumorjev ščitnice smo v času od januarja 1993 do decembra 2007 našli tri bolnike z metastatskim tumorjem v ščitnici. Primarni tumorji so bili: svetlocelični karcinom ledvic, ploščato-celični karcinom pljuč in duktalni adenokarcinom dojke.

Zaključki. Natančna anamneza, skrbna histološka preiskava in imunohistokemična analiza pomagajo pri postavitvi pravilne diagnoze.

Mezenterična fibromatoza s prizadetostjo mezenterija je podobna gastrointestinalnemu stromalnemu tumorju

Wronski M, Ziarkiewicz-Wroblewska B, Slodkowski M, Cebulski W, Gornicka B, Krasnodebski IW

Izhodišča. Fibromatoza mezenterija ali intraabdominalni dezmoidni tumor je redka bolezen. Čeprav ta tumor ne me-tastaira, je lokalno agresiven in se po odstranitvi velikokrat ponovi na mestu primarne rasti. Fibromatozo z intestinalno prizadetostjo lahko zaradi podobnosti zamenjamo z drugimi primarnimi tumorji mezenerija.

Prikaz primera. V prispevku prikazujemo primer 44-letne ženske. Bolnica je navajala dva tedna trajajočo bolečino v žlički. Laboratorijski izvidi so bili v mejah normale. S slikovnimi preiskavami smo dokazali tumor v trebuhu in postavili sum na gastrointestinalni tumor (GIST) tankega črevesa. Dokončen histološki izvid je pokazal, da odstranjen tumor ni bil GIST ampak fibromatoza mezenterija.

Zaključki. Če tumor izvira iz trebušne stene in difuzno infiltrira mezenterij, moramo pomisliti tudi na mezenterično fibromatozo.

Dozimetrično ovrednotenje 320 vrstičnega CT čitalnika

de Denaro M, Bregant P

Izhodišča. Izboljšava tehnologije večrezinskih čitalnikov vključuje tudi povečanje širine žarkov X. Nekateri novi čitalniki CT so opremljeni s 320 vrsticami detektorjev, ki omogočajo longitudinalno zaznavo v obsegu 160 mm ter 640 rezin na eno samo rotacijo. Pri takšnih parametrih dolžina tradicionalne ozke celice ("pencil chamber" 10 cm) ni več primerna za merjenje vrednosti standardno uteženega CT doznega indeksa ($CTDI_w$).

Materiali in metode. Dozimetrične meritve smo naredili na 640 rezinskem Toshiba Aquilion One CT čitalniku z uporabo običajne opreme dosegljive na oddelkih medicinske fizike.

Rezultati. Pri meritvah v zraku smo dve različni ionizacijski celici izpostavili žarku. Dozimetra sta pokazala vrednosti, ki sta se sprejemljivo ujemali. Za ovrednotenje dejanske oblike doznega profila smo uporabili filmske trakove Gafchromic XRQA. Predhodno smo na istem mestu filme kalibrirali. Iz grafičnega odziva odčitanega filma smo lahko ocenili polno širino na polovici maksimuma doznega profila (FWHM), ki predstavlja dejansko širino žarka.

Zaključki. CT dozni indeks (CTDI) ter produkt doze in dolžine (DLP) morata biti spremenjena, kadar širina žarka čitalnika CT presega 100 mm. Za dozno oceno z običajno opremo moramo upoštevati dva parametra: povprečno absorbirano dozo in dejansko širino žarka. Za meritve povprečne absorbirane doze lahko uporabimo običajno ionizacijsko celico. Pri meritvi širine doznega profila je uporaben film Gafchromic XRQA.

Preverjanje kakovosti portalnega slikanja v radioterapiji

Pesznyák C, Polgár I, Weisz C, Király R, Zaránd P

Izhodišča. Namen raziskave je bil preveriti različne vrednosti parametrov kakovosti portalnih slik v radioterapiji.

Materiali in metode. Proučili smo kakovost slik različnih sistemov za preverjanje polj. Štiri EPI naprave (Siemens OptiVue500aSi®, Siemens BeamView Plus®, Elekta iView® and Varian PortalVision™) smo proučili s PTW EPID QC PHANTOM®-om in jih primerjali z dvema sistemoma za slikanje portalnih filmov (Kodak X-OMAT® kaseto s Kodak X-OMAT V® filmom ter Kodak EC-L Lightweight® kaseto s Kodak Portal Localisation ReadyPack® filmom).

Rezultati. Primerjava vrednosti f50 in f25 modulacijskih prenosnih funkcij (MTFs) različnih sistemov je pokazala, da amorfno silikonske EPI naprave omogočajo nekoliko boljši visoki kontrast od Kodak Portal Localisation ReadyPack® filma z EC-L Lightweight® kaseto. S Kodak X-OMAT V® filmom smo dosegli slabo nizko kontrastno ločljivost: od obstoječih 27 lukenj smo zaznali le 9.

Zaključki. Raziskava je pokazala, da na osnovi fizikalnih značilnosti, ki smo jih merili, uporaba amorfno silikonskih EPI naprav omogoča najbolj kakovostne slike. Parametri EPI naprav z vrstično tekočinsko ionizacijsko celico (SLIC) so bili zelo stabilni. Pomanjkljivost starejših različic EPI naprav, kot sta SLIC in VEPID, je slaba DICOM podpora in nižje vrednosti modulacijske prenosne funkcije (MTF) (f50 in f20) v primerjavi z detektorji aSi.

Vse za rentgen
dobite pri nas!

- rentgenski filmi in kemikalije
- rentgenska kontrastna sredstva
- rentgenska zaščitna sredstva
- aparati za rentgen, aparati za ultrazvočno diagnostiko in vsa ostala oprema za rentgen

Sanolabor, d.d., Leskoškova 4, 1000 Ljubljana
tel: 01 585 42 11, fax: 01 524 90 30
www. sanolabor.si

Sanolabor
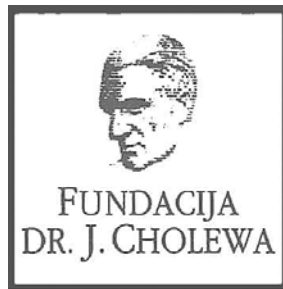
Fundacija "Docent dr. J. Cholewa"
je neprofitno, neinstitucionalno in nestrankarsko
združenje posameznikov, ustanov in organizacij, ki želijo
materialno spodbujati in poglabljati raziskovalno
dejavnost v onkologiji.

Dunajska 106
1000 Ljubljana

ŽR: 02033-0017879431
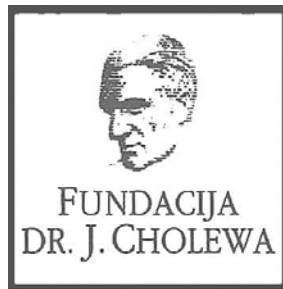
Activity of "Dr. J. Cholewa" Foundation for Cancer Research and Education – a report for the first quarter of 2011

The Dr. J. Cholewa Foundation for Cancer Research and Education is a non-profit, non-government and non-political association of individuals, institutions and organisations with the aim to support various initiatives in cancer research, prevention and education. Its target audience includes medical and other professionals, and general population. The Foundation distributes various grants and other forms of help to applicants wishing to extend existing or gain new knowledge in oncology. It also helps professional and other associations in Slovenia to organise scientific and other meetings of specific interest in different fields of advanced cancer research. On the other hand, it also supports Slovenian Cancer Association to publish various cancer information and cancer awareness brochures and booklets for general public. Importantly, the Foundation continues to support the publication of "Radiology and Oncology" international medical scientific journal that is edited, published and printed in Ljubljana, Slovenia. "Radiology and Oncology" is an open access journal, available free of charge on its website.

Within its possibilities, the Foundation supports the implementation of all advances in cancer therapy and education into everyday hospital, ambulatory and health promotion practice. Several new activities are to be added to its routine in the near future, as the need for up to date prevention and early detection measures available to Slovenian patients has grown substantially in the last few years, with a number of changes in incidence and prevalence rates of various types of cancer.

The Foundation continues with its activities in 2011 with the aim to spread the latest scientific information about cancer to specialists and other professionals in Slovenia, with important part of its activities being the education and information of general public about prevention, early detection and treatment of cancer. Hopefully, these activities may lead to greater application of the latest cancer diagnostic, therapy and education methods to medical, nursing and public environment in Slovenia.

Andrej Plesničar, MD, MSc
Tomaž Benulič, MD, MSc
Prof. Borut Štabuc, MD, PhD

Prsni ekspanderji in vsadki za rekonstrukcijo dojk

Contour Profile® Gel Family
The CPG® 300 Series

Smooth Tissue Expander Family.
Veliko število različnih oblik.

Siltex® Contour Profile® Style
6300 Tall Height

Zastopa in prodaja:

LABORMED

Labormed d.o.o. Ljubljana
Tel.: 01/436 49 00 | www.labormed.si | info@labormed.si

the power *to transform*®

MENTOR

POVZETEK GLAVNIH ZNAČILNOSTI ZDRAVILA
Ime zdravila: Temodal 20 mg, 100 mg, 140mg, 180 mg, 250 mg, Temodal 2,5 mg/ml prašek za raztopino za infundiranje **Kakovostna in količinska sestava:** Vsaka kapsula zdravila Temodal vsebuje 20 mg, 100 mg, 140 mg, 180 mg ali 250 mg temozolomida. Ena viala vsebuje 100 mg temozolomida Po rekonstituciji 1 ml raztopine za infundiranje vsebuje 2,5 mg temozolomida. Pomožna snov: Ena viala vsebuje 2,4 mmol natrija. **Terapevtske indikacije:** Zdravilo Temodal 2,5 mg/ml je indicirano za zdravljenje: odraslih bolnikov z novo diagnosticiranim multiformnim glioblastomom, sočasno z radioterapijo (RT) in pozneje kot monoterapija in otrok, starih 3 leta in več, mladostnikov in odraslih bolnikov z malignimi gliomi, npr. multiformnimi glioblastomi ali anaplastičnimi astrocitomi, ki se po standardnem zdravljenju ponovno ali napredujejo. **Odmerjanje in način uporabe:** Zdravilo Temodal 2,5 mg/ml smejo predpisati le zdravniki, ki imajo izkušnje z zdravljenjem možganskih tumorjev. *Odrasli bolniki z novo diagnosticiranim multiformnim glioblastomom* Zdravilo Temodal 2,5 mg/ml se uporablja v kombinaciji z žariščno radioterapijo (faza sočasne terapije), temu pa sledi do 6 ciklov monoterapije (monoterapijska faza) z temozolomidom (TMZ). *Faza sočasne terapije* TMZ naj bolnik jemlje v odmerku 75 mg/m2 na dan 42 dni, sočasno z žariščno radioterapijo (60 Gy, danih v 30 delnih odmerkih). Zmanjševanje odmerka ni priporočeno, vendar se boste vsak teden odločili o morebitni odložitvi jemanja TMZ ali njegovi ukinitvi na podlagi kriterijev hematološke in nehematološke toksičnosti. TMZ lahko bolnik jemlje ves čas 42-dnevnega obdobja sočasne terapije (do 49 dni), če so izpolnjeni vsi od naslednjih pogojev:
• absolutno število nevtrofilcev (ANC – Absolute Neutrophil Count) ≥ 1,5 x 109/l;
• število trombocitov ≥ 100 x 109/l;
• skupna merila toksičnosti (SMT) za nehematološko toksičnost ≤ 1. stopnje (z izjemo alopecije, navzee in bruhanja).
Med zdravljenjem morate pri bolniku enkrat na teden pregledati celotno krvno sliko.
Faza monoterapije Štiri tedne po zaključku faze sočasnega zdravljenja s TMZ in RT naj bolnik jemlje TMZ do 6 ciklov monoterapije. V 1. ciklu (monoterapije) je odmerek zdravila 150 mg/m2 enkrat na dan 5 dni, temu pa naj sledi 23 dni brez terapije. Na začetku 2. cikla odmerek povečajte na 200 mg/m2, če je SMT za nehematološko toksičnost za 1. cikel stopnje ≤ 2 (z izjemo alopecije, slabosti in bruhanja), absolutno število nevtrofilcev (ANC) ≥ 1,5 x 109/l in število trombocitov ≥ 100 x 109/l. Če odmerka niste povečali v 2. ciklu, ga v naslednjih ciklih ne smete povečevati. Ko pa odmerek enkrat povečate, naj ostane na ravni 200 mg/m2 na dan v prvih 5 dneh vsakega naslednjega cikla, razen če nastopi toksičnost. Zmanjšanje odmerka in ukinitev zdravila med fazo monoterapije opravite, kot je opisano v preglednicah 2 in 3. Med zdravljenjem morate 22. dan pregledati celotno krvno sliko (21 dni po prvem odmerku TMZ). *Odrasli in pediatrični bolniki, stari 3 leta ali več, s ponavljajočim se ali napredujočim malignim gliomom:* Posamezen cikel zdravljenja traja 28 dni. Bolniki, ki še niso bili zdravljeni s kemoterapijo, naj jemljejo TMZ v odmerku 200 mg/m2 enkrat na dan prvih 5 dni, temu pa naj sledi 23-dnevni premor (skupaj 28 dni). Pri bolnikih, ki so že bili zdravljeni s kemoterapijo, je začetni odmerek 150 mg/m2 enkrat na dan, v drugem ciklu pa se poveča na 200 mg/m2 enkrat na dan 5 dni, če ni bilo hematoloških toksičnih učinkov. **Kontraindikacije:** Preobčutljivost za zdravilno učinkovino ali katerokoli pomožno snov. Preobčutljivost za dakarbazin (DTIC). **Posebna opozorila in previdnostni ukrepi:** *Pljučnica, ki jo povzroča Pneumocystis carinii* Pilotno preskušanje podaljšane 42-dnevne sheme zdravljenja je pokazalo, da pri bolnikih, ki so sočasno prejemali TMZ in RT, obstaja še posebej veliko tveganje za nastanek pljučnice zaradi okužbe s Pneumocystis carinii (PCP). *Malignosti* Zelo redko so poročali tudi o primerih mielodisplastičnega sindroma in sekundarnih malignostih, vključno z mieloidno levkemijo. Antiemetično zdravljenje Navzea in bruhanje sta pogosto povezana z zdravljenjem s TMZ. *Antiemetično zdravljenje* se lahko da pred uporabo TMZ ali po njej. *Odrasli bolniki z novo diagnosticiranim multiformnim glioblastomom* Antiemetična profilaksa je priporočljiva pred začetnim odmerkom sočasne faze in je močno priporočljiva med fazo monoterapije. *Ponavljajoči se ali napredujoči maligni gliom* Pri bolnikih, ki so močno bruhali (stopnja 3 ali 4) v prejšnjih ciklih zdravljenja, je potrebno antiemetično zdravljenje. *Laboratorijske vrednosti* Pred jemanjem zdravila morata biti izpolnjena naslednja pogoja za laboratorijske izvide: ANC ≥ 1,5 x 109/l in število trombocitov ≥ 100 x 109/l. Na 22. dan (21 dni po prvem odmerku) ali v roku 48 ur od navedenega dne, morate pregledati celotno krvno sliko in jo nato spremljati vsak teden, dokler ni ANC > 1,5 x 109/l in število trombocitov > 100 x 109/l. Če med katerimkoli ciklom ANC pade na < 1,0 x 109/l ali število trombocitov na < 50 x 109/l, morate odmerek zdravila v naslednjem ciklu zmanjšati za eno stopnjo (glejte poglavje 4.2). Stopnje odmerka so 100 mg/m2, 150 mg/m2 in 200 mg/m2. Najmanjši priporočeni odmerek je 100 mg/m2. *Pediatrična uporaba* Kliničnih izkušenj z uporabo TMZ pri otrocih, mlajših od 3 let, ni. Izkušnje z uporabo tega zdravila pri starejših otrocih in mladostnikih so zelo omejene. *Starejši bolniki* (stari > 70 let) Videti je, da je pri starejših bolnikih tveganje za nevtropenijo ali trombocitopenijo večje, kot pri mlajših. Zato je pri uporabi zdravila TMZ pri starejših bolnikih potrebna posebna previdnost.
Moški bolniki Moškim, ki se zdravijo s TMZ je treba svetovati, naj ne zaplodijo otroka še šest mesecev po prejetem zadnjem odmerku in naj se pred zdravljenjem posvetujejo o možnostih za shranitev zmrznjenje sperme. *Natrij* To zdravilo vsebuje 2,4 mmol natrija na vialo. To je treba upoštevati pri bolnikih na nadzorovani dieti z malo natrija. **Medsebojno delovanje z drugimi zdravili in druge oblike interakcij:** Študije medsebojnega delovanja so izvedli le pri odraslih. V ločeni študiji 1. faze, sočasna uporaba TMZ in ranitidina ni povzročila spremembe obsega absorpcije temozolomida ali izpostavljenosti njegovem aktivnem presnovku monometiltriazenoimidazol karboksamidu (MTIK). Analiza populacijske farmakokinetike v preskušanjih 2. faze je pokazala, da sočasna uporaba deksametazona, proklorperazina, fenitoina, karbamazepina, ondansetrona, antagonistov receptorjev H2 ali fenobarbitala ne spremeni očistka TMZ. Sočasno jemanje z valprojsko kislino je bilo povezano z majhnim, a statistično pomembnim zmanjšanjem očistka TMZ. Študij za določitev učinka TMZ na presnovo ali izločanje drugih zdravil niso izvedli. Ker pa se TMZ ne presnavlja v jetrih in se na beljakovine veže le v majhni meri, je malo verjetno, da bi vplival na farmakokinetiko drugih zdravil.
Uporaba TMZ v kombinaciji z drugimi mielosupresivnimi učinkovinami lahko poveča verjetnost mielosupresije. **Neželeni učinki:** Pri bolnikih, ki se zdravijo s TMZ v kombinaciji z RT ali monoterapijo po RT zaradi novo diagnosticiranega multiformnega glioblastoma ali z monoterapijo pri bolnikih s ponavljajočim se ali napredujočim gliomom, so bili zelo pogosti neželeni učinki podobni; slabost, bruhanje, zaprtje, neješčnost, glavobol in utrujenost. Pri bolnikih z novo diagnosticiranim glioblastomom multiforme na monoterapiji so zelo pogosto poročali o konvulzijah, medtem ko je bil izpuščaj opisan zelo pogosto pri bolnikih z novo diagnosticiranim multiformnim glioblastomom, ki so prejemali TMZ sočasno z RT, ter pri tistih, ki so zdravilo prejemali v obliki monoterapije, pogosto pa pri tistih s ponavljajočim se gliomom. Pri obeh indikacijah so o večini hematoloških neželenih reakcij poročali pogosto ali zelo pogosto. **Imetnik dovoljenja za promet:** Schering-Plough Europe, Rue de Stalle 73, Bruselj Belgija **Način in režim izdaje zdravila:** Zdravilo Temodal 20 mg, 100 mg, 140mg, 180 mg, 250 mg se izdaja na recept (Rp/Spec), Temodal 2,5 mg/ml prašek za raztopino za infundiranje pa je namenjeno uporabi samo v bolnišnicah (H). **Datum priprave informacije:** februar 2010

1. Stupp R, et.al. Effects of radiotherapy with concomitant and adjuvant temozolomide versus radiotherapy alone on survival in glioblastoma in a randomised III study: 5-year analysis of the EORTC-NCIC trial
2. Povzetek temeljnih značilnosti zdravila Temodal

5 jakosti v **5** barvah za lažje in natančnejše dnevno odmerjanje[2]

250 mg	180 mg	140 mg	100 mg	20 mg

Resnični napredek

**Pomembno izboljšanje preživetja potrjeno
tudi ob daljšem spremljanju bolnikov[1]**

Temodal®
temozolomide
capsules

SKRAJŠAN POVZETEK GLAVNIH ZNAČILNOSTI ZDRAVILA

Samo za strokovno javnost.

Ime zdravila: Tarceva 25 mg/100 mg/150 mg filmsko obložene tablete **Kakovostna in količinska sestava:** Ena filmsko obložena tableta vsebuje 25 mg, 100 mg ali 150 mg erlotiniba (v obliki erlotinibijevega klorida).
Terapevtske indikacije: Nedrobnocelični rak pljuč: Zdravilo Tarceva je indicirano za samostojno vzdrževalno zdravljenje bolnikov z lokalno napredovalim ali metastatskim nedrobnoceličnim rakom pljuč s stabilno boleznijo po 4 ciklih standardne kemoterapije na osnovi platine v prvi liniji zdravljenja. Zdravilo Tarceva je indicirano tudi za zdravljenje bolnikov z lokalno napredovalim ali metastatskim nedrobnoceličnim rakom pljuč po neuspehu vsaj ene predhodne kemoterapije. Pri predpisovanju zdravila Tarceva je treba upoštevati dejavnike, povezane s podaljšanim preživetjem. Koristnega vpliva na podaljšanje preživetja ali drugih klinično pomembnih učinkov zdravljenja niso dokazali pri bolnikih z EGFR-negativnimi tumorji. Rak trebušne slinavke: Zdravilo Tarceva je v kombinaciji z gemcitabinom indicirano za zdravljenje bolnikov z metastatskim rakom trebušne slinavke. Pri predpisovanju zdravila Tarceva je treba upoštevati dejavnike, povezane s podaljšanim preživetjem. Koristnega vpliva na podaljšanje preživetja niso dokazali za bolnike z lokalno napredovalo boleznijo.
Odmerjanje in način uporabe: Zdravljenje z zdravilom Tarceva mora nadzorovati zdravnik z izkušnjami pri zdravljenju raka. Zdravilo Tarceva vzamemo najmanj eno uro pred zaužitjem hrane ali dve uri po tem. Kadar je potrebno odmerek prilagoditi, ga je treba zmanjševati v korakih po 50 mg. Pri sočasnem jemanju substratov in modulatorjev CYP3A4 bo morda potrebna prilagoditev odmerka. Pri dajanju zdravila Tarceva bolnikom z jetrno okvaro je potrebna previdnost. Če se pojavijo hudi neželeni učinki, pride v poštev zmanjšanje odmerka ali prekinitev zdravljenja z zdravilom Tarceva. Uporaba zdravila Tarceva pri bolnikih s hudo jetrno ali ledvično okvaro ter pri otrocih ni priporočljiva. Bolnikom kadilcem je treba svetovati, naj prenehajo kaditi, saj so plazemske koncentracije erlotiniba pri kadilcih manjše kot pri nekadilcih. Nedrobnocelični rak pljuč: Priporočeni dnevni odmerek zdravila Tarceva je 150 mg. Rak trebušne slinavke: Priporočeni dnevni odmerek zdravila Tarceva je 100 mg, v kombinaciji z gemcitabinom. Pri bolnikih, pri katerih se kožni izpuščaj v prvih 4 do 8 tednih zdravljenja ne pojavi, je treba ponovno pretehtati nadaljnje zdravljenje z zdravilom Tarceva.
Kontraindikacije: Preobčutljivost za erlotinib ali katero koli pomožno snov.
Posebna opozorila in previdnostni ukrepi: Močni induktorji CYP3A4 lahko zmanjšajo učinkovitost erlotiniba, močni zaviralci CYP3A4 pa lahko povečajo toksičnost. Sočasnemu zdravljenju s temi zdravili se je treba izogibati. Bolnikom, ki kadijo, je treba svetovati, naj prenehajo kaditi, saj so plazemske koncentracije erlotiniba pri kadilcih zmanjšane v primerjavi s plazemskimi koncentracijami pri nekadilcih. Verjetno je, da je velikost zmanjšanja klinično pomembna. Pri bolnikih, pri katerih se akutno pojavijo novi in/ali poslabšajo nepojasnjeni pljučni simptomi, kot so dispneja, kašelj in vročina, je treba zdravljenje z zdravilom Tarceva prekiniti, dokler ni znana diagnoza. Bolnike, ki se sočasno zdravijo z erlotinibom in gemcitabinom, je treba skrbno spremljati zaradi možnosti pojava toksičnosti, podobni intersticijski bolezni pljuč. Če je ugotovljena intersticijska bolezen pljuč, zdravilo Tarceva ukinemo in uvedemo ustrezno zdravljenje. Pri približno polovici bolnikov, ki so se zdravili z zdravilom Tarceva, se je pojavila driska (vključno z zelo redkimi primeri, ki so se končali s smrtnim izidom). Zmerno do hudo drisko zdravimo z loperamidom. V nekaterih primerih bo morda potrebno zmanjšanje odmerka. V primeru hude ali dolgotrajne driske, navzeje, anoreksije ali bruhanja, povezanih z dehidracijo, je treba zdravljenje z zdravilom Tarceva prekiniti in dehidracijo ustrezno zdraviti. O hipokaliemiji in ledvični odpovedi so poročali redko. Posebno pri bolnikih z dejavniki tveganja (sočasno jemanje drugih zdravil, simptomi, bolezni ali drugi dejavniki, vključno z visoko starostjo) moramo, če je driska huda ali dolgotrajna oziroma vodi v dehidracijo, zdravljenje z zdravilom Tarceva prekiniti in bolnikom zagotoviti intenzivno intravensko rehidracijo. Dodatno je treba pri bolnikih s prisotnim tveganjem za razvoj dehidracije spremljati ledvično delovanje in serumske elektrolite, vključno s kalijem. Pri uporabi zdravila Tarceva so poročali o redkih primerih jetrne odpovedi. K njenemu nastanku je lahko pripomogla predhodno obstoječa jetrna bolezen ali sočasno jemanje hepatotoksičnih zdravil. Pri teh bolnikih je treba zato premisliti o rednem spremljanju jetrnega delovanja. Dajanje zdravila Tarceva je treba prekiniti, če so spremembe jetrnega delovanja hude. Bolniki, ki prejemajo zdravilo Tarceva, imajo večje tveganje za razvoj perforacij v prebavilih, ki so jih opazili občasno (vključno z nekaterimi primeri, ki so se končali s smrtnim izidom). Pri bolnikih, ki sočasno prejemajo zdravila, ki zavirajo angiogenezo, kortikosteroide, nesteroidna protivnetna zdravila (NSAID) in/ali kemoterapijo na osnovi taksanov, ali so v preteklosti imeli peptični ulkus ali divertikularno bolezen, je tveganje večje. Če pride do tega, je treba zdravljenje z zdravilom Tarceva dokončno ukiniti. Poročali so o primerih kožnih bolezni z mehurji in luščenjem kože, vključno z zelo redkimi primeri, ki so nakazovali na Stevens-Johnsonov sindrom/toksično epidermalno nekrolizo in so bili v nekaterih primerih smrtni. Zdravljenje z zdravilom Tarceva je treba prekiniti ali ukiniti, če se pri bolniku pojavijo hude oblike mehurjev ali luščenja kože. Zelo redko so poročali o primerih perforacije ali ulceracije roženice; opazili so tudi druge očesne bolezni. Zdravljenje z zdravilom Tarceva je treba prekiniti ali ukiniti, če se pri bolnikih pojavijo akutne očesne bolezni, kot je bolečina v očeh, ali se le-te poslabšajo. Tablete vsebujejo laktozo in jih ne smemo dajati bolnikom z redkimi dednimi stanji: intoleranco za galaktozo, laponsko obliko zmanjšane aktivnosti laktaze ali malabsorpcijo glukoze/galaktoze.
Medsebojno delovanje z drugimi zdravili in druge oblike interakcij: Erlotinib se pri ljudeh presnavlja v jetrih z jetrnimi citokromi, primarno s CYP3A4 in v manjši meri s CYP1A2. Presnova erlotiniba zunaj jeter poteka s CYP3A4 v črevesju, CYP1A1 v pljučih in CYP1B1 v tumorskih tkivih. Z zdravilnimi učinkovinami, ki se presnavljajo s temi encimi, jih zavirajo ali pa so njihovi induktorji, lahko pride do interakcij. Erlotinib je srednje močan zaviralec CYP3A4 in CYP2C8, kot tudi močan zaviralec glukuronidacije z UGT1A1 *in vitro*. Pri kombinaciji ciprofloksacina ali močnega *zaviralca CYP1A2* (npr. fluvoksamina) z erlotinibom je potrebna previdnost. V primeru pojava neželenih učinkov, povezanih z erlotinibom, lahko odmerek erlotiniba zmanjšamo. Predhodno ali sočasno zdravljenje z zdravilom Tarceva ni spremenilo očistka prototipov *substratov CYP3A4*, midazolama in eritromicina. Inhibicija glukuronidacije lahko povzroči interakcije z zdravili, ki so *substrati UGT1A1* in se izločajo samo po tej poti. Močni *zaviralci aktivnosti CYP3A4* zmanjšajo presnovo erlotiniba in zvečajo koncentracije erlotiniba v plazmi. Pri sočasnem jemanju erlotiniba in močnih zaviralcev CYP3A4 je zato potrebna previdnost. Če je treba, odmerek erlotiniba zmanjšamo, še posebno pri pojavu toksičnosti. Močni *spodbujevalci aktivnosti CYP3A4* zvečajo presnovo erlotiniba in pomembno zmanjšajo plazemske koncentracije erlotiniba. Sočasnemu dajanju zdravila Tarceva in induktorjev CYP3A4 se je treba izogibati. Pri bolnikih, ki potrebujejo sočasno zdravljenje z zdravilom Tarceva in močnim induktorjem CYP3A4, je treba premisliti o povečanju odmerka do 300 mg ob skrbnem spremljanju njihove varnosti. Zmanjšana izpostavljenost se lahko pojavi tudi z drugimi zdravili, kot so fenitoin, karbamazepin, barbiturati ali šentjanževka. Če te zdravilne učinkovine kombiniramo z erlotinibom, je potrebna previdnost. Kadar je mogoče, je treba razmisliti o drugih načinih zdravljenja, ki ne vključujejo močnega spodbujanja aktivnosti CYP3A4. Bolnikom, ki jemljejo *kumarinske antikoagulante*, je treba redno kontrolirati protrombinski čas ali INR. Sočasno zdravljenje z zdravilom Tarceva in *statinom* lahko poveča tveganje za miopatijo, povzročeno s statini, vključno z rabdomiolizo; to so opazili redko. Sočasna uporaba *zaviralcev P-glikoproteina*, kot sta ciklosporin in verapamil, lahko vodi v spremenjeno porazdelitev in/ali spremenjeno izločanje erlotiniba. Za erlotinib je značilno zmanjšanje topnosti pri pH nad 5. *Zdravila, ki spremenijo pH v zgornjem delu prebavil*, lahko spremenijo topnost erlotiniba in posledično njegovo biološko uporabnost. Učinka antacidov na absorpcijo erlotiniba niso proučevali, vendar je ta lahko zmanjšana, kar vodi v nižje plazemske koncentracije. Kombinaciji erlotiniba in zaviralca protonske črpalke se je treba izogibati. Če menimo, da je uporaba antacidov med zdravljenjem z zdravilom Tarceva potrebna, jih je treba jemati najmanj 4 ure pred ali 2 uri po dnevnem odmerku zdravila Tarceva. Če razmišljamo o uporabi ranitidina, moramo zdravili jemati ločeno: zdravilo Tarceva je treba vzeti najmanj 2 uri pred ali 10 ur po odmerku ranitidina. V študiji faze Ib ni bilo pomembnih učinkov *gemcitabina* na farmakokinetiko erlotiniba, prav tako ni bilo pomembnih učinkov erlotiniba na farmakokinetiko gemcitabina. Erlotinib poveča koncentracijo platine. Pomembnih učinkov *karboplatina* ali paklitaksela na farmakokinetiko erlotiniba ni bilo. *Kapecitabin* lahko poveča koncentracijo erlotiniba. Pomembnih učinkov erlotiniba na farmakokinetiko kapecitabina ni bilo.
Neželeni učinki: *Zelo pogosti neželeni učinki* so kožni izpuščaj in driska, kot tudi utrujenost, anoreksija, dispneja, kašelj, okužba, navzea, bruhanje, stomatitis, bolečina v trebuhu, pruritus, suha koža, suhi keratokonjunktivitis, konjunktivitis, zmanjšanje telesne mase, depresija, glavobol, nevropatija, dispepsija, flatulenca, alopecija, okorelost, pireksija, nenormalnosti testov jetrne funkcije. *Pogosti neželeni učinki* so krvavitve v prebavilih, epistaksa, keratitis, paronihija, fisure na koži. *Občasno* so poročali o perforacijah v prebavilih, hirzutizmu, spremembah obrvi, krhkih nohtih, odstopanju nohtov od kože, blagih reakcijah na koži (npr. hiperpigmentacija), spremembah trepalnic, hudi intersticijski bolezni pljuč (vključno s smrtnimi primeri). *Redko* pa so poročali o jetrni odpovedi. *Zelo redko* so poročali o Stevens-Johnsonovem sindromu/toksični epidermalni nekrolizi ter o ulceracijah in perforacijah roženice.
Režim izdaje zdravila: H/Rp. **Imetnik dovoljenja za promet:** Roche Registration Limited, 6 Falcon Way, Shire Park, Welwyn Garden City, AL7 1TW, Velika Britanija. **Verzija:** 2.0/10. **Informacija pripravljena:** februar 2011.

EGFR M+

Zadeli smo pravo tarčo

Izredno učinkovito zdravljenje prvega reda pri nedrobnoceličnem pljučnem raku z mutacijo EGFR

Iressa je prva in edina tarčna monoterapija, ki dokazano podaljša preživetje brez napredovanja bolezni v primerjavi z dvojno kemoterapijo kot zdravljenje prvega reda pri bolnikih z napredovalim nedrobnoceličnim pljučnim rakom z mutacijo EGFR. [1]

AstraZeneca
ONKOLOGIJA

IRESSA®
gefitinib

Megace®

megestrolacetat 40mg/ml
peroralna suspenzija

učinkovita in preizkušena možnost zdravljenja anoreksije-kaheksije

Megace®

... še vedno EDINO ZDRAVILO, ki je v Sloveniji registrirano za zdravljenje anoreksije-kaheksije pri bolnikih z napredovalim rakom [1,2] - predpisovanje na zeleni recept v breme ZZZS [6]

Megace®

- izboljša apetit [1,5]
- pomaga ohraniti in pridobiti telesno težo [3,4,5]
- izboljša splošno počutje bolnikov [3,4]

Megace®

SKRAJŠAN POVZETEK GLAVNIH ZNAČILNOSTI ZDRAVILA: MEGACE 40 mg/ml peroralna suspenzija

Sestava: 1 ml peroralne suspenzije vsebuje 40 mg megestrolacetata. **TERAPEVTSKE INDIKACIJE:** Zdravljenje anoreksije-kaheksije ali nepojasnjene, pomembne izgube telesne mase pri bolnikih z AIDS-om. Zdravljenje anorektično-kahektičnega sindroma pri napredovalem raku. **ODMERJANJE IN NAČIN UPORABE:** Pri aidsu je priporočeni začetni odmerek Megace za odrasle 800 mg (20 ml peroralne suspenzije) enkrat na dan eno uro pred jedjo ali dve uri po jedi in se lahko med zdravljenjem prilagodi glede na bolnikov odziv. V raziskavah bolnikov z aidsom so bili klinično učinkoviti dnevni odmerki od 400 do 800 mg/dan (10 do 20 ml), uporabljani štiri mesece. Pri anorektično-kahektičnem sindromu zaradi napredovalega raka je priporočljiv začetni odmerek 200 mg (5 ml) na dan; glede na bolnikov odziv ga je mogoče povečati do 800 mg na dan (20 ml). Običajni odmerek je med 400 in 800 mg na dan (10–20 ml). V raziskavah bolnikov z napredovalim rakom so bili klinično učinkoviti dnevni odmerki od 200 do 800 mg/dan (5 do 20 ml), uporabljani najmanj osem tednov. Pred uporabo je potrebno plastenko s suspenzijo dobro pretresti. Uporaba pri otrocih: Varnosti in učinkovitosti pri otrocih niso dokazali. Uporaba pri starostnikih: Zaradi pogostejših okvar jeter, ledvic in srčne funkcije, pogostejših sočasnih obolenj ali sočasnega zdravljenja z drugimi zdravili je odmerek za starejšega bolnika treba določiti previdno in običajno začeti z najnižjim odmerkom znotraj odmernega intervala. **KONTRAINDIKACIJE:** Preobčutljivost za megestrolacetat ali katerokoli pomožno snov. **POSEBNA OPOZORILA IN PREVIDNOSTNI UKREPI:** Uporaba gestagenov med prvimi štirimi meseci nosečnosti ni priporočljiva. Pri bolnikih s tromboflebitisom v anamnezi je treba zdravilo Megace uporabljati previdno. Zdravljenje z zdravilom Megace se lahko začne šele, ko so bili vzroki hujšanja, ki jih je mogoče zdraviti, ugotovljeni in obravnavani. Megestrolacetat ni namenjen za profilaktično uporabo za preprečitev hujšanja. Učinki na razmnoževanje virusa HIV niso ugotovljeni. Med zdravljenjem z megestrolacetatom in po prekinitvi kroničnega zdravljenja je treba upoštevati možnost pojava zavore nadledvične žleze. Morda bo potrebno nadomestno zdravljenje s stresnimi odmerki glukokortikoidov. Megestrolacetat se v veliki meri izloči prek ledvic. Ker je verjetnost zmanjšanega delovanja ledvic pri starostnikih večja, je pri določitvi odmerka potrebna previdnost, prav tako je koristno spremljanje ledvične funkcije. Peroralna suspenzija vsebuje saharozo. Bolniki z redko dedno intoleranco za fruktozo, malabsorpcijo glukoze/galaktoze ali pomanjkanjem saharoza-izomaltaze ne smejo jemati tega zdravila. Peroralna suspenzija vsebuje tudi majhne količine etanola (alkohola), in sicer manj kot 100 mg na odmerek. **INTERAKCIJE:** Aminoglutetimid: poročali so o zmanjšanju koncentracije progestogena v plazmi z možno izgubo terapevtskega delovanja zaradi inducirane presnove. Sočasno jemanje megestrolacetata (v obliki peroralne suspenzije) in zidovudina ali rifabutina ne povzroča sprememb farmakokinetičnih parametrov. **NEŽELENI UČINKI:** Pogosti (≥ 1/100, < 1/10): navzea, bruhanje, driska, flatulenca, izpuščaj, metroragija, impotenca, astenija, bolečina, edem. Neznana pogostnost (pogostnosti ni mogoče oceniti iz razpoložljivih podatkov): poslabšanje osnovne bolezni (širjenje tumorja), adrenalna insuficienca, kušingoidni izgled, Cushingov sindrom, diabetes mellitus, motena toleranca za glukozo, hiperglikemija, spremembe razpoloženja, sindrom karpalnega kanala, letargija, srčno popuščanje, tromboflebitis, pljučna embolija (v nekaterih primerih usodna), hipertenzija, navali vročine, dispneja, zaprtje, alopecija, pogosto uriniranje. **Vrsta ovojnine in vsebina:** Plastenka z 240 ml suspenzije. **Režim izdaje:** Rp/Spec. **Imetnik dovoljenja za promet:** Bristol-Myers Squibb spol. s r.o., Olivova 4, Praga 1, Češka; **Odgovoren za trženje v Sloveniji:** PharmaSwiss d.o.o., Ljubljana, tel: 01 236 4 700, faks: 01 236 4 705; MGS-120609. **Pred predpisovanjem preberite celoten povzetek glavnih značilnosti zdravila!**

Reference: 1. Povzetek glavnih značilnosti zdravila Megace – 12. junij 2009; **2.** Register zdravil Republike Slovenije XI – leto 2008; **3.** Beller, E., 1997. Ann Oncol 8: 277-283; **4.** Čufer, T, 2002. Onkologija 9(2): 73-75; **5.** Yavuzsen, T., 2005. J Clin Oncol 23(33): 8500-8511; **6.** Bilten Recept 7(1), 22.5.2009

MEG1109-07; november, 2009

Bristol-Myers Squibb

PharmaSwiss
Choose More Life

odprto

Vir
Sodelovanje
Izobraževanje
Jasnost
Zavezanost

Novartis Oncology prinaša spekter inovativnih zdravil,
s katerimi poskuša spremeniti življenje bolnikov z rakavimi
in hematološkimi obolenji.

Ta vključuje zdravila kot so Glivec® (imatinib), Tasigna® (nilotinib),
Afinitor® (everolimus), Zometa® (zoledronska kislina), Femara®
(letrozol), Sandostatin® LAR® (oktreotid/i.m. injekcije) in Exjade®
(deferasiroks).

Novartis Oncology ima tudi obširen razvojni program,
ki izkorišča najnovejša spoznanja molekularne genomike,
razumskega načrtovanja in tehnologij
za odkrivanje novih učinkovin.

glivec®
imatinib

Tasigna®
(nilotinib)

AFINITOR®
(everolimus) tablete

ZOMETA®
zoledronska kislina

Femara®
(letrozol)

Sandostatin® LAR®
oktreotid/i.m. injekcije

EXJADE®
deferasiroks

NOVARTIS
ONCOLOGY

TANTUM® VERDE

Lajšanje bolečine in oteklin pri vnetju v ustni votlini in žrelu, ki nastanejo zaradi okužb in stanj po operaciji in kot posledica radioterapije (t.i. radiomukozitis).

Tantum Verde 1,5 mg/ml oralno pršilo, raztopina

Kakovostna in količinska sestava
1 ml raztopine vsebuje 1,5 mg benzidaminijevega klorida, kar ustreza 1,34 mg benzidamina. V enem razpršku je 0,17 ml raztopine. En razpršek vsebuje 0,255 mg benzidaminijevega klorida, kar ustreza 0,2278 mg benzidamina. En razpršek vsebuje 13,6 mg 96 odstotnega etanola, kar ustreza 12,728 mg 100 odstotnega etanola, in 0,17 mg metilparahidroksibenzoata (E218).

Terapevtske indikacije
Samozdravljenje: lajšanje bolečine in oteklin pri vnetju v ustni votlini in žrelu, ki so lahko posledica okužb in stanj po operaciji. Po nasvetu in navodilu zdravnika: lajšanje bolečine in oteklin v ustni votlini in žrelu, ki so posledica radiomukozitisa.

Odmerjanje in način uporabe
Uporaba 2- do 6-krat na dan (vsake 1,5 do 3 ure). Odrasli: 4 do 8 razprškov 2- do 6-krat na dan. Otroci od 6 do 12 let: 4 razprški 2- do 6-krat na dan. Otroci, mlajši od 6 let: 1 razpršek na 4 kg telesne mase; do največ 4 razprške 2 do 6-krat na dan.

Kontraindikacije
Znana preobčutljivost za zdravilno učinkovino ali katerokoli pomožno snov.

Posebna opozorila in previdnostni ukrepi
Pri manjšini bolnikov lahko resne bolezni povzročijo ustne/žrelne ulceracije. Če se simptomi v treh dneh ne izboljšajo, se mora bolnik posvetovati z zdravnikom ali zobozdravnikom, kot je primerno. Zdravilo vsebuje aspartam (E951) (vir fenilalanina), ki je lahko škodljiv za bolnike s fenilketonurijo. Zdravilo vsebuje izomalt (E953) (sinonim: izomaltitol (E953)). Bolniki z redko dedno intoleranco za fruktozo ne smejo jemati tega zdravila. Uporaba benzidamina ni priporočljiva za bolnike s preobčutljivostjo za salicilno kislino ali druga nesteroidna protivnetna zdravila. Pri bolnikih, ki imajo ali so imeli bronhialno astmo, lahko pride do bronhospazma. Pri takih bolnikih je potrebna previdnost.

Medsebojno delovanje z drugimi zdravili in druge oblike interakcij
Pri ljudeh raziskav o interakcijah niso opravljali.

Nosečnost in dojenje
Tantum Verde z okusom mentola 3 mg pastile se med nosečnostjo in dojenjem ne smejo uporabljati.

Vpliv na sposobnost vožnje in upravljanja s stroji
Uporaba benzidamina lokalno v priporočenem odmerku ne vpliva na sposobnost vožnje in upravljanja s stroji.

Neželeni učinki
Bolezni prebavil Redki: pekoč občutek v ustih, suha usta.
Bolezni imunskega sistema Redki: preobčutljivostna reakcija.
Bolezni dihal, prsnega koša in mediastinalnega prostora Zelo redki: laringospazem.
Bolezni kože in podkožja Občasni: fotosenzitivnost. Zelo redki: angioedem.

Rok uporabnosti
4 leta. Zdravila ne smete uporabljati po datumu izteka roka uporabnosti, ki je naveden na ovojnini. Posebna navodila za shranjevanje Za shranjevanje pastil niso potrebna posebna navodila. Plastenko z raztopino shranjujte v zunanji ovojnini za zagotovitev zaščite pred svetlobo. Shranjujte pri temperaturi do 25°C. Shranjujte v originalni ovojnini in nedosegljivo otrokom.

CSC   ANGELINI

Instructions for authors

The editorial policy

Radiology and Oncology is a multidisciplinary journal devoted to the publishing original and high quality scientific papers, professional papers, review articles, case reports and varia (editorials, short communications, professional information, book reviews, letters, etc.) pertinent to diagnostic and interventional radiology, computerized tomography, magnetic resonance, ultrasound, nuclear medicine, radiotherapy, clinical and experimental oncology, radiobiology, radiophysics and radiation protection. Therefore, the scope of the journal is to cover beside radiology the diagnostic and therapeutic aspects in oncology, which distinguishes it from other journals in the field.

The Editorial Board requires that the paper has not been published or submitted for publication elsewhere; the authors are responsible for all statements in their papers. Accepted articles become the property of the journal and, therefore cannot be published elsewhere without the written permission of the editors.

Submission of the manuscript

The manuscript written in English should be submitted electronically to: gsersa@onko-i.si. In the case the figures are too big to be submitted electronically, authors are asked to send along the printed copy of the manuscript, together with all the files on CD, to the editorial office. The type of computer and word-processing package should be specified (Word for Windows is preferred).

Editorial Office Radiology and Oncology
Zaloska cesta 2
P.O. Box 2217
SI-1000 Ljubljana
Slovenia
Phone: +386 (0)1 5879 434,
Tel./Fax: +386 (0)1 5879 434,
E-mail: gsersa@onko-i.si

All articles are subjected to the editorial review and the review by independent referees. Manuscripts which do not comply with the technical requirements stated herein will be returned to the authors for the correction before peer-review. The editorial board reserves the right to ask authors to make appropriate changes of the contents as well as grammatical and stylistic corrections when necessary. Page charges will be charged for manuscripts exceeding the recommended page number, as well as additional editorial work and requests for printed reprints. All articles are published printed and on-line as the open access. To support the open access policy of the journal, the authors are encouraged to pay the open access charge of 500 EUR.

Preparation of manuscripts

Radiology and Oncology will consider manuscripts prepared according to the Uniform Requirements for Manuscripts Submitted to Biomedical Journals by International Committee of Medical Journal Editors (http://www.icmje.org/). The manuscript should be typed double-spaced with a 3-cm margin at the top and left-hand side of the sheet. The manuscript should be written in grammatically and stylistically correct language. Abbreviations should be avoided. If their use is neccessary, they should be explained at the first time mentioned. The technical data should conform to the SI system. The manuscript, including the references, must not exceed 15 typewritten pages, and the number of figures and tables is limited to 8. If appropriate, organize the text so that it includes: Introduction, Materials and methods, Results and Discussion. Exceptionally, the results and discussion can be combined in a single section. Start each section on a new page, and number each page consecutively with Arabic numerals.

The Title page should include a concise and informative title, followed by the full name(s) of the author(s); the institutional affiliation of each author; the name and address of the corresponding author (including telephone, fax and E-mail), and an abbreviated title. This should be followed by the abstract page, summarizing in less than 250 words the reasons for the study, experimental approach, the major findings (with specific data if possible), and the principal conclusions, and providing 3-6 key words for indexing purposes. Structured abstracts are preferred. Slovene authors are requested to provide title and the abstract in Slovene language in a separate file. The text of the research article should then proceed as follows:

Introduction should summarize the rationale for the study or observation, citing only the essential references and stating the aim of the study.

Materials and methods should provide enough information to enable experiments to be repeated. New methods should be described in detail.

Results should be presented clearly and concisely without repeating the data in the figures and tables. Emphasis should be on clear and precise presentation of results and their significance in relation to the aim of the investigation.

Discussion should explain the results rather than simply repeating them and interpret their significance and draw conclusions. It should discuss the results of the study in the light of previously published work.

Illustrations and tables must be numbered and referred to in the text, with the appropriate location indicated. Graphs and photographs, provided electronically, should be of appropriate quality for good reproduction. Color graphs and photographs are encouraged. Picture size must be 2.000 pixels on the longer side. In photographs, mask the identities of the patients. Tables should be typed double-spaced, with a descriptive title and, if appropriate, units of numerical measurements included in the column heading.

References must be numbered in the order in which they appear in the text and their corresponding numbers quoted in the text. Authors are responsible for the accuracy of their references. References to the Abstracts and Letters to the Editor must be identified as such. Citation of papers in preparation or submitted for publication, unpublished observations, and personal communications should not be included in the reference list. If essential, such material may be incorporated in the appropriate place in the text. References follow the style of Index Medicus. All authors should be listed when their number does not exceed six; when there are seven or more authors, the first six listed are followed by "et al.". The following are some examples of references from articles, books and book chapters:

Dent RAG, Cole P. *In vitro* maturation of monocytes in squamous carcinoma of the lung. *Br J Cancer* 1981; **43**: 486-95.

Chapman S, Nakielny R. *A guide to radiological procedures.* London: Bailliere Tindall; 1986.

Evans R, Alexander P. Mechanisms of extracellular killing of nucleated mammalian cells by macrophages. In: Nelson DS, editor. *Immunobiology of macrophage.* New York: Academic Press; 1976. p. 45-74.

Authorization for the use of human subjects or experimental animals

Manuscripts containing information related to human or animal use should clearly state that the research has complied with all relevant national regulations and institutional policies and has been approved by the authors' institutional review board or equivalent committee. These statements should appear in the Materials and methods section (or for contributions without this section, within the main text or in the captions of relevant figures or tables).

When reporting experiments on human subjects, authors should indicate whether the procedures followed were in accordance with the Helsinki Declaration. Patients have the right to privacy; therefore the identifying information (patient's names, hospital unit numbers) should not be published unless it is essential. In such cases the patient's informed consent for publication is needed, and should appear as an appropriate statement in the article.

The research using animal subjects should be conducted according to the EU Directive 2010/63/EU and following the Guidelines for the welfare and use of animals in cancer research (*Br J Cancer 2010; 102: 1555 – 77*). Authors must identify the committee approving the experiments, and must confirm that all experiments were performed in accordance with relevant regulations.

Transfer of copyright agreement

For the publication of accepted articles, authors are required to send the Transfer of Copyright Agreement to the publisher on the address of the editorial office. A properly completed Transfer of Copyright Agreement, signed by the Corresponding Author on behalf of all the authors, must be provided for each submitted manuscript. A form can be found on the journal's webpage.

Conflict of interest

When the manuscript is submitted for publication, the authors are expected to disclose any relationship that might pose real, apparent or potential conflict of interest with respect to the results reported in that manuscript. Potential conflicts of interest include not only financial relationships but also other, non-financial relationships. In the Acknowledgement section the source of funding support should be mentioned. The Editors will make effort to ensure that conflicts of interest will not compromise the evaluation process of the submitted manuscripts; potential editors and reviewers will exempt themselves from review process when such conflict of interest exists. The statement of disclosure must be in the Cover letter accompanying the manuscript or submitted on the form available on http://www.icmje.org/coi_disclosure.pdf

Page proofs will be sent by E-mail or faxed to the corresponding author. It is their responsibility to check the proofs carefully and return a list of essential corrections to the editorial office within three days of receipt. Only grammatical corrections are acceptable at this time.

Reprints: The electronic version of the published papers will be available on www.versitaopen.com free of charge.

Lilly Onkologija

Vsaka odprta vrata lahko pomenijo novo odkritje.

Z več kot 60 tarčnimi zdravili v razvoju, se naša prizadevanja
v iskanju pristopov zdravljenja po meri bolnika, šele pričenjajo.

Lilly Onkologija

Niti dva bolnika z rakom nista enaka. Zato si Lilly Onkologija prizadeva, da razvije tako edinstvene pristope zdravljenja, kot so edinstveni ljudje, ki zdravljenje potrebujejo. Veliko smo prispevali k izboljšanju izidov zdravljenja in – z vsakimi vrati, ki jih odpremo – naredimo še en korak naprej. Naša prizadevanja v zagotavljanju zdravljenja po meri bolnika se nadaljujejo.

Znanost približujemo posamezniku.

SIALM00022

Lilly

Odgovori, ki štejejo.